Aus dem Institut für Klinische Neuroimmunologie

der Ludwig-Maximilians-Universität München

Direktoren: Prof. Dr. Reinhard Hohlfeld & Prof. Dr. Martin Kerschensteiner

Detection of autoreactive CD8$^+$ T cells *in situ* and investigation of their antigen-specificities

Dissertation

zum Erwerb des Doktorgrades der Naturwissenschaften

an der medizinischen Fakultät

der Ludwig-Maximilians-Universität München

vorgelegt von

Qingqing Zhou

aus

Henan, China

2017

Gedruckt mit der Genehmigung der medizinischen Fakultät

der Ludwig-Maximilians-Universität München

Supervisor: PD. Dr. Klaus Dornmair

Referees:

1. Prof. Dr. Peter Jon Nelson
2. Prof. Dr. Jürgen Bernhagen
3. Prof. Dr. Elfriede Nößner

Dean: Prof. Dr. med. dent. Reinhard Hickel

Date of the oral defence: 16. 11. 2017

Eidesstattliche Versicherung

Zhou, Qingqing

Name, Vorname

Ich erkläre hiermit an Eides statt,

dass ich die vorliegende Dissertation mit dem Thema

„Detection of autoreactive CD8$^+$ T cells *in situ* and investigation of their antigen-specificities"

selbständig verfasst, mich außer der angegebenen keiner weiteren Hilfsmittel bedient und alle Erkenntnisse, die aus dem Schrifttum ganz oder annähernd übernommen sind, als solche kenntlich gemacht und nach ihrer Herkunft unter Bezeichnung der Fundstelle einzeln nachgewiesen habe.

Ich erkläre des Weiteren, dass die hier vorgelegte Dissertation nicht in gleicher oder in ähnlicher Form bei einer anderen Stelle zur Erlangung eines akademischen Grades eingereicht wurde.

München, 16.11.2017

Ort, Datum

Unterschrift Doktorandin

I dedicate this work to my family.

Table of contents

Summary ..... **I**

Zusammenfassung ..... **III**

Acknowledgements ..... **V**

1 Introduction **1**

1.1 Immune Responses 1

1.1.1 Innate Immune Response 1

1.1.2 Adaptive Immune Response 1

1.2 $CD8^+$ T cells and Their Receptor Complex 3

1.2.1 Diversity of TCR Gene Rearrangement 3

1.2.2 Structure and Function of TCR-CD3 Complex 5

1.3 Antigen Recognition by $CD8^+$ T Cells 6

1.4 Positive and Negative Section of T Cells in Thymus 8

1.5 Autoimmunity and Autoimmune Disease 9

1.6 Multiple Sclerosis 9

1.6.1 Pathology and Etiology 11

1.6.2 The Dominant Role of T lymphocytes in MS 12

1.6.3 Mucosal Associated Invariant T Cells (MAITs) and MS 12

1.7 Identification of Autoreactive T Cells in MS 14

1.8 Characterization of Specific Antigens of TCR in MS 15

1.9 Objectives 18

2 Materials and Methods **19**

2.1 Materials 19

2.1.1 Devices 19

2.1.2 Consumables and Chemicals 20

2.1.3 Chemical kits and specific reagents 20

2.1.4 Buffers, Mediums, and Solutions 21

2.1.5 Primers 22

2.1.6 Plasmids 25

2.1.7 Antibodies 26

2.1.8 Eukaryotic Cell Lines and *Escherichia coli* Strains 27

2.1.9 Human Tissue Samples 28
2.2 Molecular Biology based Methods 30
2.2.1 Isolation of Total RNA 30
2.2.2 Isolation of Plasmid DNA 30
2.2.3 Quantitation of DNA and RNA 30
2.2.4 Assessment of RNA Integrity 31
2.2.5 Separation of DNA Fragments 31
2.2.6 DNA Extraction 32
2.2.7 Ethanol Precipitation of DNA 32
2.2.8 DNA Sequencing 32
2.2.9 Amplification of TCR chains from Single T Cells 33
2.2.10 Plasmid Recovery PCR 37
2.2.11 PCR Purification 38
2.2.12 TOPO TA Cloning 38
2.3 Microbiology based Methods 39
2.3.1 Bacterial *E.coli* Culture Conditions 39
2.3.2 Determination of *E.coli* Cells' Density 39
2.3.3 Preparation of *E.coli* Culture Glycerol Stocks 39
2.3.4 Reviving Bacteria from a Glycerol Stock 40
2.3.5 Bacterial Transformation by Heat Shock 40
2.3.6 Bacteria Transformation by Electroporation 41
2.4 Cell Biology based Methods 42
2.4.1 Cultivation of Eukaryotic Cells 42
2.4.2 Determination of Cell Numbers 43
2.4.3 Freezing and Thawing of Cell Lines 44
2.4.4 Cell Re-cloning for Stably Transfected T Hybridoma Cell Line 44
2.4.5 Cell Transfection by FuGENE® HD Reagent 45
2.4.6 Cell Transfection by Nucleofection 45
2.4.7 Co-cultivation with T Hybridoma cells 46
2.4.8 T hybridoma Cell Activation Assays 46
2.4.9 Flow Cytometry Analysis 48
2.4.10 Identification of Single T Cells from CSF Specimens 49
2.5 Immunology-based Methods 51
2.5.1 Preparation of Tissue Cryosections 51

2.5.2 Immunofluorescence of the Immune Cells in Human Tissue 51
2.6 Laser Capture Microdissection 52
2.7 Characterization of Antigen Coding Plasmids from COS-7 cells 53
2.7.1 Isolation of Candidate COS-7 Cells by Micromanipulation 53
2.7.2 Reconstruction of PCR Products into Expression Plasmids 53
2.7.3 Reactivation of T Hybridoma Cells 54
2.7.4 Antigen Coding Plasmids Enrichment by plasmid subpools 54
3 Results 57
3.1 Immunofluorescence of the Immune Cells on Human Tissue Cryosection 57
3.2 Morphological Identification of Activated $CD8^+$ T Cells in the Lesion of MS Brain 64
3.3 Identification of Matching TCR α- and β-Chains from MS Patients 67
3.3.1 Rapid Immunostaining of Single $CD8^+$ T Cells for Microdissection 68
3.3.2 Effective Treatments on Tissue to Minimize the Degradation of RNA Quality 72
3.3.3 Optimization of the Unbiased PCR Technology to Identify Paired TCR α- and β-Chains 76
3.3.4 Identification of TCR β-chains from Single $CD8^+$ T Cells Infiltrating in the MS Brain ... 84
3.3.5 Characterization of Paired αβ-TCRs from Single T Cells of the MS CSF Specimens 86
3.4 Resurrection of Disease-Related $CD8^+$ T cells *in vitro* 91
3.4.1 Expression of Recombinant TCRs and Co-Receptor CD8 *in vitro* 92
3.4.2 TCR Activation *in vitro* by CD3 Cross-linking 94
3.5 Identification of Specific Antigens of Recombinant TCRs 96
3.5.1 PECP Libraries Employed for Antigen Unbiased Search 96
3.5.2 Reduction of T-cell Spontaneous Activation by Re-cloning 97
3.5.3 Search of Positive APCs upon TCR Activation 99
3.5.4 Recovery of Antigen Coding Plasmids from Single Positive APCs 106
3.5.5 TCR Reactivation by Antigen Pools Isolated from Single APCs 107
4 Discussion 113
4.1 Localization of Immune Cells in MS Brain 113
4.1.1 Immunofluorescence Staining of Immune Cells 113
4.1.2 Distribution of Clusters of Activated $CD8^+$ T-Cells 115
4.1.3 Prospects for Investigation of Immune Cells in MS Brain 116
4.2 Identification of the MS-Related TCR αβ-Chains 116
4.2.1 Distinguishing of Activated $CD8^+$ T Cells from Irrelevant Bystanders 117
4.2.2 Minimization of RNA Degradation 118

4.2.3 Molecular Analysis of Paired αβ-TCRs from Single T Cells in MS Patients 120
4.3 Subcloning of 58-BV1-BJ2.3-AV7.2-AJ24.2 T hybridoma cells 124
4.4 Investigation of HLA Restriction of the TCR BV1-BJ2.3-AV7.2-AJ24.2 124
4.5 Technical Challenges of Antigen Identification 125
4.5.1 Activation Background of TCR BV1-BJ2.3-AV7.2-AJ24.2 125
4.5.2 Identification of the Antigenic Plasmid by *E.coli* Subpools 126
4.6 Outlook 126
5 Appendix 129
5.1 Abbreviations 129
5.2 Indexes of Figures and Tables 131
5.3 Control Staining with Isotype Antibody 133
5.4 Vector Maps 137
5.4.1 Map of pcDNA™ 6/V5-His 137
5.4.2 Map of pcDNA™ 3.1D/V5-His-TOPO® 137
5.4.3 Map of pCR™ 2.1-TOPO® 138
5.5 Curriculum Vitae 139
5.6 References 141

Summary

Multiple sclerosis (MS) is a chronic inflammatory disorder of the central nervous system (CNS), typically with relapsing-remitting (RR) course. It is characterized by demyelination and infiltration of most probably autoreactive T lymphocytes into the brain parenchyma, and by oligoclonal bands persisting in the cerebrospinal fluid (CSF) of MS patients. $CD8^+$ T cells are the dominant T-cell population of infiltrates, which are presumably accelerating the inflammation in MS brain. Clonal expansions of $CD8^+$ T cells are often detected *in situ*, and are most likely related to the immunopathogenesis of MS. However, it remained unclear how those autoreactive $CD8^+$ T cells trigger an immune attack and which molecular antigenic target(s) they recognize.

This study investigates $CD8^+$ T cell clones and their specific antigen(s) in the MS-related inflammatory tissues. To this end, an unbiased method to determine the paired αβ-T cell receptors (TCR) of single T cells on frozen tissue slides was improved. This includes optimization of a protocol of the fluorescence staining to identify single activated $CD8^+$ T cells, and modification of a multiplex RT-PCR based method for the high yield of TCR-αβ pairs. Five significant points were accomplished with the optimized approach: (i) By immunohistochemistry, activated $CD8^+$ T cells were shown to be accumulated in the MS lesions. (ii) Single activated $CD8^+$ T cells were distinguished from irrelevant bystander cells. (iii) Degradation of RNA on tissue slide resulted from the fluorescence staining was minimized. (iv) Identical TCR β-chains detected in different tissue blocks indicate that $CD8^+$ T cell infiltration is antigen-restricted. (v) TCR repertoires of $CD4^+$ and $CD8^+$ T-cell subpopulations were studied in the CSF of MS patients.

In parallel, the HLA restriction of a TCR that consisits of BV1-BJ2.3 and AV7.2-AJ24.2 chains was investigated. This TCR was identified from brain-infiltrating $CD8^+$ T cells of a MS patient. High numbers of activated T cells were detected with *HLA-C*0701* restricted plasmid-encoded combinatorial peptide libraries. The result indicates that *HLA-C*0701*, but not the other two HLA class I molecules (*HLA-A*0101* and *HLA-B*0801*) of the MS patient, might be the correct antigen-presenting HLA molecule for TCR BV1-BJ2.3-AV7.2-AJ24.2. In the long-term, these results may contribute to the understanding of the immunopathogenesis of MS, and autoimmune diseases in generally.

Zusammenfassung

Multiple Sklerose (MS), ist eine chronisch entzündliche Erkrankung des Zentralnervensystems (ZNS). Charakteristische Merkmale sind ihr schubförmig remittierender Verlauf, die Demyelinisierung und Infiltrierung des Hirnparenchym durch vermutlich autoreaktive T-Lymphozyten und die persistierenden oligoklonalen Banden in der Zerebrospinal Flüssigkeit (ZSF) der MS Patienten. Entzündungsbeschleunigende $CD8^+$ T-Zellen sind die dominierende T-Zell Population der Infiltrate. Die klonalen Expansionen dieser $CD8^+$ T-Zellen werden häufig *in situ* detektiert und stehen höchstwahrscheinlich im Zusammenhang mit der Immunopathogenese von MS. Allerdings ist es bislang unklar, wie diese autoreaktiven $CD8^+$ T-Zellen einen Immunangriff auslösen. Zudem ist nicht bekannt, welche molekularen Antigene sie erkennen.

Diese Studie untersucht $CD8^+$ T-Zellklone und ihre spezifischen Antigene in MS betroffenen entzündlichen Geweben. Für diesen Zweck wurde ein Verfahren zur Bestimmung der gepaarten αβ-T-Zellrezeptoren (TZR) einzelner T-Zellen auf gefrorenen Gewebe-Objektträgern verbessert. Dazu wurde ein Protokoll zur Fluoreszenzfärbung für die Identifizierung von einzeln aktivierten CD8 T-Zellen optimiert und ein auf Multiplex-RT-PCR-basierendes Verfahrens für hohe TZR αβ-Paar Ausbeuten modifizeirt.

Fünf signifikante Punkte konnten mit dem optimierten Ansatz erreicht werden:

(i) Mittels Immunohistochemie konnte die Akkumulierung von aktivierten $CD8^+$ T-Zellen in den MS-Läsionen gezeigt werden. (ii) Es konnten einzeln aktivierte $CD8^+$ T-Zellen von irrelevanten Bystanderzellen unterschieden werden. (iii) Die RNA Degradierung auf Gewebeschnitten während der Fluoreszenzfärbung konnte minimiert werden. (iv) Der Nachweis von identischen TZR-β Ketten in verschiedenen Gewebeblöcken einer Biopsie zeigte, dass die $CD8^+$ T-Zellinfiltration vermutlich Antigen-spezifisch sind. (v) Zudem konnten die TZR-Repertoires von $CD4^+$ und $CD8^+$ T-Zell-Subpopulationen im ZSF von MS-Patienten untersucht werden.

Parallel dazu wurde die HLA-Restriktion eines TZR, der aus BV1-BJ2.3 und AV7.2-AJ24.2 Ketten besteht, untersucht. Dieser TZR war aus hirninfiltrierenden $CD8^+$ T-Zellen eines MS-Patienten kloniert worden. Eine hohe Anzahl von aktivierten T-Zellen wurden beobachtet, wenn kombinatorischen Peptidbibliotheken verwendet wurden, die zusammen mit *HLA-C*0701*-Molekülen präsentiert wurden. Dieses Ergebnis deutet darauf hin, dass bei diesem MS Patienten *HLA-C*0701*, jedoch nicht die beiden weiteren HLA-Klasse-I-Moleküle des Patienten (*HLA-A*0101* und *HLA-B*0801*) das richtige Antigen-präsentieren, also das spezifische Restriktionselement für den TZR BV1-BJ2.3-AV7.2-AJ24.2 darstellen. Langfristig könnten diese Ergebnisse zum Verständnis der Immunpathogenese von MS und Autoimmunerkrankungen im Allgemeinen beitragen.

Acknowledgements

It is a pleasure to show my sincere gratitude to all who have made invaluable contributions to my research. First and foremost, my deepest gratitude goes to my supervisor **PD Dr. Klaus Dornmair**, for his instructive advice and useful suggestions on my research project. He has participated in all the stages of the preparation of this thesis. Without his generous encouragement and patient guidance, the thesis would not have reached its present form. I have learned a lot from his scientific research thinking and knowledge. At the same time, I am also grateful to **Prof. Reinhard Hohlfeld** for his scientific advice to my research, and how to be a real scientist in the future. Next, I would like to thank **China Scholarship Council (CSC)** for their generous financial supporting and the opportunity to have the advanced studies at the Ludwig Maximilians University of Munich in Germany.

I am also thankful to be a member of this wonderful group. I would like to thank two outstanding colleagues, **Dr. Kathrin Held** and **Dr. Eduardo Beltran**, who help me a lot no matter the life in Germany or how to get along with the workmates. Meanwhile, I would like to give my great appreciation to a nice person, **Aline Plappert**, who is the first friend since I came to Germany, and always help me to solve problems no matter in life or at work. I must thank **Joachim Malotka** and **Ingrid Eiglmeier**, who introduced me the techniques in the lab and provide a great work atmosphere. Many thanks are given to **Simone Brändle**, **Matea Konjevic**, **Geraldine Rühl**, **Dr. Margarete Schönwetter-Steer**, **Reinhard Mentele**, and **Martina Sölch**, who gave me much support in the past four years! We always have a pleasant conversation during the work and fulfilled collaborations through which many projects are connected.

Last but not the least, sincere thanks would go to my beloved family for their understanding and my lovely friends for their kind consideration in the past four years!

It is needless to say that this thesis would not be finished without the great support from any of you!

1 Introduction

1.1 Immune Responses

The environment of human and other mammals is obviously populated by both pathogenic and non-pathogenic microbes, which contains huge amounts of variable toxic or allergenic substances that may threat the normal homeostasis. A host defense against the infection by potential pathogens is defined as immune responses, which are combined with two fronts, the fast and non-specific innate immune response and the antigen-specific adaptive immune response.

1.1.1 Innate Immune Response

When the pathogens encounter the human body for the first time, the innate immune response mounts several physical and chemical barriers against the infection. (i) The complement system is immediately activated to recognize and destroy the foreign organisms, even promote clearance procedures of dead cells or antibody complexes. (ii) Phagocytic white blood cells, like macrophages, neutrophils, and natural killer cells are recruited to the site of infection to ingest and kill microbes by producing some toxic chemicals and degradative enzymes. (iii) Antimicrobial proteins are secreted on the mucosal surfaces to prevent microbes from entering the body. Innate immune responses occur quickly upon exposure to an infectious organism; however, they do not lead a lasting immunity against virus or bacteria-derived pathogens.

1.1.2 Adaptive Immune Response

Unlike innate defense mechanisms, the adaptive immune response is capable of eliminating infections more efficiently because of the accurately specific recognizing functions of lymphocytes. These cells can recognize and respond to particular antigens through the highly specialized antigen receptors presented on the surface of lymphocytes. After the original infection is eliminated, the activated lymphocytes and secreted antibodies can be persisted in the human body even for many years, which

allow another faster and more intense response when a second infection will happen. Therefore, the adaptive immune response is more efficient than the innate immune response against the specific pathogens. The adaptive immune system contains two branches: one is humoral immunity mediated by B cells and their antibodies, and the other is cellular immunity mediated by $CD8^+$ T cells and $CD4^+$ T cells.

The immune response, mediated by antibodies, complement proteins, and antimicrobial peptides in the extracellular fluids, is termed as humoral immunity. B lymphocytes are the main immune cells involved in the humoral immune responses. Naïve B cells can be activated and differentiated into plasma cells that produce and secrete antibodies to kill the specific soluble antigens. Meanwhile, some naïve B cells may develop into memory B cells that will quickly lead to an immune response against the reinfection by the same antigens in a long-lasting immunity. Moreover, B cells serve as professional APCs to recognize and present the pathogenic antigens to cytotoxic T cells.

Once pathogens have entered the infected cells, antibodies in the extracellular fluid are not capable of encountering and even eliminating them. However, another significant immune response mediated by T lymphocytes will be triggered. T cells are capable of detecting peptide antigens derived from different types of pathogens. Peptide antigens derived from intracellular pathogens in the cytoplasm are transferred to the surface with major histocompatibility complex (MHC) class I molecules and recognized by $CD8^+$ T lymphocytes. These $CD8^+$ T cells will differentiate into cytotoxic T cells (CTLs) that release a series of cytotoxins and proteases (such as perforin granulysin, and granzyme) to kill the target cells. However, peptide antigens derived from bacteria or toxins are carried to the cell surface by MHC class II molecules and presented to $CD4^+$ T cells. These T cells further differentiate into subtypes of effector T cells, termed as T helper 1 (Th1) and T helper 2 (Th2). Th1 cells can not only exclusively induce B cells to produce IgG antibodies that effectively opsonize extracellular pathogens, but also efficiently activate the phagocytosis of macrophages to engulf the infected cells. Cytokine interleukin-4 (IL-4) secreted by Th2 cells can stimulate naïve antigen-specific B cells to produce IgM antibodies acting on the humoral immune response. The highly specialized dendritic

cells (DCs) are the most important APCs during the activation of naïve T cells. They can present pathogenic antigens to the effector T cells to trigger the adaptive immune response.

1.2 $CD8^+$ T cells and Their Receptor Complex

$CD8^+$ T cells, also called as killer T cells, are indispensable warriors of the adaptive immune system for protecting the human body from infection and attacks of tumors, viruses (and other pathogens). The specific antigen is loaded onto MHC class I molecule and brought to the surface of the infected cell, which will be recognized by the specific TCR expressed on $CD8^+$ T cell. There are three major mechanisms involved in the cytotoxicity of $CD8^+$ T cells, which are (i) the secretion of cytokines (such as Tumor necrosis factor alpha (TNF-α) and Interferon gamma (INF-γ)), (ii) the production and release of cytotoxic granules (such as perforin and granzyme), which kill the target cells, and, (iii), the destruction of the infected cell directly by Fas/FasL interactions.

1.2.1 **Diversity of TCR Gene Rearrangement**

The genes coding for different chains of T-cell receptor are composed of numerous and intermittent segments that are rearranged somatically to produce heterodimeric TCR, either αβ-chains (90% - 95% of T cells) or γδ-chains (5% - 10% of T cells). Most of the $CD8^+$ T cells express αβ-TCRs. Because of the hypervariety of pathogenic antigens recognized by $CD8^+$ T cells, rearrangement of αβ-TCRs generates various antigen recognition sites in the binding grooves of the variable domains. The rearrangement of TCR gene segments occurs during the development of T lymphocytes in the thymus and is similar to that of immunoglobulin gene segments. After gene rearrangement, TCR α- and β-chains both consist of a variable (V) amino-terminal region, a jointing (J) and a constant (C) gene segments whereas a diversity (D) gene element is exclusively included in TCR β-chain. The rearrangement of αβ-heterodimer of TCR is shown in Figure 1-1 (A).

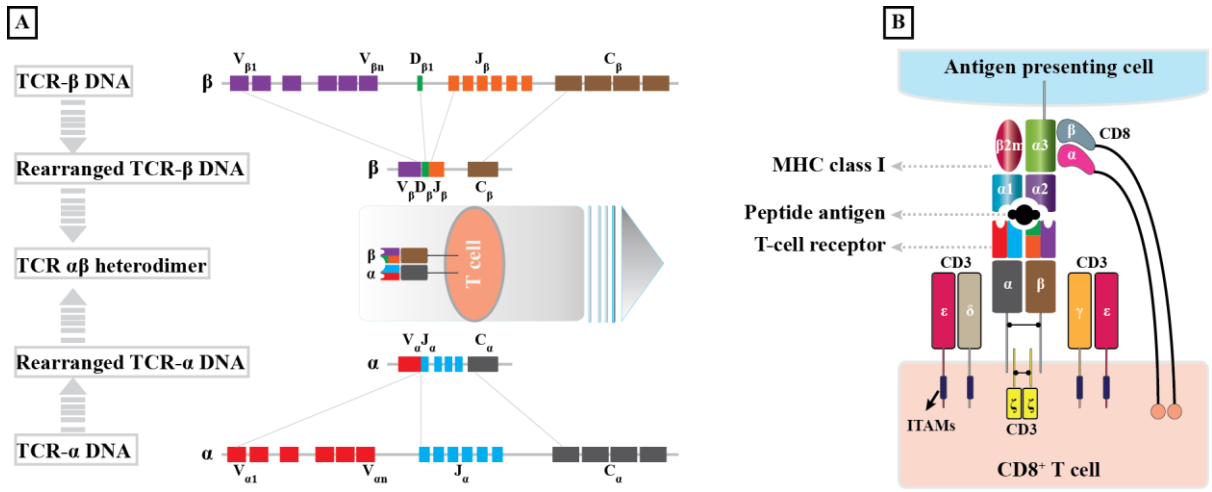

Figure 1-1: TCR gene recombination and the formation of TCR-pMHC I complex

(A) Rearrangement of TCR α/β gene locus. Human TCR β gene locus contains a combination of the variable (V), diversity (D), jointing (J) and constant (C) gene segments as same as the components of TCR α gene locus missing D gene segments. The rearrangement of Vβ, Dβ, as well as Jβ gene segments, generates a functional VnDnJ-region exon that is transcribed and spliced to connect Cβ gene segment. After mRNA translation, TCR β-chain is yielded. TCR α gene locus is rearranged in the same way, and then TCR αβ heterodimer is synthesized and expressed on the surface of T cells. **(B)** Structure of a T cell receptor-peptide-bound major histocompatibility complex (TCR–pMHC). TCR-CD3 complex contains the TCR heterodimer (TCR α-and β-chains) and CD3 molecule that binds to the immunoreceptor tyrosine-based activation motifs (ITAMs) for intracellular cell signaling. CDR3 regions bound to antigenic peptide (black) presented by MHC class I molecule (consisting of three domains: α1-α3 and beta-2 microglobulin) are associated with CD8 dimer on the surface of $CD8^+$ T cell. (Modified from Woodsworth et al., 2013)

The rearrangement of TCR β-chain begins with a random combination of a Vβ- and Dβ-segments that is then added to a Jβ-segment. To enhance the diversity of TCR, the hypervariable nucleotide sequence, N(D)N, is formed by the insertion or deletion of palindromic (P) or non-germline (N) nucleotides at the junctions between the V, D (only in TCR β-chains) and J gene segments. After transcription to mRNA, the V(D)J segments are connected to the Cβ-segment by splicing. Meanwhile, TCR α-chain is produced by the junction of a Vα- and Jα-segments followed by a Cα-segment. TCR α- or β-chain contains three hypervariable complementarity determining regions (CDRs) located in the variable domain termed as CDR1, CDR2, and CDR3. CDR1 and CDR2 are considered to interact with the MHC complex, however, CDR3 encoded by the hypervariable N(D)N nucleotides is the main CDR responsible for the formation of the antigen-binding site and antigen recognition.

1.2.2 **Structure and Function of TCR-CD3 Complex**

Majority of $CD8^+$ T cells express the TCR heterodimer that consists of two transmembrane glycoprotein chains, i.e., α- and β-chains. Both two chains are linked by a disulfide bond. For better antigen recognition and intracellular signal transduction, a set of proteins are also included in the TCR complex (Figure 1-1, B). (i) CD8 is a transmembrane glycoprotein, which is predominantly expressed on the surface of cytotoxic and effector T cells. It contains α- and β-chains and exclusively binds the class I MHC molecule. The interaction of CD8 and class I MHC complex increases the connection between TCR and its target cell for antigen recognition. (ii) CD3 is a group of non-polymorphic signaling molecules, which is made up of one γ and δ as well as two ε and ζ molecules. These molecules can assist TCR to transmit an intracellular signal when the TCR binds a peptide-bound major histocompatibility complex (pMHC). The intracellular domains of CD3 molecules contain several copies of a sequence motif termed as Immunoreceptor Tyrosine-based Activation Motifs (ITAMs) that serve either as tyrosine kinase substrates or as binding sites for SH2 domains of other kinases after phosphorylation. However, the precise molecular mechanism underlying this highly modified complex is still not completely identified. The TCR-CD3 complex could promote a series of signaling cascades driving the activation of the nuclear factor of activated T cells (NFAT), which in turn facilitates expression of activation-associated molecules such as interleukin-2 (IL-2). In addition, NFAT-dependent promoters can be used as a reporter protein for detection of TCR activation.

1.3 Antigen Recognition by $CD8^+$ T Cells

Major histocompatibility complex molecules in human, also named as human leukocyte antigen (HLA), is a set of cell surface proteins essentially for presenting the pathogenic peptide to its counterpart T lymphocyte. Typical MHC molecules are divided into two subgroups: MHC class I and MHC class II. MHC class I molecule is composed of three domains-α1, α2 and α3, interacting with a unit of the non-MHC molecule β2 microglobulin (β2M) that can specifically be recognized by $CD8^+$ T cells (Figure 1-1, B). Because any nucleated cells can be infected by viruses, almost all such cells could express class I MHC molecules. A crystal structure of TCR-pMHC complex is shown in Figure 1-2. On the contrary, class II MHC molecules are composed of two α- and β-chains of almost the same size. Each chain has a conserved region (α2, β2) and a variable peptide-binding domain (α1, β1). The latter two domains could specifically be recognized by $CD4^+$ T cells. Only professional APCs (e.g., B lymphocytes, dendritic cells and macrophages) express class II MHC molecules to present antigens to effector $CD4^+$ T cells. Because of more than 10,000 of variant alleles located at class I and class II *loci* according to the IMGT-HLA database (latest updated in July 2014), an individual generally possesses three different class I MHC molecules (e.g., HLA-A, -B, -C) as well as three class II MHC molecules (e.g., HLA-DP, -DQ, -DR). However, because of the MHC polymorphism and the codominant expression of MHC gene locus, MHC molecules express on almost all nucleated cells. Therefore, almost every person is heterozygous at MHC *loci*, except for some specific cases that same alleles are shown in the corresponding MHC locus on both homologous chromosomes (Table 2-13).

$CD8^+$ T cells specifically recognize short linear antigenic peptide with about 8-10 amino acids presented by class I MHC molecules. The antigenic peptide is digested by the proteasome in the cytosol and then translocated into the lumen of the endoplasmic reticulum (ER) accomplished by the transporter associated with antigen processing transporter (TAP). Then the peptide-loading process will proceed in the lumen of ER with the help of a large multimeric protein complex consisting of TAP, tapasin, calreticulin, calnexin, and Erp57. Once the correct peptide is loaded onto the MHC class I molecule, the MHC-peptide complex is dissociated from ER and translocated via the Golgi apparatus

to the cellular surface. In addition, to bind a particular MHC molecule, the peptide has the same or similar amino acid residues at two or three particular positions in the antigen binding sites of peptide sequence. They are the specific amino acids named as “anchor positions” or “anchor residues”. These “anchor residues” can enhance the interactions between antigenic peptide and MHC molecule. In addition, T cells can recognize the “non-self” antigens in the presence of self-MHC molecules. If the auto-antigens are recognized, MHC restriction can prevent T cells from an autoimmune response against host tissues.

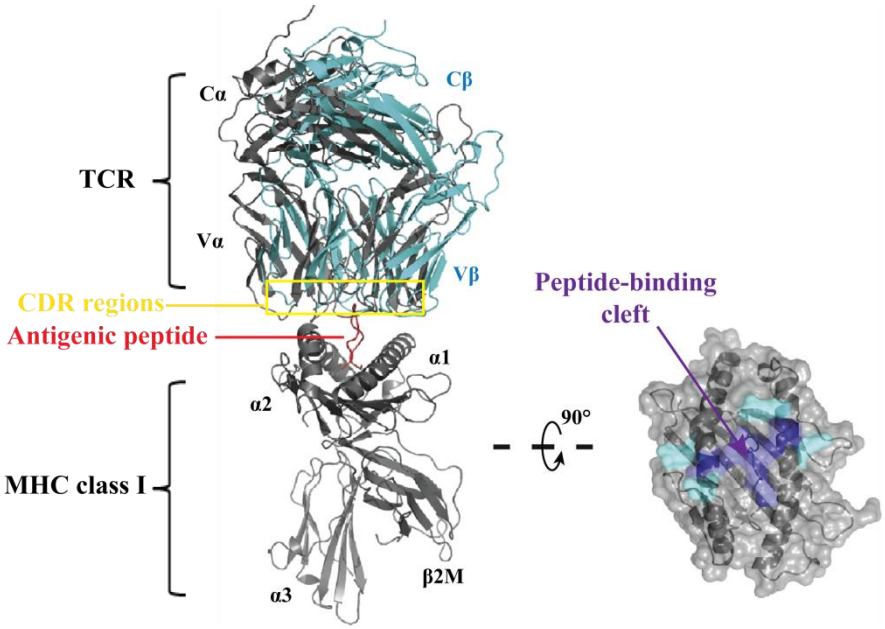

Figure 1-2: Crystal structure of a TCR–pMHC complex

Side (left) and aerial (right) view of a αβ-TCR molecule in complex with an MHC class I molecule that expresses the antigenic peptide (colored in red). The MHC class I molecule (colored in gray) contains α1, α2, and α3 domains as well as a β2M molecule, in which the α1 and α2 domains contact the antigen, while the α3 domain is associated with β2M. The TCR consists of one α-chain (colored in black) and one β-chain (colored in cyan), in which the CDR regions (in the frame) of the two TCR chains interact with the antigenic peptide. The surface depiction of the pMHC from an aerial view is presented on the right. The peptide-bind cleft formed between α1 and α2 domains of MHC is colored in blue, at which the antigenic peptide binds to the MHC molecule. (modified from Kass et al., 2014)

1.4 Positive and Negative Section of T Cells in Thymus

After the TCR α- and β-chains are successfully rearranged the T cells need to undergo positive and negative selection before leaving the thymus. The further development of $CD4^+$ and $CD8^+$ T cells in the thymus is vital for the proper recognition of foreign antigens presented by the self-HLA molecules and preventing the autoimmunity (Sprent et al., 1988).

Positive selection occurs in the thymic cortex, where the double-positive thymocytes ($CD4^+CD8^+$) are presented with self-antigens binding to self-MHC molecules on the surface of thymic cortical epithelial cells (Nikolic-Zugic and Bevan, 1990). Only those thymocytes capable of interacting with MHC molecules appropriately, i.e., not too high affinity or no affinity, will survive and continue with the negative selection in the medulla of the thymus. On the contrary, all that do not or strongly interact with MHC class I or II molecule will be destroyed. In this stage, MHC restriction decides the differentiation of $CD4^+$ and the $CD8^+$ T cell lineage (Zerrahn et al., 1997). However, this process can not eliminate those thymocytes that may arise an autoimmune attack on the body.

In the process of negative selection, T cells that react strongly with a self-antigen presented on the self-MHC complex of medullary thymic epithelial cells are deleted in the thymus (Hinterberger et al., 2010). These auto-recognized T cells die by apoptosis. The remaining thymocytes exit the thymus and become matured naïve T cells, which will differentiate into $CD4^+$ T helper cells or $CD8^+$ T killer cells when encountering their specific pathogens. As an important aspect of central tolerance (Griesemer et al., 2010), this process can effectively prevent the formation of autoreactive T cells that might induce autoimmune diseases, such as multiple sclerosis.

Therefore, more than 95% of precursor T cells are eliminated with these two mechanisms. The self-MHC restricted, self-tolerant, and single positive T cells can enter into the peripheral blood and lymphoid system (Starr et al., 2003). Otherwise, once the T cells escape the two mechanisms and develop into self-reactive T cells, an autoimmune disease occurs (Section 1.4).

1.5 Autoimmunity and Autoimmune Disease

If the antibodies and immune cells target the body's healthy tissues, an autoimmune reaction will occur. The immune response against "self"-antigens is termed as autoimmunity, and the disease caused by such exceptional immune response is an autoimmune disease. The significant syndrome of an autoimmune disease is inflammation, and is often restricted to certain organs of the body. When an autoimmune attack occurs only in a specific organ like muscle, this is the case of Myositis, in which autoreactive T cells attack the muscle fibers and lead to a chronic inflammation of muscle (Mantegazza et al., 1993). An example on an autoimmune attack that targets different organs like the joints, heart, kidneys, liver, lung and skin, Systemic lupus erythematosus (SLE), might be mediated by anti-DNA antibodies (Diamond et al., 1992). So far, the loss of immune tolerance leading to autoimmune diseases and the underlying immunopathogenesis are not well understood.

1.6 Multiple Sclerosis

Multiple sclerosis is a chronic inflammatory disorder of the CNS. Its hallmarks are demyelination in the CNS, oligoclonal bands in the CSF, and the infiltration of T cells in the brain parenchyma. After entering the CNS from the peripheral circulation via a disrupted blood-brain barrier (BBB), the T cells will induce an inflammatory cascade that results in the infiltration of immune cells, multifocal inflammatory demyelination, and axonal loss (Hohlfeld et al., 2016). Such inflammatory episodes occur with unpredictable intervals usually last days to months. Relapses and remissions may happen during the patient's whole lifetime. The disease was firstly systematically defined by French neurologist Jean-Martin Charcot in the late 19th century (Compston, 1988). Charcot observed that the diagnosis of MS requires the presence of multiple white-matter lesions disseminated in CNS. Based on an investigation in 2013 (Global Burden of Disease Study, 2015), about 2.3 million of people in different regions around the world are still suffered from MS. About 20,000 people died from MS in that year compared to 12,000 in 1990. Moreover, MS patients are mainly diagnosed the limit time at age 20 to 50, and the incidence rate is twice as high in women as in men (Milo and Kahana, 2010).

Currently there are many ways to diagnose the autoimmune diseases, such as magnetic resonance imaging (MRI), CSF analysis, and the recording of evoked potentials (Brownlee et al., 2017). In the diagnosis of MS, increased secretion of intrathecal IgG and its distribution as “oligoclonal bands (OCB)” in the CNS are considered the most significant immunological hallmarks for MS patients (Stangel et al., 2013; Awad et al., 2010). There might be unknown antigens persisting in the CSF, which are recognized by MS-related B cells.

According to the clinical diagnosis, the conventional types of MS patterns are categorized in Figure 1-3, which include relapsing-remitting (RR) MS, secondary progressive (SP) MS, primary progressive (PP) MS, and progressive relapsing (PR) MS (Lublin, 2014). In addition, some patients, who have preclinical MS but may not be examined with a clinical attack by MRI, will experience the clinical attack within five years (Callan et al., 2000; Compston and Coles, 2008). This specific pattern is classified as a “radiologically isolated syndrome” (RIS). The identification for oligoclonal bands of IgG in the CSF of patient with a “clinically isolated syndrome” (CIS) doubles the risk of progression to MS independent of MRI analysis (Marcus and Waubant, 2013).

Several treatments especially for MS, are developed, including immunomodulating therapies specific to autoreactive T and B lymphocytes (Dornmair et al., 2003; Hohlfeld et al., 2008), stem cell transplantation (Uccelli and Mancardi, 2010), anti-inflammatory drugs (Babij and Perumal, 2015), hormonal regulation (Deckx et al., 2013) and vitamin D (Ascherio et al., 2014; Munger et al., 2004). However, some aggressive treatments have the unknown risks for MS patients, which need more experimental evidences with long-term follow-up (Comi et al., 2017; Way and Popko, 2016).

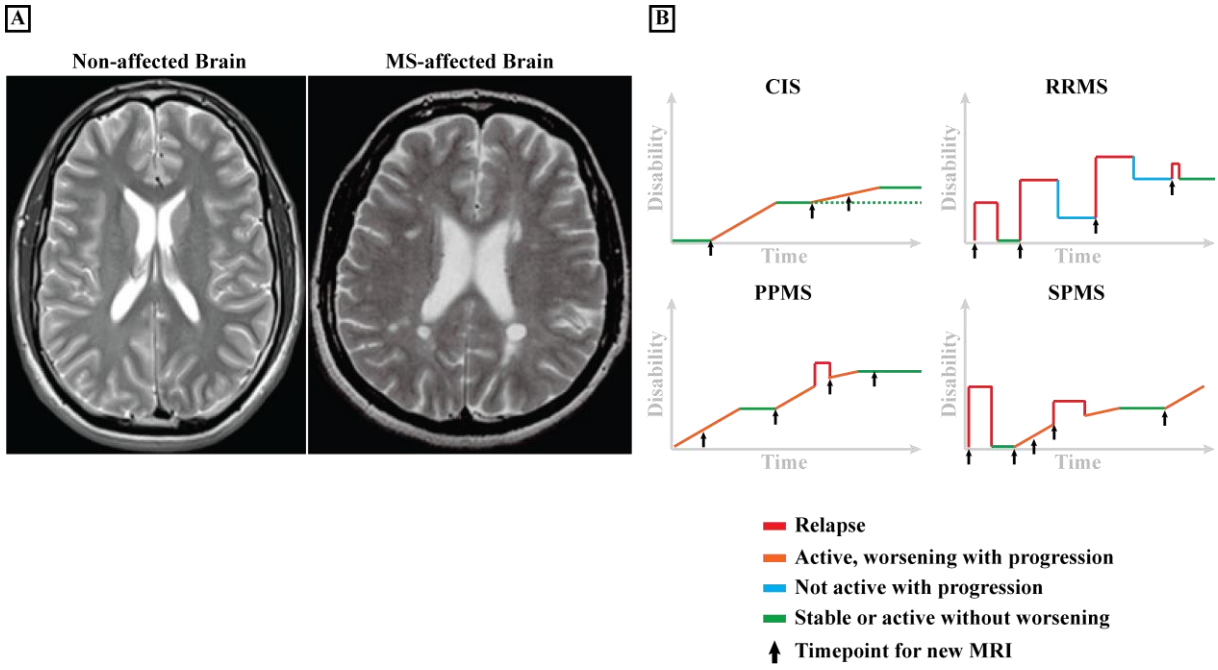

Figure 1-3: Overview of the progress and diagnosis of MS

Diagnosis of MS with MRI displays the difference between healthy and infected brains. **(B)** Four disease courses have been identified in MS: clinically isolated syndrome (CIS), relapsing-remitting MS (RRMS), primary progressive MS (PPMS) and secondary progressive MS (SPMS), according to International Advisory Committee on Clinical Trials of MS in 2013. (The source of MRI pictures came from the website: http://spinms.ca/; and the defining the clinical course of MS was adapted from Lublin et al., 2014)

1.6.1 Pathology and Etiology

During the progress of MS, demyelination is a significant diagnostic criterion to determine an MS lesion, which is not only excluded in the white matter but also extended to the gray matter, particularly in the cortex (Hohlfeld and Wekerle, 2001). Except for demyelination, many somatic immune cells, such as lymphocytes, macrophages, plasma cells and mononuclear cells are accumulated in the perivascular spaces of medium-sized or small veins within a MS plaque (Lassmann et al., 2001). However, the symptoms of MS are variable among different lesions of the same patient as well as different patients. An autoimmune-mediated pathomechanism is indeed involved in the progress of MS (Hohlfeld and Dornmair, 2007). Effective therapeutic tools are developed based on the immune mechanisms of inflammation, demyelination, or remyelination. However, whether the interaction of genetic background and unknown environmental factors will affect the development of MS is still uncertain (Oksenberg et al., 2001; Sawcer et al., 2014).

1.6.2 The Dominant Role of T lymphocytes in MS

The demyelinated plaque is a pathological hallmark of focal white-matter lesions in MS patients. It is characterized by immune cell infiltration. The infiltrates may be composed of T and B lymphocytes as well as macrophages. Moreover, these presumably autoreactive T cells may persist in the blood of MS patient for many years (Skulina et al., 2004). In the T-cell subsets, $CD4^+$ T cells are considered to play a role in the immunopathogenesis of MS (Bielekova et al., 2004). However, more evidences indicate $CD8^+$ T cells might be the main subpopulation within the CNS lesions of MS patients (Friese and Fugger, 2009). These $CD8^+$ T cells are clonally expanded in the brain lesions and in CSF (Babbe et al., 2000; Skulina et al., 2004). One study evaluated that the proportion of $CD8^+$ T cells ranges from 60% in active lesions to more than 85% in its onset of active lesions or inactive plaques (Berthelot et al., 2008; Junker et al., 2007). The presiding T and B cells are still massively outnumbered in the demyelinated patches by macrophages and microglia cells. However, the molecular mechanism of T cells in the underlying immunopathogenesis of MS is not well understood.

1.6.3 Mucosal Associated Invariant T Cells (MAITs) and MS

Human Mucosal-associated invariant T cells (MAITs) are innate-like T-cells that are abundant and comprising 10% of the $CD8^+$ T-cell compartment in blood (Le Bourhis et al., 2011). MAITs are distinguished by a specific expression of a semi-invariant TCR (Vα7.2-Jα33/12/20) and restricted by the evolutionarily conserved MHC Class I related protein (MR1) (Huang et al., 2005). Recent evidence indicates that MAITs might recognize a newly identified class of antigens termed as vitamin B metabolites existing in most bacteria and yeasts (Kjer-Nielsen et al., 2012; Milo and Kahana, 2010; Pellkofer et al., 2009). Except for the bacteria-derived ligand, MAITs can also be activated by Ki67 antigen involved in the inflammatory bowel diseases (Serriari et al., 2014). Although MAITs are developing into the significant players in human immune system, the role of MAIT cells is unapparent so far. The specific antigens recognized by MAITs still need to be investigated.

The connection of MAITs and MS is initially demonstrated by Illes et al., that T populations possessed TCR AV7.2-AJ33 have infiltrated in CNS lesions from MS patients as well as in the peripheral nervous system from a patient with chronic inflammatory demyelinating polyneuropathy (CIDP) (Illes et al., 2004). With the development of MS, the number of MAIT cells in the peripheral blood of MS patients is reduced, especially during the remission and relapse stage of MS (Miyazaki et al., 2011). MAIT cells might be related to the immunopathogenesis of MS. In a previous study (Held et al., 2015), four TCRs are characterized from the brain biopsy of an MS patient, which are consisted of the identical TCR β-chain (Vβ1-Jβ2.3) and four similar TCR α-chains (Figure 1-3). The four α chains contain the common Vα7.2 region but different Jα regions (Jα16, Jα 33, Jα 24, and Jα58) as well as the various sequences covering the CDR3 region. One MS-derived TCR (Vβ1Jβ2.3-Vα7.2Jα33), which carries the typical MAIT TCR (Porcelli et al., 1993; Tilloy et al., 1999), is clonally expanded in the brain of MS patient. The other three α chains are homologous at the peptide level, but they are not carrying the canonical region of MAIT α-chain (Va7.2-Ja33). During the investigation of TCR $V\beta1^+$ T-cell population in active brain lesions of MS patients, they are more related to $V\alpha7.2^+$ α-chains with different Jα regions (Held et al., 2015). Although these T cells show MAIT cell-related features, there is no direct evidence to tell they are MAIT-cell subset or hypervariable $CD8^+$ T-cell repertoire.

	V region	n (D) n	J region	# of cells	Detected in
A. TCR-β chain sequence	Vβ1	C A S S I S G R K D T Q Y F G P G	Jβ2.3	36	Blood; Brain
B. Matching TCR-α chain sequence	Vα7.2	C A V Q E P S G S L T F G E G	Jα58	1	Brain
	Vα7.2	C A V R D S N Y Q L I W G A G	Jα33	7	Brain
	Vα7.2	C A V R D Q A T D S W G K L Q F G A G	Jα24	1	Brain
	Vα7.2	C A V R D N L E L L F A R G	Jα16	6	Blood

CDR3

Homologous

Figure 1-4: Sequences of paired T-cell receptor (TCR) α- and β-chains derived from MS patient

(A) Identical TCR β-chain (Vβ1-Jβ2.3) is identified in the active brain lesion and peripheral blood of MS patient. **(B)** Four homologous TCR α-chains correspond to the same TCR β-chain. Except one α-chain (Vα7.2-Jα16) is expanded in the peripheral blood, the rest three TCR (Vα7.2-Jα58, Vα7.2-Jα33, and Vα7.2-Jα24) are detected in the early active brain lesion. All TCR α-chains contain the identical V-region but different J-region as well as similar CDR3 region (in the green frame) where sequence homologies are found (in the yellow frame). The conserved region of each J segment is underlined. (Modified from Held et al., 2015)

1.7 Identification of Autoreactive T Cells in MS

Autoreactive T cells play a crucial role in the immunopathogenesis of MS. Identification of these T cells might help us to better understand the pathogenic and possible protective mechanisms involved in the development of MS. Except for the classification of the T sub-populations by the glycoproteins (CD4/CD8) on the cell surface and the cytokines (IL-2, IL-4, IL-17, and TNF-γ), the T cells can be characterized by the presence of an antigen-specific TCR on the cell surface. Obviously, the clonally expanded TCRs or monoclonal TCRs are most interesting for the investigation of the immunopathogenesis of T cell-mediated autoimmune diseases. However, because of the short survival of live T cells *in vitro* (Dooms and Abbas, 2002), the research in this direction has been hindered for many years. It is urgent to find a way to distinguish relevant clones from an oligoclonal background *in vivo* (Hofbauer et al., 2003; Matsumoto et al., 2003) and the entire repertoire (~10^{15}) of all possible αβ-TCR heterodimers (Davis and Bjorkman, 1988).

The early studies mainly focus on the analysis of the whole repertoire of TCR β-chain either by restriction fragment length polymorphisms (RFLP) (Beall et al., 1989; Biddison et al., 1989) or by reverse transcription of RNA from brain biopsy of MS patients (Wucherpfennig et al., 1992). However, these methods are not suited for distinguishing paired TCR clones of autoreactive T cells from the bystander cells. Moreover, an *in situ* oligoclonal expanded T cell clone within a biopsy sample can be detected by CDR3-spectratyping analysis (Pannetier et al., 1995), which indicates that characterization of the disease-related TCR β-chains from clonally expanded T cells is available. Recently, monoclonal antibodies are produced to recognize particular variable regions of TCR β-chains (such as Vβ1, Vβ5, and Vβ13), which are used to detect the certain T cells in biopsy samples by immunofluorescence staining. By combining CDR3 spectratyping with immunofluorescence staining method, single T cells of interest are isolated by laser capture microdissection (LCM). Subsequently, the matched TCR α- and β-chains from these single T cells are characterized by clonally specific PCRs (Seitz et al., 2006). In addition, to identify the clonally expanded TCR α- and

β-chains for the autoreactive T cells of MS patients, next generation sequencing (NGS) is more efficient than CDR3-spectratyping on bulk T cell populations (Gerdes et al., 2016; Held et al., 2015).

However, many commercial antibodies to certain Vβ-regions are unavailable. Therefore, the entire TCR β-chain repertoire can not be analyzed. Moreover, because TCR α-chain genes are more variable than β-chain genes (Lefranc and Lefranc, 2001), and because very rarely anti-α-chain antibodies are available for immunofluorescence staining (Dornmair et al., 2009), detection of TCR α-chains had been more difficult than β-chains. Thus, an "unbiased approach" was established to overcome this obstacle (Seitz et al., 2006). This approach was based on firstly detecting the V element of the β chain by an antibody, secondly amplifying the entire VnDnJ region of β chain by multiplex RT-PCR using a Vβ specific primer, and thirdly amplifying the corresponding α chain using a set of α-chain primers that cover the entire α repertoire. Later, a primer-set was developed that could determine the matched TCR αβ-chains from any single T cell of interest without prior knowledge of their particular TRAV or TRBV usage (Kim et al., 2012). The activated T cells accumulate in the distinct lesions of MS brain, which are possibly considered autoreactive T cells. These T cells of interest could be detected by the commercial antibodies against a common T cell marker and an activation marker, which might have a close contact to an APC or target cell.

1.8 Characterization of Specific Antigens of TCR in MS

The identification of antigenic peptides derived from the processing of antigenic protein is an essential step in understanding the pathogenesis of such diverse processes as the response to infectious agents, and the immune surveillance of cancer as well as autoimmune diseases. So far, several approaches were developed to determine the possible antigens of TCRs. The recognition of candidate antigens, such as viruses, experimental autoimmune encephalomyelitis (EAE)-related glycoproteins (e.g., Myelin basic protein and Myelin basic protein), could be tested (Hohlfeld et al., 2015; Hohlfeld et al., 2016). A report indicates that soluble TCR molecules may recognize the randomized peptide libraries expressed by insect cells (Crawford et al., 2006). However, this approach is limited by the low affinity

of TCRs to their MHC-peptide complex and by rare appropriate HLA-matched APCs from MS patients. Another approach is to use the patient-derived full-length complementary DNA (cDNA) libraries to identify the potential antigens from tumors (Boon et al., 2006; Van Der Bruggen et al., 2002; Wong et al., 1999). However, the cDNA library should contain the full-length in-frame cDNA originated from affected tissue, which is not always available *in vitro*. Besides, correct antigen processing machinery is necessary for the screening of cDNA library (Vyas et al., 2008). Moreover, using the 'motif-recognition' properties of TCR molecules, synthetic combinatorial peptide libraries were established to screen the antigenic peptide in quantitative terms (Zhao et al., 2001). In the chronic Lyme disease, a report indicates that the potentially relevant antigens are recognized both by $CD4^+$ T cells from the host and by *Borrelia burgdorferi* (Hemmer et al., 1999). Nevertheless, the antigenic peptide is highly diluted by many irrelevant bystander peptides in the library and incapable of recovery by cloning. Because of these reasons, very rarely specific antigens of human T cells have been characterized so far.

Therefore, a new strategy was developed to overcome the requirement for accurate antigen processing. This approach is based on the plasmid-encoded combinatorial peptide libraries (PECP), through which mimotopes might be identified (Siewert et al., 2012). The schematic overview of this antigen search technology is illustrated in Figure 1-5. In detail, COS-7 cells served as APCs are co-transfected with plasmids encoding the patient's HLA class I alleles and the plasmids coding PECP libraries consisted of short peptides with random sequences but defined lengths. Simultaneously, $58^{-/-}$ T hybridoma cells, a variant cell line of the DO-11.10.7 mouse T hybridoma that does not express TCR α/β chains (Letourneur and Malissen, 1989), are used to generate the functional T cells which can express the putatively disease-related TCR, human CD8, and green fluorescent protein (sGFP) under the control of the NFAT promoter. After the co-culturing of T hybridoma cells together with transfected COS-7 cells, the activated T hybridoma cells will turn to green under the fluorescence microscope, and the underlying positive APC can be isolated by micromanipulation. One problem is that some 58 cells turn green spontaneously for unknown reasons (Section 3.5.2 and 4.5.1). Due to spontaneous Ca^{2+} influx,

the spontaneous activation is observed in T cells (Kawakami, 2016). To minimize the spontaneous activation, T hybridoma cell clones that show minimal activation spontaneously should be selected by sub-cloning. Moreover, these cells should be in good condition during antigen search experiments (Section 4.5.1). Subsequently, the potential antigen-coding plasmid will be identifed by subcloning with several rounds of plasmids enrichment by *E.coli* culture (Siewert et al., 2012).

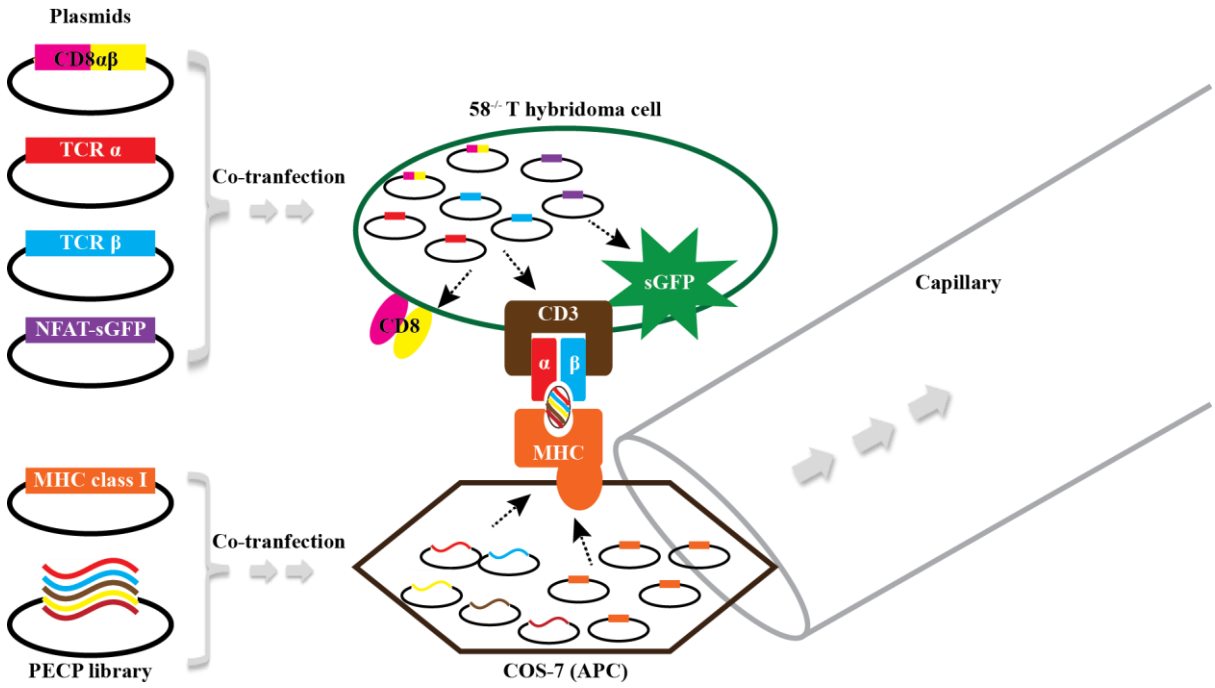

Figure 1-5: Overview of an approach for antigen identification from putatively disease-related TCR molecules

The experimental strategy is based on the PECP library (multi-colored lines) that is con-transfected with appropriate HLA molecule (MHC class I, orange) into COS-7 as an APC. With the help of large T antigen on the plasmids, intracellular plasmids are amplified and candidate antigen (pMHC complexes) is presented on the surface of COS-7 cell. At the same time, TCR-deficient mouse T hybridoma cells $58^{-/-}$ cell as a detector is stably transfected with plasmids coding for a putatively disease-related TCR (α-chain: red; β-chain: blue) and human CD8 molecule (α-chain: magenta; β-chain: yellow) as well as sGFP reporter protein under the control of the NFAT promoter (purple). Once the TCR binds the correct antigenic peptide (multi-color) presented by the suitable MHC molecules, the T hybridoma cells will be activated and fluorescent green and the underlying APC will be isolated with the help of a capillary, which is then employed for the recovery of antigen coding plasmids. (Modified from Siewert et al., 2012)

1.9 Objectives

Although high numbers of $CD8^+$ T cells are infiltrating the brain lesions and give a great risk to proliferate into clonally expanded sub-populations, the identity and the mimicry reaction of $CD8^+$ T cells involved in the immunopathogenesis of MS are still not known. Recent evidence indicates the predomination of brain-infiltrating $CD8^+$ T cells over the other immune cells such as $CD4^+$ T cells and macrophages in MS lesions (Babbe et al., 2000). Moreover, it is also of interest to determine their target cells in MS lesions, which might help us to understand the antigen presenting process and the recognition of autoantigens by the autoreactive $CD8^+$ T cells. To characterize the clonally expanded $CD8^+$ T cells and their presumed antigenic mimotopes from MS patients, six objectives will be accomplished in the thesis as followed:

i. Immunolocalization of immune cells infiltrated in the active brain lesions of MS patients;
ii. Identification of single activated $CD8^+$ T cells in the active brain lesions of MS patients, and the cells interacting with those $CD8^+$ T cells;
iii. Microdissection of these single T cells with sufficient RNA preservation;
iv. Optimization of the "unbiased method" to obtain the high yield of paired αβ-TCRs from these T cells;
v. Application of the improved protocol for the single T cell analysis on clonally expanded T cells from brain and CSF samples of MS patients;
vi. Searching for antigenic peptides of certain TCR molecules by screening of unbiased plasmid encoded peptide libraries.

2 Materials and Methods

2.1 Materials

2.1.1 Devices

Table 2-1 presents the devices used for the experiments.

Table 2-1: List of devices

Name	Model	Company
Bacteria shaker	Innova® 44	New Brunswick Scientific
Centrifuge	Avanti® JXN-26	Beckman Coulter
	Centrifuge 5417 R	Eppendorf
	Heraeus® Multifuge X3R	Thermo Fisher Scientific
	Optima L-90K	Beckman Coulter
Class 2 microbiological safety cabinet	FlowSafe® B-[MaxPro]²- 130/160	Berner
CO_2 Incubator	Galaxy® 170 S/R	New Brunswick Scientific
Cryostat	CM3050 S	Leica System
Electroporator	Gene Pulser	Bio-Rad
Flow Cytometer	FACS Calibur	Becton Dickinson
Fridge and Freezer	KP 3120 Comfort	Liebherr
	TP 1410 Comfort	Liebherr
	GNP 1066 Premium NoFrost	Liebherr
	GNP 3013 Comfort NoFrost	Liebherr
	HERAfreeze® HFU T Series -86°C	Thermo Fisher Scientific
	Innova® U725 Upright -86°C	New Brunswick Scientific
Gel Documentation	AlphaImage DE500	Alpha Innotech
Gel Electrophoresis	Power supply: LKB ECPS	Pharmacia
Microbiological Incubators	BD 115	Binder
Microscopes and accessories	Axioplan 2	Zeiss
	AxioVert 25	
	AxioVert 200M	
	Robo-Mover	P.A.L.M. Microlaser Technologies
	Microinjector CellTram Vario	Eppendorf
	Micromanipulator LN25 Mini	Luigs und Neumann
4D-Nucleofector™ X unit	AAF-1002X	lonza
PCR Cyclers	GeneAmp PCR System 9600	Perkin Elmer
	Mastercycler® Gradient Thermal Cycler	Eppendorf
	Mastercycler® pro	
	TC-E-48DA	Genetouch
pH-meter	S20 SevenEasy™ pH	Mettler Toledo
RNA Quality Analysis	2100 Bioanalyzer	Agilent
Spectrophotometers	Nanodrop ND-2000	Thermo Fisher Scientific
	UV-1600PC	VWR
Thermomixer	Comfort 25436	Eppendorf
Water Bath Incubation	1002-1013	GFL
Water Purification System	Milli-Q® Reference	Millipore

2.1.2 Consumables and Chemicals

The general consumables, such as pipette tips, centrifugation tubes, graduated pipettes and cell culture materials, were purchased from the Biozym, BD Falcon, Nunc, and Corning, respectively. The sterile DNase/RNase-free centrifugation tubes and polypropylene pipette tips were bought from Biozym. They are particular to minimize the adsorption of nucleic acids and proteins. Unless otherwise mentioned, all the chemicals were obtained from companies BD Falcon or Sigma-Aldrich.

2.1.3 Chemical kits and specific reagents

Table 2-2 presents the chemical kits and specific reagents used for the experiments.

Table 2-2: List of chemical kits and specific reagents

Name	Company	Application
Agilent RNA 6000 Pico Kit	Agilent	RNA quality analysis
Amersham Cy3 mAb Labelling Kit	GE Healthcare	Antibody label
Anti-Mouse IgG2a+b MicroBeads Kit	MACS	Cell isolation
Anti-PE MicroBeads UltraPure Kit	MACS	Cell isolation
Bovine Serum Albumin solution	Sigma-Aldrich	A blocking agent
CD3 Microbeads Kit	MACS	Cell isolation
DAPI	Sigma-Aldrich	Nucleic acid staining
dNTP (10 mM each)	Qiagen	PCR
FuGENE® HD Transfection Reagent	Promega	Plasmid transfection
Glycogen (20 mg/ml)	Roche	Precipitation of nucleic acids
Hispeed Plasmid Maxi Kit	Qiagen	Plasmid purification from Bacteria
HistoGene™ LCM Immunofluorescence Staining Kit	Arcturus	IHC
iProof™ High-Fidelity Master Mix (2×)	Bio-Rad	Plasmid recovery PCR
MiniElute® Gel Extraction Kit	Qiagen	DNA purification from agarose gels
OneStep RT-PCR Kit	Qiagen	Single cell PCR
Pan T Cell Isolation Kit	MACS	Cell isolation
pcDNA3.1™ Directional TOPO® Expression Vector Kit	Invitrogen	Cloning of PCR products
PCR Buffer (10×)	Roche	PCR
Pellet Paint® Co-Precipitant	Millipore	DNA precipitation
peqGOLD 50 bp DNA-ladder	Peqlab	DNA ruler
peqGREEN DNA/RNA dye	Peqlab	Dye of Nucleic Acid
PicoPure™ RNA Isolation Kit	Life Technologies	RNA purification
Propidium iodide	Sigma-Aldrich	Staining of dead cell
Protector RNase Inhibitor	Roche	Single cell PCR
Protein Block Serum-Free	Dako	IHC
QIAprep® Spin Miniprep Kit	Qiagen	Plasmid isolation
QIAquick® Gel Extraction Kit	Qiagen	DNA purification from agarose gels
QIAquick® PCR Purification Kit	Qiagen	PCR products purification
Random Primers	Invitrogen	RT-PCR
RNase OUT™ Recombinant Ribonuclease Inhibitor	Invitrogen	Single cell PCR
RNeasy® Mini Kit	Qiagen	RNA purification
Sodium Acetate (3 M, pH=5.2)	Millipore	DNA precipitation
Taq-DNA-Polymerase (5 U/µl)	Roche	Single cell PCR
TOPO TA Cloning® Kit	Life Technologies	Cloning of PCR products
ToPro®-3 Iodide 642/661 (1 mM)	Invitrogen	Staining of dead cell
TRIzol® RNA Isolation Reagents	Invitrogen	Isolation of total RNA
Trypan Blue solution (0.4%)	Sigma-Aldrich	Staining of dead cell
Trypsin-EDTA solution	Sigma-Aldrich	Trypsinization of Adherent cells

2.1.4 **Buffers, Mediums, and Solutions**

Table 2-3 shows the buffers, medium and solutions used for the experiments.

Table 2-3: List of buffers, medium, and solutions

Name	Chemical composition	
Cell freezing medium	10% (v/v)	DMSO
		FBS Superior
DNA loading buffer (6×)	30% (v/v)	Glycerol
	0.25% (w/v)	Bromophenol blue
	0.25% (w/v)	Xylene cyanol FF
DEPC treated water	Dissolve 0.1% diethylpyrocarbonate (DEPC) in H_2O; incubate at room temperature overnight, autoclave.	
FACS buffer	1% (v/v)	FBS Superior
		PBS (1×, pH=7.4)
LB^{amp} medium (pH=7.0)	1% (w/v)	NaCl
	1% (w/v)	Tryptone
	0.5% (w/v)	Yeast extract
	5 N	NaOH (adjust the pH)
	0.14 mM	Ampicillin
		RNase-free H_2O
LB^{amp} plate	1.5% (w/v)	Bacto agar
	0.14 mM	Ampicillin
		LB medium (pH=7.0)
MACS buffer	0.5%	Bovine Serum Albumin (BSA)
	2 mM	EDTA (disodium salt)
		PBS (1×, pH=7.2)
PBS buffer (10×, pH=7.4)	1.37 M	NaCl
	27 mM	KCl
	100 mM	Na_2HPO_4
	18 mM	KH_2PO_4
		RNase-free H_2O
S.O.C. Medium	2%	Tryptone
	0.5%	Yeast Extract
	10 mM	NaCl
	2.5 mM	KCl
	10 mM	$MgCl_2$
	10 mM	$MgSO_4$
	20 mM	Glucose
TBE electrophoresis buffer (10×)	1 M	Tris base
	1 M	Boric acid
	0.02 M	EDTA (disodium salt)
		RNase-free H_2O
Tissue blocking buffer	1% (w/v)	BSA
	0.1% (w/v)	Cold fish skin gelatin
	0.5% (w/v)	Triton X-100
	0.05% (w/v)	Sodium aside
	0.01 M	PBS (1×, pH=7.4)
Trypan Blue solution (0.04%)	10% (v/v)	Trypan Blue solution (0.4%)
		PBS (1×, pH=7.4)
RPMI-1640/complete	500 ml	RPMI-1640 Medium
	10% (v/v)	FBS Superior
	100 U/ml	Penicillin (10,000 U/ml)
	100 µg/ml	Streptomycin (10,000 µg/ml)
	1 mM	Sodium Pyruvate (100 mM)
	2 mM	L-Glutamine
	1×	MEM Non-essential Amino Acid Solution (100×)

2.1.5 **Primers**

All the primers used in this thesis were synthesized and HPLC-purified by Metabion. The final concentration of them is 100 μM. Primers designated with "for" (forward primer) elongate the coding strand and primers designated with "rev" (reverse primer) extend the non-coding strand of DNA. The appendages "out" or "in" refer to the position of primers in nested PCRs. To avoid cross-contaminations, we separated the primers in small volume aliquots and stored them at -20°C. Table 2-4 to 2-8 present the nucleotide sequences of primers and their specificity. The primers designed for the variable regions of the TCR α- and β-chains are named according to the Arden nomenclature (Arden et al., 1995). The reverse primers (Cβ-mid3 and Cβ-mid4) and the anchor primers (UP_{new}, $VP1^{+}_{new}$ to $VP9^{+}_{new}$) are newly designed during the thesis, but all the rest primers were created by Katherina Siewert, Sabine Seitz, and Song-Min Kim (Kim et al., 2012; Seitz et al., 2006; Siewert et al., 2012). Primer "UP_{new}" is modified from primer "UP" without the first two nucleotides, and primers "$VP1^{+}_{new}$ to $VP9^{+}_{new}$" are designed to add the new anchor primer "UP_{new}" to 5-end of primers "VP1 to VP9". The formula $T_m = 4(G + C) + 2(A + T)$ is used to calculate melting temperature (T_m) of all oligonucleotide primers mentioned in the thesis.

Table 2-4: Primers used for reverse transcription (RT) reaction of single T cells

The first three reverse primers were designed by Sabine Seitz (Seitz et al., 2006) and the latter two primers were created by Song-Min Kim (Kim et al., 2012).

Name	Specificity	Nucleotide sequence (5'→3')
Cα-RT-imp	Cα	GCCACAGCACTGTTGC
Cβ-RT	Cβ	GAAGAAGCCTGTGGCC
Cβ-RT-2	Cβ	GWAGAAGCCTGTGGCC
Cα-out	Cα	GCAGACAGACTTGTCACTGG
Cβ-out	Cβ	TGGTCGGGGWAGAAGCCTGTG

Table 2-5: Primers used for specific amplification of TCR β-chain of single T cells

All primers VP1 to VP9 are synthesized with an "UP_{new}" sequence at their 5'-end (termed as $VP1^{+}$ to $VP9^{+}$). Nucleotides exchanges (underlined) are introduced here to avoid primer interactions. Degenerate primers contain bold red letters to indicate nucleotide exchanges. VP1 to VP9, Cβ-in and anchor primer (UP) were designed by Song-Min Kim (Kim et al., 2012).

Name	Vβ specificity	Nucleotide sequence (5'→3')
VP1	1, 5, 16, 17, 23	T**S**Y**T**TTGTCTCCTGGGAGCA
VP2	22, 25	CCTGAAGTCGCCCAGACTCC
VP3	18, 24	GTCATSCAGAACCCAAGA**Y**ACC
VP4	2, 4	GG**W**TATCTGT**M**AG**M**GTGGAACCTC
VP5	3, 11, 12, 13, 14, 15	ATGTACTGGTATCGACAAGA**Y**C
VP6	20	CACTGTGGAAGGAACATCAAACC
VP7	6, 8, 21	TCTCCACTCT**S**AAGATCCAGC
VP8	6	CAG**R**ATGTA**R**AT**Y**TCAGGTGTGATCC
VP9	7, 9	CCAGAC**W**CCAA**R**A**Y**ACCTGGTCA
$VP1^{+}_{new}$		AGCACGACTTCCAAGACTCAC**Y**TTTGTCTCCTGGGAGCA
$VP2^{+}_{new}$		AGCACGACTTCCAAGACTCACCTGAT<u>T</u>GTCGC<u>C</u>CAGACTCC
$VP3^{+}_{new}$		AGCACGACTTCCAAGACTCAGTCAT**S**CAGAACCCAAGA**Y**ACC
$VP4^{+}_{new}$		AGCACGACTTCCAAGACTCAGG**W**TATCTGT**M**AG**M**GTGGAACCTC
$VP5^{+}_{new}$		AGCACGACTTCCAAGACTCAATGTACTGGTATCGACAAGA**Y**C
$VP6^{+}_{new}$		AGCACGACTTCCAAGACTCACACTGTGGAAGGAACATCAAACC
$VP7^{+}_{new}$		AGCACGACTTCCAAGACTCATCTCCACTCT**S**AAGATCCAGC
$VP8^{+}_{new}$		AGCACGACTTCCAAGACTCACAG**R**ATGTA**R**AT**Y**TCAGGTGTGATCC
$VP9^{+}_{new}$		AGCACGACTTCCAAGACTCA<u>T</u>CAGAC**W**CCAARA**Y**ACCTGGTCA
UP		ACAGCACGACTTCCAAGACTCA
UP_{new}		AGCACGACTTCCAAGACTCA
Cβ-mid3	Cβ	TGTGGCCTTTTGGGTGTGG
Cβ-mid4	Cβ	TGGGTGTGGGAGATCTCTG
Cβ-in	Cβ	TCTGATGGCTCAAACACAGC

Table 2-6: Primers used for pre-amplification of TCR α-chain of single T cells

Degenerate primers contain bold red letters to indicate nucleotide exchanges. All the forward primers for TCR α-chain were designed by Sabine Seitz (Seitz et al., 2006).

Name	Vα specificity	Nucleotide sequence (5'→3')
$Vα\text{-}1^{14}$-for-out	1.1, 1.4	AG**S**AGCCTCACTGGAGTTG
$Vα\text{-}1^{235}$-for-out	1.2, 1.3, 1.5	CTGAGGTGCAACTACTCATC
Vα-2-for-out	2.1, 2.2, 2.3	CA**R**TGTTCCAGAGGGAGCC
Vα-3,25-for-out	3.1, 25.1	GAA**R**ATG**Y**C**W**CCATGAACTGC
Vα-4,20-for-out	4.1, 4.2, 20.1	**W**TGCTAAGACCACCCAGCC
Vα-5-for-out	5.1	AGATAGAACAGAATTCCGAGG
Vα-6,14-for-out	6.1, 14.1, 14.2	**RY**TGCACATATGACACCAGTG
Vα-7-for-out	7.1, 7.2	CACGTACCAGACATCTGGG
Vα-8,21-for-out	8.1, 8.2, 21.1	CCTGAG**Y**GTCCAGGA**R**GG
Vα-9-for-out	9.1	GTGCAACTATTCCTATTCTGG
Vα-10,24-for-out	10.1, 24.1	A**S**TGGAGCAGAG**Y**CCTCAG
Vα-11-for-out	11.1	TCTTCAGAGGGAGCTGTGG
Vα-12-for-out	12.1	GGTGGAGAAGGAGGATGTG
Vα-13,19,26-for-out	13.1, 19.1, 24.1, 26.1	**S**AA**S**TGGAGCAGAGTCCTC
Vα-15-for-out	15.1	CCTGAGTGTCCGAGAGGG
Vα-16-for-out	16.1	ATGCACCTATTCAGTCTCTGG
Vα-17-for-out	17.1	TGATAGTCCAGAAAGGAGGG
Vα-18-for-out	18.1	GTCACTGCATGTTCAGGAGG
Vα-22,31-for-out	22.1, 31.1	CCCT**W**CCCTTTTCTGGTATG
Vα-23,30-for-out	23.1, 30.1	GGCA**R**GAYCCTGGGAAAGG
Vα-27-for-out	27.1	CTGTTCCTGAGCATGCAGG
Vα-28-for-out	28.1	AGACAAGGTGGTACAAAGCC

Vα-29-for-out	29.1	CAACCAGTGCAGAGTCCTC
Vα-32-for-out	32.1	GCATGTACAAGAAGGAGAGG

Table 2-7: Primers used for the specific amplification of TCR α-chain of single T cell

All the forward primers for TCR α-chain were created by Sabine Seitz (Seitz et al., 2006).

	Name	Vα specificity	Nucleotide sequence (5'→3')
	Cα-rev-in	Cα	AGTCTCTCAGCTGGTACACG
SET1	Vα-4/1-for-in	4.1	ACAGAAGACAGAAAGTCCAGC
	Vα-4/2-for-in	4.2	GTCCAGTACCTTGATCCTGC
	Vα-6-for-in	6.1	GCAAAATGCAACAGAAGGTCG
	Vα-8/1-for-in	8.1	CAGTGCCTCAAACTACTTCC
	Vα-8/2-for-in	8.2	GCCTCAGACTACTTCATTTGG
	Vα-14-for-in	14.1, 14.2	ACAGAATGCAACGGAGAATCG
	Vα-24-for-in	24.1	CCTTCAGCAACTTAAGGTGG
	Vα-28-for-in	28.1	TCTCTGGTTGTCCACGAGG
SET2	Vα-2/1-for-in	2.1, 2.3	TGGAAGGTTTACAGCACAGC
	Vα-2/2-for-in	2.2	TGGAAGGTTTACAGCACAGG
	Vα-5-for-in	5.1	CAGCATACTTACAGTGGTACC
	Vα-10-for-in	10.1	TCACTGTGTACTGCAACTCC
	Vα-12-for-in	12.1	TACAAGCAACCACCAAGTGG
	Vα-22-for-in	22.1	AGGCTGATGACAAGGGAAGC
	Vα-31-for-in	31.1	GTGGAATACCCCAGCAAACC
SET3	Vα-7-for-in	7.1, 7.2	CTCCAGATGAAAGACTCTGC
	Vα-13-for-in	13.1	TTAAGCGCCACGACTGTCG
	Vα-17-for-in	17.1	CTGTGCTTATGAGAACACTGC
	Vα-18-for-in	18.1	CCTTACACTGGTACAGATGG
	Vα-21-for-in	21.1	TGCTGAAGGTCCTACATTCC
	Vα-23-for-in	23.1	GTGGAAGACTTAATGCCTCG
	Vα-32-for-in	32.1	TCACCACGTACTGCAATTCC
SET4	Vα-3-for-in	3.1	TTCAGGTAGAGGCCTTGTCC
	Vα-11-for-in	11.1	AGGGACGATACAACATGACC
	Vα-15-for-in	15.1	CCTCCACCTACTTATACTGG
	Vα-19-for-in	19.1	CCTGCACATCACAGCCTCC
	Vα-25-for-in	25.1	AGACTGACTGCTCAGTTTGG
	Vα-26-for-in	26.1	CCTGCATATCACAGCCTCC
	Vα-29-for-in	29.1	ACTGCAGTTCCTCCAAGGC
SET5	Vα-1/235-for-in	1.2, 1.3, 1.5	AAGGCATCAACGGTTTTGAGG
	Vα-1/14-for-in	1.1, 1.4	CTGAGGAAACCCTCTGTGC
	Vα-9-for-in	9.1	ATCTTTCCACCTGAAGAAACC
	Vα-16-for-in	16.1	TCCTTCCACCTGAAGAAACC
	Vα-20-for-in	20.1	ACGTGGTACCAACAGTTTCC
	Vα-27-for-in	27.1	ACTTCAGACAGACTGTATTGG
	Vα-30-for-in	30.1	CTCTTCACCCTGTATTCAGC

Table 2-8: Primers used for recovery of antigen-coding plasmids

Nucleotides underlined are the insert site of pcDNA3.1D/V5-His-TOPO. All primers used for experiments were designed by Katherina Siewert (Siewert et al., 2012).

Name	Nucleotide sequence (5'→3')
pcDNA-for-1	CACTGCTTACTGGCTTATCG
pcDNA-for-2	CGACTCACTATAGGGAGACC
pcDNA-2nd-for	TCCGGCGCGCCACCATG
pcDNA-2nd-for-TOPO	CACCTCCGGCGCGCCACCATG
pcDNA-rev-1	ACTAGAAGGCACAGTCGAGG
pcDNA-rev-2	CTGATCAGCGGGTTTAAACTC
pcDNA-rev-3	TGGTGATGGTGATGATGACC
pcDNA-2nd-rev-10	CTAGACTCGAGCGGCCGC
pHSE-res-for	GGTTATTGTCTCATGAGCGG
pHSE-res-rev	AGCTGGCGTAATAGCGAAG

2.1.6 Plasmids

Table 2-9 lists the plasmids used for the experiments.

Table 2-9: Plasmid constructions

Plasmid	Length	Resistance Genes	Application	Resources
pHSE3'-HLA-A*0101	9.2 kb	Amp^R, Neo^R	Expression of human HLA-A* 0101 in COS-7 cells	Klaus Dornmair
pHSE3'-HLA-A*0201	9.2 kb	Amp^R, Neo^R	Expression of human HLA-A* 0201 in COS-7 cells	
pHSE3'-HLA-B*0801	9.2 kb	Amp^R, Neo^R	Expression of human HLA-B* 0801 in COS-7 cells	
pHSE3'-HLA-C*0701	9.2 kb	Amp^R, Neo^R	Expression of human HLA-C* 0701 in COS-7 cells	
pHSE3'-hMR1	11.2 kb	Amp^R, Neo^R	Expression of human MR1 in COS-7 cells	
pcDNA6/V5-HisA	5.1 kb	Amp^R, Bls^R	Backbone plasmid for truncated protein expression	Invitrogen
pcDNA6/V5-HisA-sGFP	5.9 kb	Amp^R, Bls^R	Expression of sGFP in COS-7 cells	Katherina Siewert
pcDNA6/V5-HisA-N27 lib	5.1 kb	Amp^R, Bls^R	PECP library, coding for random nonamer peptides	Katherina Siewert
pcDNA6/V5-HisA-A1^{39} Lib	5.1 kb	Amp^R, Bls^R	PECP library, coding for nonamer peptides with I, V and L at the positions 2, 6 and 9, respectively	Katherina Siewert Latika Bhonsle
pcDNA6/V5-HisA-A2^{269} Lib	5.1 kb	Amp^R, Bls^R	PECP library, coding for nonamer peptides with I, V and L at the positions 2, 6 and 9, respectively	Katherina Siewert
pcDNA6/V5-HisA-B8^{359} Lib	5.1 kb	Amp^R, Bls^R	PECP library, coding for nonamer peptides with I, V and L at the positions 2, 6 and 9, respectively	Katherina Siewert Latika Bhonsle
pcDNA6/V5-HisA-C7^{9} Lib	5.1 kb	Amp^R, Bls^R	PECP library, coding for nonamer peptides with I, V and L at the positions 2, 6 and 9, respectively	Katherina Siewert Latika Bhonsle
pcDNA™3.1D/V5-His-TOPO	5.5 kb	Amp^R, Neo^R	Recloning of peptides coded on PECP libraries for mimotope search	Invitrogen
pCR™ 2.1-TOPO®	3.9 kb	Amp^R, Kan^R	Cloning of PCR products directly from a PCR reaction	Invitrogen

2.1.7 **Antibodies**

Table 2-10 to 2-11 present the antibodies for immunofluorescence staining and flow cytometers analysis, respectively. Unless there are special annotations, all antibodies listed in this thesis are directly against human antigens.

Table 2-10: Antibodies employed for immunofluorescence staining

×: non-specific staining detectable in human tissues. † The antibody is self-labeled with Cy3 mAb labeling kit (Bioscience), according to the manufacturer's instructions.

A. Primary antibodies

Target antigen	Clone (isotype)	Working Concentration	Company
CD3ε	Polyclonal (rabbit IgG)	1:500	Dako
CD3ζ	K25-407.69 (mouse IgG2a)	1:10	BD BioSciences
CD8α†	LT8 (mouse IgG1)	1:50-1:100	AbD serotec
	SK1 (mouse IgG1)	1:50	BD BioSciences
CD8β	5F2 (mouse IgG1)	1:20-1:50	Santa cruz
	2ST8.5H7 (mouse IgG2a)	1:50-1:100	BD BioSciences
	F-5 (mouse IgG2a)	×	Santa cruz
	SIDI8BEE (mouse IgG1)	×	Ebioscience
CD57	HNK-1 (mouse IgM)	1:50	Biolegend
CD68	PG-M1 (mouse IgG3)	1:1	Dako
	EBM11 (mouse IgG1)	1:500	Dako
	KP1 (mouse IgG1)	1:200	Dako
CD69	FN50 (mouse IgG1)	1:100	AbD serotec
CD83	HB15e (mouse IgG1)	1:250	BD BioSciences
CD134	443318 (rat IgG2a)	1:25	R&D
	7H163 (mouse IgG1)	1:100-1:200	Usbiological
	ACT35 (mouse IgG1)	1:5	BD BioSciences
	H-10 (mouse IgG2a)	1:50-1:200	Santa cruz
	W4-3 (rat IgG2a)	1:50-1:200	MBL
CD137	Polyclonal (goat IgG)	1:200	RD
	BBK-2 (mouse IgG1)	1:200	Abcam
ICAM-3	ICAM-3.3 (mouse IgG1)	1:500	R&D
Vα7.2	3C10 (mouse IgG1)	1:15	Biolegend
Vβ1	BL37.2 (rat IgG1)	1:25	Beckman coulter

B. Secondary antibodies

Target antigen	Species	Conjugation	Company
Goat IgG	Rabbit	Alexa Fluor® 488	Invitrogen
Mouse IgG	Goat	Alexa Fluor® 488	Invitrogen
Mouse IgG2a	Goat	Alexa Fluor® 488	Invitrogen
Rabbit IgG	Goat	Alexa Fluor® 594	Invitrogen
Rat IgG	Goat	Alexa Fluor® 488	Invitrogen
Rat IgG	Goat	Cy3	Jackson ImmunoResearch
α-FITC	Goat	Alexa Fluor® 488	Invitrogen

C. Isotype controls

Target antigen	Clone	Conjugation	Company
Mouse IgG1	X40	FITC	BD BioSciences
	MOPC-21	PE	BD BioSciences
Rat IgG2a	R35-95	PE	BD BioSciences
	X39	FITC	BD BioSciences

D. The dye for cell nuclei

Name	Stock solution	Working concentration	Company
DAPI	5 mg/ml	10 µl in 50 ml 1× PBS solution	ThermoFisher scientific

Table 2-11: Antibodies employed for flow cytometers

† This is anti-mouse antibody.

A. Primary antibodies

Target antigen	Clone (isotype)	Conjugation	Company
mCD3ε†	145-2C11 (Armenian hamster IgG1)	APC, FITC, PE	BD BioSciences
CD8α	SK1 (mouse IgG1)	APC, FITC	BD BioSciences
CD8β	2ST8.5H7 (mouse IgG2a)	PE	BD BioSciences
Vβ1	BL37.2 (rat IgG1)	FITC, PE	Beckman coulter
Vβ17	E17.5F3.15.13 (mouse IgG1)	PE	Beckman coulter
Vα7.2	3C10 (mouse IgG1)	APC, FITC	Biolegend

B. Isotype controls

Anti-	Clone (isotype)	Conjugation	Company
Trinitrophenol (TNP)	A19-3 (Armenian hamster IgG1)	APC, FITC, PE	BD BioSciences
-	MOPC-21 (mouse IgG1)	APC, FITC, PE	BD BioSciences
Trinitrophenol (TNP)	G155-178 (mouse IgG2a)	PE	BD BioSciences

C. Fluorescence dyes for dead cells

Name	Stock solution	Working concentration	Company
ToPro-3	1 mM in DMSO	1:6,000	Invitrogen
Propidiumiodid	1 mg/ml in PBS	1:500	Sigma-Aldrich

2.1.8 Eukaryotic Cell Lines and *Escherichia coli* Strains

Table 2-12 presents the eukaryotic cell lines and the *E.coli* strains used in this thesis.

Table 2-12: List of eukaryotic cell lines and *E.coli* strains

Except for COS-7 cell line, all the other cell lines were generated in the lab of PD. Dr. Klaus Dornmair, and all *E.coli* strains were purchased from Invitrogen. † Colony forming units (cfu)/µg pUC19 plasmid.

A. Eukaryotic cell lines

Name	Description	Reference
COS-7	African green monkey kidney cell line, adherent, transformed with SV40, produces T antigen	ATCC® CRL-1651™
COS-7-A2	COS-7 cells with stable expression of human HLA-A*0201	Klaus Dornmair, Katherina Siewert
EBV-16488	EBV-transducted B cells derived from polymyositis patient 16488, stable expression of HLA-A2, HLA-A26, HLA-B8, HLA-B38, HLA-C7, HLA-C12, suspended	Klaus Dornmair
EBV-17490	EBV-transduced B cells derived from polymyositis patient 17490, stable expression of HLA-A2, HLA-A3, HLA-B35, HLA-B40, HLA-C3, HLA-C4, suspended	Klaus Dornmair
EBV-FE	EBV-transducted B cells derived from MS patient FE, stable expression of HLA-A1, HLA-B8, HLA-C7, suspended	Klaus Dornmair

58α$^-$β$^-$	TCR deficient mouse T hybridoma recipient cell line, suspended	Klaus Dornmair
58-JM22	Derivative cell line from 58α$^-$β$^-$, stably expressing human Vα10.1-Jα42-Vβ17Jβ2.7 TCR and human CD8 molecule, additionally expressing sGFP under the control of the NFAT promoter, suspended	Klaus Dornmair
58-FE-BV1-BJ2.3-AV7.2-AJ24.2	Derivative cell line from 58α$^-$β$^-$, stably expressing human Vα7.2-Jα24.2-Vβ1Jβ2.3 TCR and human CD8 molecule, additionally expressing sGFP under the control of the NFAT promoter, suspended	Klaus Dornmair, Latika Bhonsle, David Laplaud

B. *E.coli* strains

***E.coli* strains**	**Genotype**	**Transformation Efficiency**[†]
ElectroMAX™ DH10B™ T1 Phage Resistant Cells	F$^-$ *mcr*A Δ(*mrr-hsd*RMS-*mcr*BC) φ80*lac*ZΔM15 Δ*lac*X74 *rec*A1 *end*A1 *ara*D139 Δ(*ara, leu*)7697 *gal*U *gal*K λ$^-$ *rps*L *nup*G	1×10^{10}
MAX Efficiency® DH5α F'IQ™ Competent Cells	F-φ80*lac*ZΔM15 Δ(*lac*ZYA-*arg*F) U169 *rec*A1 *end*A1 *hsd*R17 (rk-, mk+) *pho*A *sup*E44 λ$^-$ *thi*$^-$1 *gyr*A96 *rel*A1/F´ *pro*AB+ *lac*IqZΔM15 zzf::Tn5 [KmR]	3×10^{8}
One Shot® TOP10 Chemically Competent Cells	F$^-$ *mcr*A Δ(*mrr-hsd*RMS-*mcr*BC) φ80*lac*ZΔM15 Δ*lac*X74 *rec*A1 *ara*D139 Δ(*ara-leu*) 7697 *gal*U *gal*K *rps*L (Str^R) *end*A1 *nup*G λ-	1×10^{9}

2.1.9 **Human Tissue Samples**

All patients and voluntary donors allowed scientific examination of their biopsies or blood samples. Immunological and CSF investigation were approved by the ethics committee of the Ludwig Maximillian's University, Munich.

2.1.9.1 Human brain and tonsil biopsies

Brain biopsies from two MS patients are used in this thesis. Patient FE was diagnosed with a malignant glioma in the right temporooccipital lobe of the brain at the age of 49 and then the affected region of the brain was surgically removed and stored at -80°C. Followed by the presence of oligoclonal immunoglobulin in the CSF and three relapses in the next five years, the patient had a diagnosis of MS Type III (Hu and Lucchinetti, 2009). He is homozygous for the HLA class I gene locus (Skulina et al., 2004), and possesses the alleles *HLA-A*0101*, *HLA-B*0801*, *HLA-C*0701*, *HLA-DRB1*0301*, *HLA-DRB3*0101*, *HLA-DQA1*05* and *HLA-DQB1*0201*. Brain biopsies from patient RF were obtained from Ph.D. David-Axel Laplaud from University of Nantes, France. The HLA composition analyzed in this study is presented in Table 2-13.

In addition, two tonsil biopsies were obtained from Dr. Markus Krumbholz. One tonsil biopsy was from a healthy donor, and another tonsil biopsy was from an inflammation patient donor.

Table 2-13: HLA typing results of MS patients FE and RF

The HLA alleles were determined by genomic HLA typing with the identification code (ID) of the MS patients displayed in column 1. The haplotype for patient FE is homozygous as only one allele was detected for each of the *loci*. However, patient RF is heterozygous for all *loci*. – Not detectable in the *loci*.

	HLA-						
Patient ID	**A***	**B***	**C***	**DRB1***	**DRB3***	**DQA1***	**DQB1***
FE	0101	0801	0701	0301	0101	05	0201
RF	0301	0702	-	0102	-	-	0501
	2402	1402		1501			0602

2.1.9.2 Human blood and CSF specimens

In cooperation with Dr. Lisa Ann Gerdes, the CSF and blood samples were taken either from selected MS twins or newly diagnosed patients. These MS patients were diagnosed with Clinically Isolated Syndrome (CIS), Radiologically Isolated Syndrome (RIS), Neurological Disorder after Treatment of Metastatic Melanoma with Ipilimumab (MP), or encephalitis against N-methyl-D-aspartate receptor. Some of the samples were immediately stored in liquid nitrogen, and the rest were used for TCR analysis. The HLA typing for each patient has been done in the lab of Immunogenetics (LMU, Munich). The results are summarized in Table 2-14. MS twins (Twin #01) are homozygous at each of the *loci*, but the rest of patients analyzed in this study are heterozygous. Besides, blood lymphocytes from voluntary donors are employed for αβ-TCRs identification.

Table 2-14: Diagnostic performance of HLA typing for MS patients.

The HLA alleles of the MS patients are determined by genomic HLA typing with the identification code (ID). Identical twins always have identical MHCs. The haplotype for patient Twin #01 are homozygous as only one allele is detected for each of the *loci*, but the rest of patients are heterozygous for all *loci*. – Not detectable in the *loci*.

	HLA-A		**HLA-B**		**HLA-C**		**HLA-DRB1**		**HLA-DQB1**	
Patient ID	**Allele 1**	**Allele 2**	**Allele 1**	**Allele 2**	**Allele 1**	**Allele 2**	**Allele 1**	**Allele 2**	**Allele 1**	**Allele 2**
RIS #01	*11	*31	*35	*35	*04	-	*11	*15	*03	*06
RIS #02	*03	*68	*41	*44	*05	*17	*07	*13	*02	*06
RIS #03	*03	-	*07	*51	*07	-	*15	-	*06	-
RIS #04	*02	*68	*44	*47	*06	*07	*11	*15	*03	*06
RIS #05	*24	*26	*27	*49	*01	*07	*01	*15	*05	*06
RIS #06	*24	*68	*07	*51	*07	*15	*08	*09	*03	*04
RIS #07	*02	*03	*07	*37	*06	*07	*11	*15	*03	*06
RIS #08	*01	*03	*07	*35	*04	*07	*15	-	*06	-
RIS #09	*02	-	*15	-	*03	*03	*04	*15	*03	*06
RIS #10	*03	*24	*08	*39	*07	-	*03	*15	*02	*06
Twin #01	*24	-	*07	-	*07	-	*15	-	*06	-
Twin #02	*31	*32	*15	*35	*04	-	*13	*15	*06	*06
Twin #03	*01	*02	*08	*51	*07	*15	*03	*15	*02	*06
Twin #04	*01	*03	*14	*35	*08	*12	*04	*08	*03	*03
Twin #05	*02	*30	*08	*42	*07	*17	*03	*13	*02	*03

2.2 Molecular Biology based Methods

2.2.1 Isolation of Total RNA

50-100 mg of tissue samples was homogenized in 1 ml TRIzol reagent using a pipette or grinding tool and incubated at room temperature for 5 minutes to permit complete dissociation of the nucleoprotein complex. Then 0.2 ml of chloroform per ml TRIzol-tissue was added to the sample and it was shaken vigorously for 15 seconds. After incubation at room temperature for five minutes and centrifugation at 4°C at 20,800× g for 15 minutes, the sample was separated into a lower red phenol-chloroform phase, an interphase, and a colorless upper aqueous phase. The upper phase contained most of the RNA exclusively. Then the upper phase was gently transferred into an RNase-free tube by pipetting. 5-10 µg of glycogen (20 mg/ml, Roche) and 0.7 ml of isopropanol (70%) were added for RNA precipitation, and then the sample was incubated at -20°C for 20 minutes. After centrifugation at 4°C at 20,800× g for 20 minutes, the RNA pellet was resuspended in 1 ml of 80% ethanol and subsequently centrifuged at 4°C at 20,800× g for 5 minutes. Finally, the RNA pellet was dried in a vacuum for 30 minutes and completely dissolved in 20 µl of DEPC treated water (Invitrogen). The concentration of RNA was determined as described in Section 2.2.3.

2.2.2 Isolation of Plasmid DNA

Different commercial kits were used to isolate the plasmid DNA from *E.coli* culture. Briefly, QIAprep Spin Miniprep Kit (Qiagen) was used to isolate plasmid DNA (≤ 20 µg) from 1-2 ml of *E.coli* cultures. However, HISpeed Plasmid kit (Qiagen) was employed to obtain a high yield of plasmid DNA (up to 750 µg) especially for the generation of PECP libraries.

2.2.3 Quantitation of DNA and RNA

Two methods were used to quantitate solutions of nucleic acids. The first one was to use a spectrophotometer (NanoDrop 2000, Thermo Fisher Scientific) to measure the amount of ultraviolet radiation absorbed at a wavelength of 260 nm (OD_{260}). OD_{260}/OD_{280} ratio is an indication of nucleic

acid purity, such as pure DNA had an OD_{260}/OD_{280} ratio of around 1.8 and purified RNA has an OD_{260}/OD_{280} ratio of around 2.0. Phenol or protein contamination might cause low rates of OD_{260}/OD_{280}. The second one was to quantify the amount of DNA by judging its concentration as compared to a standard molecular mass marker after the agarose gel electrophoresis.

2.2.4 **Assessment of RNA Integrity**

Intact RNA is essential for successful RT-PCR analysis. The assessment of RNA integrity is a critical step for obtaining gene expression data. The 2100 Bioanalyzer (Agilent) and Agilent RNA 6000 Pico Kit were used to determinate the RNA integrity. Briefly, the RNA sample was diluted with DEPC treated water (Invitrogen) and subsequently was denatured at 70°C for 2 minutes. Then the RNA integrity was measured as the manufacturer's introduction. Finally, the data was displayed in the electropherogram and densitometry plot through the software "Agilent Technologies 2100 Bioanalyzer 2100 Expert, VB.02.06.SI418" (Agilent). The quality of RNA was classified by "RNA integrity number" (RIN), based on a numbering system (level 1-10), which represents that level 1 means the most degraded RNA and level 10 means the most intact RNA. The RIN-value represents the ratio between 28S rRNA and 18S rRNA offset against further factors. Moreover, the ratio of the 18S to 28S ribosomal subunits also plays a significant role in determining the degree of degradation of RNA sample.

2.2.5 **Separation of DNA Fragments**

Gel electrophoresis can easily separate different size of DNA fragments. In an electrical field, the negatively charged DNA moves towards to positive electrode through an agarose gel matrix. Agarose gel was prepared in 1× TBE buffer with fluorescence dye peqGREEN (peQlab), which is used to visualize the DNA with the UV-induced emission of fluorescence (λ=295 to 490 nm). PeqGREEN is a non-carcinogenic and non-toxic DNA/RNA fluorescence dye. In the condition of 90-150 V and 50 mA, the DNA fragments are completely separated in 40 minutes. The lengths of the DNA segments

are determined by a DNA standard of known concentration or a molecular mass marker, such as peqGOLD 50 bp DNA-ladder, Peqlab).

2.2.6 DNA Extraction

After separating by gel electrophoresis, the DNA fragment was excised from the gel with a clean, sterile razor blade under a UV transilluminator. Then DNA was purified from the gel by the Gel Extraction kit (Qiagen) by the manufacturer's instructions. Finally, the extracted DNA was eluted in 30 µl of EB buffer and stored at -20°C.

2.2.7 Ethanol Precipitation of DNA

Ethanol precipitation is the most widely used method for concentration and purification of DNA. This approach is accomplished by adding salt and ethanol to a DNA solution. Briefly, the DNA solution was mixed with 1/10 volume of 3 M sodium acetate (pH=5.2) and about 2-3 volumes of 100% ethanol. The mixture was frozen overnight at -80°C. Then the mixture was centrifuged at 20,800× g in a standard microcentrifuge at 4°C for one hour. After the supernatant was carefully removed by a pipette, the DNA pellet was rinsed twice with cold 70% ethanol and centrifuged at 4°C at 20,800× g for 15 minutes. Finally, The DNA pellet was air-dried for another 15 minutes and then resuspended in DEPC treated water. In addition, Pellet Paint® Co-precipitant (Novagen) can be employed to visualize the DNA pellet during precipitation procedure.

2.2.8 DNA Sequencing

The sequencing service performed DNA sequencing analyses at the Faculty of Biology at the Ludwig Maximillian's University (LMU), Munich. The template was prepared in a total volume of 7 µl with diluted DNA and primer. According to the protocol "Cycle, Clean & Run BigDye v3.1", the sequence of DNA was analyzed. The sequencing data were presented by the software "Chromas Lite V2.01".

2.2.9 **Amplification of TCR chains from Single T Cells**

Polymerase chain reaction (PCR) is a widely used method for generation of multiple copies from a single copy or a segment of DNA through several cycles of annealing, amplification, and denaturation. The TCR α- and β-chains of single T cells could be amplified by multiplex RT-PCR-based method. The unbiased PCR approaches were established by Song-Min Kim and optimized during this thesis. All the reactions were performed in the Mastercycler™ pro-PCR System (Eppendorf). DEPC treated water instead of DNA template was served as a negative control in each PCR reaction. PCR products were analyzed by the gel electrophoresis.

2.2.9.1 Workflow

The relative positions of primers for the unbiased amplification of TCR α- and β-chains are illustrated in Figure 2-1.

2.2.9.2 Reverse transcription (RT)

Single isolated T cells were used as template to synthesize the complementary cDNA strands that were further amplified by PCR. The RT reaction was carried out with the OneStep® RT-PCR Kit (Qiagen) according to the manufacturer's instruction. 20 µl of RT reaction mix with 0.3 µM of the Cα-RT-imp and Cβ-RT-2 oligonucleotide primers (Table 2-4) were added to the sample containing the single T cell. RNaseOUT™ Recombinant Ribonuclease Inhibitor (Invitrogen) was additionally added to the sample to avoid the RNA degradation. The details of RT reaction mix are presented below:

Reagent	**Volume (µl)**	**Final concentration**
RNase-free H_2O	13.78	
5× one step RT-PCR buffer	4	1×
dNTP	0.8	0.4 mM each
Cα-RT-imp	0.06	0.3 µM
Cβ-RT-2	0.06	0.3 µM
Enzyme Mix	0.8	
RNaseOUT Inhibitor	0.5	20 units
Total	20	

20 µl of RT reaction mix was directly added into the cap of the PCR tube that contained the isolated single T cell. Subsequently, the sample was centrifuged at 4°C at 20,800× g for 5 minutes and then cDNA synthesis proceeded at 50°C for 30 minutes.

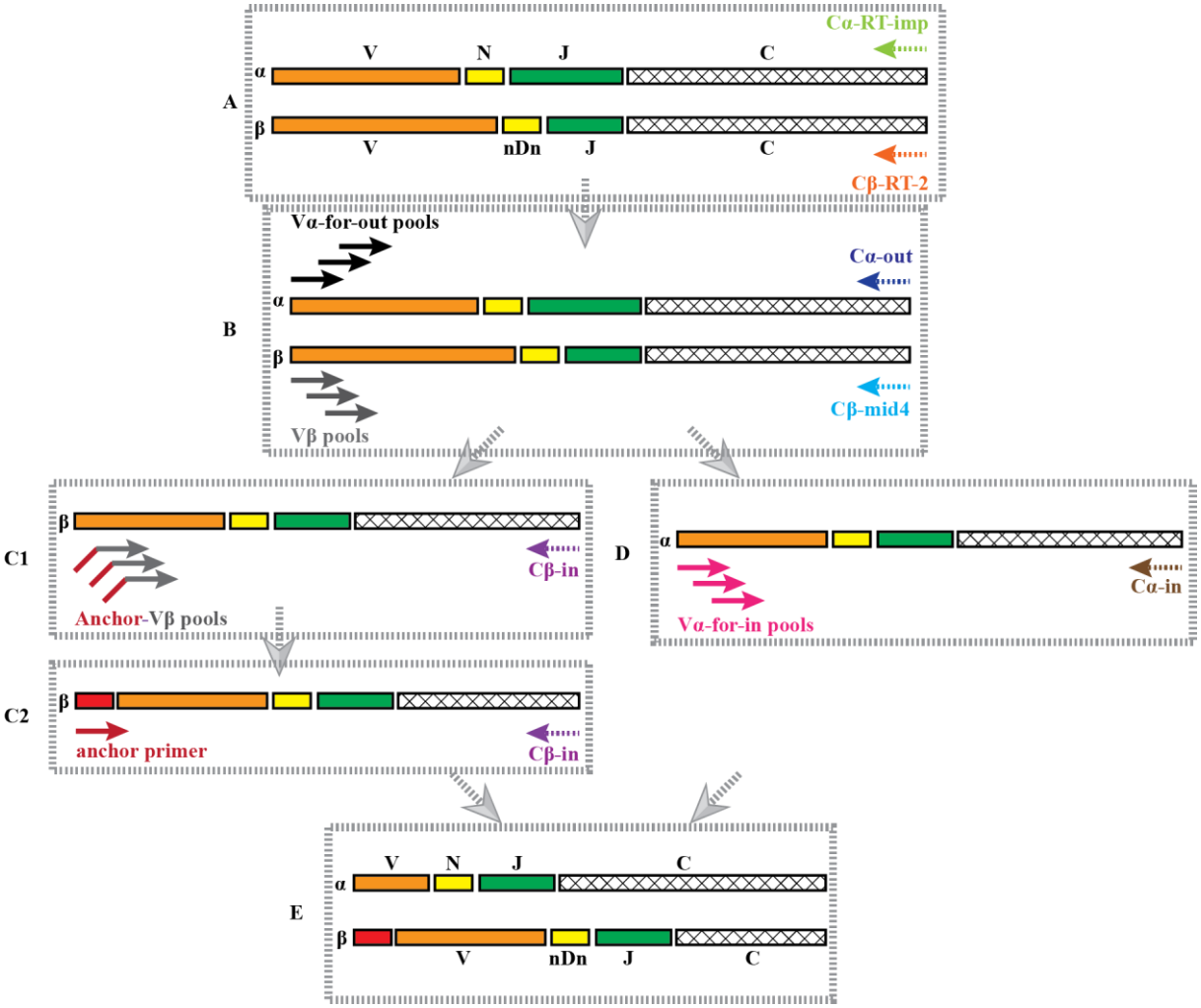

Figure 2-1: PCR strategy for identifying the paired TCR α- and β-chains from single T cells

Step 1 (A) Total mRNA from paired TCR α- and β-chains (**E**) was transcribed into cDNA via the primers Cα-RT-imp and Cβ-RT-2 which bind to the constant gene regions of αβ chains. **Step 2 (B)** Pre-amplification of the paired αβ chains by the former primers (Vα-for-out pools Vβ pools) and the reverse primers (Cα-out, Cβ-mid4). **Step 3 (C)** Specific amplification of the Vβ genes by two steps: firstly, an anchor sequence (Universal Primer) was added to the 5'-site of each variable gene region of β-chain with a semi-nested PCR (**C1**) using the primers Vβ pools and Cβ-in; secondly, the Vβ genes were amplified with the anchor primer and primer Cβ-in (**C2**). **Step 4 (D)** Specific amplification of the TCR α-chains by semi-nested PCR from the pre-amplification PCR products (**B**) using the primer Vα-for-in pools and primer Cα-in. Orange: variable gene regions V; yellow: diversity gene regions nDn/N; green: joining gene regions J; stripe: constant gene regions C. Figure was modified from Kim et al., 2012.

2.2.9.3 Pre-amplification of TCR α- and β-chains of single cells

After reverse transcription, 5 µl of PCR mix from the OneStep® RT-PCR Kit (Qiagen) was added to the previous reaction to obtain a final volume of 25 µl. The PCR mix contained 0.072 µM of Vα- and Vβ-oligonucleotide primers each as well as 0.08 µM of Cα-out and Cβ-mid4 oligonucleotide primers. The primer pools for the Vα-repertoire consisted of 24 oligonucleotide primers are described in Table 2-6. The primer pools for Vβ- repertoire consisted of nine oligonucleotide primers (VP1 to VP9) are given in Table 2-5. A pool of all V regions primers (called "V-primers"), and a pool of all the C segments primers (called "C-primers") were prepared in advance. These primers were used to pre-amplify the TCR αβ-chains. The details of PCR mix are presented below:

Reagent	Volume (µl)	Final concentration
RNase-free H_2O	2.8	
5× OneStep RT-PCR buffer	1	1×
dNTP	0.2	0.08 mM each
V-primers	0.6	0.072 µM each
C-primers	0.2	0.08 µM each
Enzyme Mix	0.2	
Total	5	

Thermocycling conditions for a touchdown PCR:

Step	Temperature (°C)	Time (Minute)	Cycles
Initial Denaturation	95	15	1×
Denaturation	94	1	4×
Hybridization	61	1	
Elongation	72	1	
Denaturation	94	1	4×
Hybridization	58	1	
Elongation	72	1	
Denaturation	94	1	40×
Hybridization	56	1	
Elongation	72	1	
Final Extension	72	10	1×
Hold	4-10	∞	∞

Finally, the PCR product was employed as a template for the subsequent identification of TCR α- and β-chains.

2.2.9.4 Characterization of TCR β-chains of single cells

The specific amplification of TCR β-chains contains two PCR steps (Figure 2-1, C1-C2). The first step introduced a new universal primer (UP_{new}) segment comprising 20 nucleotides (AGCACGACTTCCAAGACTCA) as an anchor to the 5' -end of each VP1 to VP9 primers ($VP1^+$-new to $VP9^+$-new). The nucleotide sequences of $VP2^+$-new and $VP9^+$-new were modified to avoid primer interactions (Table 2-5). 1 µl of PCR product from Section 2.2.9.3 was added to a PCR mix containing 0.11 µM of anchored Vβ-oligonucleotide primers ($VP1^+_{new}$ to $VP9^+_{new}$) and 0.1 µM of Cβ-in oligonucleotide primer. A pool of $VP1^+_{new}$ to $VP9^+_{new}$ primers called "VP^+-pool" was prepared in advance. The details of PCR mix are presented below:

Reagent	Volume (µl)	Final concentration
RNase-free H_2O	16.28	
10× PCR buffer with $MgCl_2$	2	1×
dNTP	0.4	0.2 mM each
VP^+-pool	0.2	0.11 µM
Cβ-in	0.02	0.1 µM
Taq	0.1	0.025 U/µl
DNA	1	
Total	20	

For the first PCR step, the well-mixed sample was initially denatured at 94°C for 2 minutes. Then PCR program was set up for 30 cycles (denatured at 94°C for 30 seconds, annealed at 56°C for 1 minute and elongated at 72°C for 1 minute). Finally, the reaction was extended at 72°C for 10 minutes.

The second PCR step was to amplify the TCR β-chain transcripts with an anchor primer (UP_{new}) and a reverse primer (Cβ-in). Briefly, 1 µl of PCR product from the first step was added to a PCR mix. The PCR mix was comprised of 2 µl 10× PCR buffer with $MgCl_2$ (Roche), 0.4 µl dNTP (10 mM each), 0.5 µM of oligonucleotide primers (Cβ-in and UP_{new}), and 0.1 µl of Taq DNA Polymerase (5 U/µl, Roche). The PCR program began with the initial denaturation at 94°C for 2 minutes and followed by 20 cycles (denatured at 94°C for 30 seconds, annealed at 58°C for 1 minute and elongated at 72°C for 1 minute. Afterwards, a final elongation step was set up at 72°C for 10 minutes. The PCR product was

collected by agarose gel electrophoresis. After DNA extraction from agarose gel (Section 2.2.6), the DNA was sequenced as described in Section 2.2.8.

2.2.9.5 Amplification of the matching TCR α-chain

Only the single T cells that had yielded a PCR product for the TCR β-chains were employed for characterization of the matching TCR α-chains. 36 different primers were designed for the V regions of TCR α-chains and divided into five sets, named "Vα-in-set X" (X=1 to 5). 1 µl of PCR product from Section 2.2.9.3 was separately added to five PCR mixes. Each PCR mix contained 0.5 µM of Vα-in-set X primers and reversed primer (Cα-rev-in). The details of a PCR mix are presented below:

Reagent	**Volume (µl)**	**Final concentration**
RNase-free H_2O	15.5	
10× PCR buffer with $MgCl_2$	2	1×
dNTP	0.2	0.1 mM each
Vα-in-set X	1	0.5 µM
Cα-rev-in	0.1	0.5 µM
Taq	0.2	
DNA	1	
Total	20	

Touchdown PCR was carried out with an initial denaturation at 95°C for 2 minutes. Then the PCR program was run for four cycles each with annealing temperature at 61°C, 58°C and 56°C for 1 minute, respectively. Subsequently, 40 cycles were run at 53°C. Each cycle contained denaturation and extension steps at 94°C and 72°C each for 1 minute. Finally, the extension of PCR product was at 72°C for 10 minutes and collected by agarose gel electrophoresis. After DNA extraction from agarose gel (Section 2.2.6), the DNA was sequenced as described in Section 2.2.8.

2.2.10 **Plasmid Recovery PCR**

Single APCs that contain the antigen-coding plasmids were isolated by a microcapillary as described in Section 2.7.1. A PCR program is immediately performed with the flowing PCR mix.

Reagent	Volume (µl)	Final concentration
RNase-free H_2O	49	
pcDNA 2nd for TOPO	0.5	0.5 µM
pcDNA-rev-3	0.5	0.5 µM
iProof™ HF Master Mix (2×)	50	1×
Total	100	

The well-mixed sample was initially denatured at 98°C for 3 minutes. Then PCR program was set up for 40 cycles (denaturing at 98°C for 20 seconds, annealing at 56°C for 20 seconds and elongating at 72°C for 30 seconds). Finally, PCR product was extended at 72°C for 10 minutes. After PCR purification (Section 2.2.11), the DNA was inserted into an expression vector (pcDNA™ 3.1D/V5-His-TOPO) for characterization of antigen coding plasmids (Section 2.7.2).

2.2.11 **PCR Purification**

PCR purification could efficiently remove excess primers, nucleotides, DNA polymerase and salts from PCR reactions, and it is an essential step for DNA construction. QIAquick PCR purification kit (Qiagen) was used to purify PCR product under the manufacturer's introductions. After purification, most primers and primer-dimers (<40 bp) were removed. Purified DNA was ready for antibody-labeling, DNA amplification, sequencing and re-cloning.

2.2.12 **TOPO TA Cloning**

TOPO TA cloning technology is used to directly insert the Taq polymerase-amplified PCR products into a plasmid vector. The linearized pCR™ 2.1-TOPO® TA vector carries the 3'-thymidine (T) overhangs to directly ligate to the 3'-adenine (A) overhangs of Taq polymerase-amplified PCR products. The PCR product was cloned into the TOPO® vector with the TOPO® TA Cloning® kit (Invitrogen) according to the manufacturer's description. The ligated product was then transformed into chemically competent *E.coli* cells (Section 2.3.5).

2.3 Microbiology based Methods

2.3.1 Bacterial *E.coli* Culture Conditions

Escherichia coli (*E.coli*) cells grow on a solid (LB plate) or in a liquid growth medium (LB broth). Solid and liquid medium contain the similar composition, but an extra agar (15 g/l) is added to the solid medium. The LB culture medium is autoclaved at 121°C for 20 minutes to avoid the contaminations. If necessary, antibiotics such as ampicillin and kanamycin are added to the culture medium to select the antibiotic-resistant plasmids. The *E.coli* cells are grown in a liquid growth medium at 37°C with 180 rpm for 16 hours or on an LB plate at 37°C overnight.

2.3.2 Determination of *E.coli* Cells' Density

The density of E.coli cells was determined by measuring the optical density (OD) at a wavelength of 600 nm. Two kinds of spectrophotometers, UV-1600 PC (VWR) and Nanodrop ND-2000 (Peqlab), were occupied to measure the OD_{600} value[1] of *E.coli* cells' density according to the manufacturer's introductions. An equal volume of fresh LB medium served as a negative control. Furthermore, the diluted *E.coli* cells were uniformly plated on LB plate with appropriate antibiotics and incubated at 37°C overnight. The clone numbers of *E.coli* cells were determined by the numbers of colonies on the plate.

2.3.3 Preparation of *E.coli* Culture Glycerol Stocks

The quality of *E.coli* strains highly influences the transformation efficiency and the subsequent analysis of recombinant plasmids. Correctly storing the *E.coli* strains is important to make competent cells retain high transformation efficiency. Agar plate and liquid LB medium are only suitable for short-term storage of *E.coli* cells at 4°C. Preparation of a Glycerol bacteria stock kept at -80°C is the best way to maintain the high transformation efficiency of bacteria strains. Glycerol can stabilize the

[1] OD_{600} value corresponds to the cell density or cell number in a given *E.coli* culture volume; OD_{600}=1 equals to 1×10^9 *E.coli* cells per millimeter of LB medium.

frozen bacteria, prevent damage to the cell membranes and keep the cells alive. Briefly, once a new *E.coli* strain was purchased, a small portion of the bacteria was transferred to a liquid LB medium and incubated in a shaker at 37°C with 225 rpm for 2-8 hours. Then a suitable amount of culture medium was uniformly coated on an LB plate with appropriate antibiotics, and subsequently the plate was incubated overnight at 37°C. Afterwards, a single colony was picked and cultured overnight in a fresh LB medium containing appropriate antibiotics at 37°C. Then 180 µl of 86% sterile glycerol was added to a 2 ml screw-cap culture vial and mixed with 820 µl of liquid *E.coli* cells. Finally, the glycerol stock with *E.coli* cells was stored at -80°C.

2.3.4 **Reviving Bacteria from a Glycerol Stock**

E.coli cells were revived from a glycerol stock, which was thawed on ice and centrifuged at 4°C with 3000× g for 15 minutes. Then the bacteria pellet was resuspended in 5 ml of fresh LB medium containing appropriate antibiotics and cultured at 37°C/225 rpm for 1 hour. Subsequently, a small portion of bacteria suspension was uniformly plated on an LB plate with appropriate antibiotics and incubated at 37°C overnight. Finally, a single colony was picked and cultured in fresh LB medium containing appropriate antibiotics overnight at 37°C/180 rpm. In addition, the density of bacteria was measured as described in Section 2.3.2.

2.3.5 **Bacterial Transformation by Heat Shock**

Transformation is a process that bacterial cells can take up foreign DNA from the environment by creating pores in bacterial cell membranes. These bacterial cells are called competent cells. Heat shock is a basic technique to transform the plasmid DNA into *E.coli* competent cells. In this thesis, *E.coli* One Shot® TOP10 competent cells were employed for the heat shock transformation according to the manufacturer's description. Briefly, the competent cells were completely thawed on ice. Then about 2 µl of plasmid DNA (10 pg-100 ng) was immediately added to the competent cell solution and the mixture was incubated in an ice-water bath for 30 minutes. After that, the sample was stimulated at 42°C for 45 seconds (heat shock) and quickly incubated in an ice-water bath. Finally, 250 µl of S.O.C.

medium (Invitrogen) was added, and the sample was incubated at 37°C with 225 rpm for one hour. PUC19 and DEPC treated water instead of the plasmid DNA served as positive control and negative control, respectively. Moreover, to check whether the transformation successfully or not, a small portion of transformed *E.coli* cells was cultured on LB plate containing the appropriate antibiotics overnight at 37°C. The successfully transformed *E.coli* cells will be further used for plasmid isolation.

2.3.6 **Bacteria Transformation by Electroporation**

Electroporation is another highly efficient strategy to introduce the foreign nucleic acids into many cell types, including bacteria and mammalian cells. In this section, electroporation was used to transform plasmid DNA into the ElectroMAX™ DH10B™ T1 Phage-Resistant Competent Cells (Invitrogen). Briefly, the dissolved competent cells were immediately added to a reaction tube that contained 2 µl of DNA sample. Then the mixture was pipetted into a chilled cuvette (0.1 cm, Bio-Rad) and directly electroporated in GenePulser® II electroporator (Bio-Rad) using the following conditions: 2.0 kV, 200 Ω, and 25 µF. Subsequently, 1 ml of S.O.C. medium (Invitrogen) was added to the cells in the cuvette. The cell suspension was transferred to a 14 ml snap-cap tube and then incubated at 37°C with 225 rpm for one hour. A positive control was prepared with pUC19 instead of DNA sample and a negative control with cells only (without DNA) was included as well. Afterwards, the transformed cells were transferred into 20 ml of LB medium containing appropriate antibiotics and incubated at 37°C with 180 rpm overnight. Meanwhile, a small portion of transformed cells was spread on LB plate containing appropriate antibiotics and incubated at 37°C overnight. The successfully transformed *E.coli* cells will be further used for plasmid isolation.

2.4 Cell Biology based Methods

2.4.1 Cultivation of Eukaryotic Cells

Unless otherwise specified, all cell lines were cultured in the RPMI-1640 medium with 10% FCS and incubated in a humid atmosphere of 5% CO_2 at 37°C.

2.4.1.1 COS-7 cell line

COS-7 (ATCC®) is an adherent and fibroblast-like cell line that came from the kidney of an African Green Monkey, *Cercopithecus aethiops*. It is immortalized by transformation with a mutant strain of the Simian vacuolating virus 40 (SV40) that codes for the wild-type T-antigen. Thus, a vector bearing the SV40 promoters can be substantially replicated in COS-7 cells using the large T-antigen. COS-7 cells mainly display adherent growth to glass or plastic surfaces with RPMI-1640 complete medium. Cells can be sub-cultured with a ratio of 1:4 to 1:8 with the following protocol. The cells were rinsed with Trypsin-EDTA solution (Sigma-Aldrich) and incubated at 37°C for 10 minutes. Once the cells were detached from the surface, the trypsinization reaction was stopped by adding the RPMI-1640 + L-Glutamine medium containing 5% FCS to the cells. Then the cells were centrifuged at 4°C at 300× g for 5 minutes, and the supernatant was discarded. Afterwards, the cell pellet was thoroughly resuspended in 6-8 ml of growth medium by pipetting up and down. Finally, an aliquot of cells suspension was transferred to a new culture vessel that contained fresh growth medium. The COS-7-A2 cell line was stably transfected with pHSE3'-HLA-A2 and expressed human *HLA-A*0201*. In the growth medium of culturing COS-7-A2 cells, the antibiotic G418 (1.5 mg/ml) was added to select HLA-$A2^+$ COS-7 cells (Table 2-15).

2.4.1.2 58 $\alpha^-\beta^-$ cell line

58 $\alpha^-\beta^-$ T hybridoma cell line can be used as a recipient for TCR α/β gene transfection to obtain cell lines that express the functional TCR molecules at their surfaces. Thus, two stable transfected cell

lines, 58-JM22 and 58-FE-BV1-BJ2.3-AV7.2-AJ24.2, were created by Katherina Siewert and Latika Bhonsle (Siewert et al., 2012) to express TCR JM22 and BV1-BJ2.3-AV7.2-AJ24.2 on their surfaces (Table 2-12). Besides the TCRs, the two cell lines also expressed human CD8 molecule and an NFAT-GFP pcDNA construct. They are soluble cells and could be cultured in RPMI-1640 complete medium in addition to appropriate antibiotics for selection of stably transfected cells (Table 2-15).

Table 2-15: Antibiotic selection for stable transfection of eukaryotic cell lines

Stable Transfection	Antibiotics	Final Concentration	Cell line
HLA-A*0201	G418	1.5 mg/ml	COS-7-A2
CD8αβ	Puromycin	1.0 µg/ml	58-JM22
NFAT-sGFP	Blasticidin	3.0 µg/ml	58-FE-BV1-BJ2.3-AV7.2-AJ24.2
TCR α-chain	Hygromycin	0.3 mg/ml	
TCR β-chain	G418	1.5 mg/ml	

2.4.1.3 EBV-transducted B cell line

Human B lymphocytes can be immortalized by transduction of Epstein-Barr virus (EBV) (Hellebrand et al., 2006). In this thesis, three EBV-transducted B cell lines, EBV-B-16488, EBV-B-17490 and EBV-FE cell lines (Table 2-12), were used to investigate potential antigens. They were cultivated in RPMI-1640 complete medium as well.

2.4.2 **Determination of Cell Numbers**

The number of cells were determined by counting cells using a hemocytometer under a microscope. During cell counting, trypan blue solution (0.4%, Sigma-Aldrich) was used for staining dead cells in blue. Briefly, the cell suspension was prepared in a balanced salt solution (e.g., 1× PBS). Then 50 µl of cells was pipetted to an equal volume of trypan blue (dilution factor=2). Finally, 10 µl of cells was added to the hemocytometer and counted under a microscope. The concentration of live cells (seen as bright cells) is calculated by the percentage of visible cells using an equation below:

$$Live\ Cells\ per\ milliliter = \frac{Numbers\ of\ live\ cells\ counted}{Numbers\ of\ large\ squares\ counted} \times Dilution\ factor \times 10^4$$

2.4.3 **Freezing and Thawing of Cell Lines**

Cryopreservation is necessary to maintain cells in the long term. Storage of cells in liquid nitrogen is the best way to ensure a reliable, career-long source of cells. Moreover, a particular freezing medium containing DMSO or glycerol is used to reduce the possibility of ice crystal formation, which does damage to cells and causes cell death. Briefly, cells were centrifuged at 4°C at 300× g for 5 minutes, and the supernatant was completely discarded. Afterwards, the cell pellet was resuspended in freezing medium (Table 2-3). The optimized cell concentration is from 2×10^6 to 5×10^6 cells per milliliter. Subsequently, 1.5 ml of cells was pipetted into a sterile Corning® cryovial. Then the vial was placed in a Nalgene® freezing container (Thermo Scientific) and stored at -80°C for 48 hours. The appropriate freezing container contains isopropanol and allows the sample slowly cool down with approximately 1°C per hour. Two days later, the frozen cells were transferred into liquid nitrogen tank for long-term storage.

Cell thawing should be quickly accomplished in a 37°C water bath to avoid the ice crystals to destroy the cells. Briefly, the frozen vial was quickly removed from the liquid N_2 storage and immediately placed in a water bath (37°C) until the cells were completely dissolved. Then the cell suspension was transferred to a centrifuge tube containing 10 ml of culture medium and spun down at 300× g for 5 minutes. Subsequently, the supernatant was completely removed, and the cell pellet was resuspended in 10 ml of fresh, appropriate culture medium. Finally, the cell suspension was placed in a small T25 flask and incubated in a 5% CO_2 incubator. If necessary, antibiotics were added for transfection selection after two days of first cultivation.

2.4.4 **Cell Re-cloning for Stably Transfected T Hybridoma Cell Line**

For better investigation of potential antigens, the two stable transfected T hybridoma cell lines should satisfy two criteria. (i) The numbers of unwanted single green T cells should be as low as possible (Section 1.8). (ii) The cells should have a strong response in the presence of antigenic stimuli. These signals can be observed by fluorescence microscopy and flow cytometry analysis. Re-cloning was

employed to select a stable clone from these hybridoma cells. Briefly, 90 cells were diluted in 60 ml of fresh RPMI-1640 complete medium. Then 200 µl of cell suspension per well was added to three BD Falcon® cell culture plate (96 wells). Subsequently, three plates of cells were convolved with the plastic wrap and incubated at 37°C in an incubator for 5-7 days. Afterwards, only single cell cluster was transferred to a new BD Falcon® cell culture plate (24 wells) for further proliferation. Finally, the individual clones were stimulated by CD3 cross-linking and the activation results were analyzed by flow cytometry.

2.4.5 **Cell Transfection by FuGENE® HD Reagent**

Transfection is a process to deliver nucleic acids (either DNA or RNA) into mammalian or insect cells by various methods including lipid transfection and chemical and physical methods such as electroporation. FuGENE® HD Transfection Reagent (Promega) was used to transfect plasmids DNA into COS-7 cells. It is a non-liposomal transfection reagent to insert RNA or plasmid DNA into cultured cells.

The protocol of transfection with FuGENE® HD Transfection Reagent was optimized based on the manufacturer's protocol. Briefly, before the transfection, COS-7 cells were seeded for at least three hours at a density of 500,000 cells per dish in 3 ml of RPMI-1640 complete medium. About 2 µg of plasmid DNA was diluted in 100 µl of pre-warmed RPMI-1640 medium without serum. Then 7 µl of the FuGENE® HD Transfection Reagent was added to the diluted DNA. After vortexing briefly, the DNA was incubated at room temperature for 15 minutes. Afterwards, the transfected DNA was slowly added to the COS-7 cell suspension. Finally, the cells were incubated at 37°C for 48-72 hours. The transfection efficiency was measured by an assay appropriate for the reporter gene pcDNA-sGFP.

2.4.6 **Cell Transfection by Nucleofection**

Nucleofection also referred to as “Nucleofector Technology”, is an electroporation-based transfection method that enables the DNA to enter the nucleus directly. In this thesis, SE Cell Line 4D-

Nucleofector® X Kit L was used to transfect plasmid DNA into a COS-7 cell line, according to the manufacturer's instruction. Briefly, 1×10^6 COS-7 cells harvested by trypsinization were centrifuged at 125× g for 10 minutes at room temperature. Then the supernatant was completely removed, and the cell pellet was carefully resuspended in 100 µl of Nucleofector® Solution (Lonza). Afterwards, 2 µg of plasmid DNA was added to the cell suspension. The cell/DNA solution was subsequently transferred into a certified cuvette. Meanwhile, the appropriate Nucleofector® Program CM-130 was selected. Then the cuvette with cell/DNA suspension was inserted into the Nucleofector® Cuvette Holder (Lonza). The chosen program was immediately applied. The cuvette was taken out from the holder and incubated at room temperature for 10 minutes immediately when the transfection was finished. Thereupon, 1 ml of pre-warmed RPMI-1640 complete medium was added to the cuvette and then the cell suspension was gently transferred into a cell culture dish containing 2 ml pre-warmed RPMI-1640 complete medium. Finally, the cells were incubated in a humidified 37°C/5% CO_2 incubator. If necessary, antibiotics were added to the culture medium two days after transfection.

2.4.7 **Co-cultivation with T Hybridoma cells**

24 or 48 hours after transfection, T hybridoma cells were seeded onto the transfected COS-7 cells for reactivation assays. The transfected COS-7 cells should be rinsed twice with PBS before co-culturing with T hybridoma cells to avoid un-transfected plasmid DNA to adhere to the surface of COS-7 cells. About 1.5×10^6 of T hybridoma cells in 3 ml of RPMI-1640 complete medium were added onto the transfected COS-7 cells and then the cells were incubated in a humidified 5% CO_2 incubator at 37°C for 16 hours before reactivation assays.

2.4.8 **T hybridoma Cell Activation Assays**

2.4.8.1 T hybridoma cell activation by CD3 cross-linking

To examine whether the stably transfected T hybridoma cells could be activated or not, we analyzed the expression of NFAT-sGFP in T hybridoma cells upon CD3 activation. Briefly, 96-well plate was

coated with the antibody against mouse CD3ε (1:500 dilution in PBS) and then incubated at 37°C for 2 hours. Subsequently, the cell suspension was added to the antibody. After 16 hours incubation, the sGFP expressing cells were tested by fluorescence microscopy or flow cytometers.

2.4.8.2 T hybridoma cell activation by EBV antigens

To find out whether the stable TCR-transfected T hybridoma cells could recognize the antigens derived from EBV or not, we analyzed the expression of NFAT-sGFP in T hybridoma cells upon co-cultivation with autologous EBV-transformed B cells. After 16 hours incubation, the sGFP expression cells were observed by microscopy and the cell supernatant was examined by IL-2 measurement.

2.4.8.3 Activation of 58-JM22 by the synthetic peptide flu (58-66)

As a source of antigenic stimuli, the synthetic peptide flu (58-66) was recognized by the stable TCR-transfected T hybridoma cell line 58-JM22 (Siewert et al., 2012). The peptide was used as a positive control for the recognition of 58-JM22 cells. Briefly, 50,000 COS-7 cells (stably expressing *HLA-A*0201*) per cm^2 were seed on the plate and incubated at 37°C for 3 hours. Then the synthetic peptide flu (58-66) with a final concentration of 5 µM was pulsed on cultured COS-7-A2 cells for 3 hours before the addition of 58-JM22 cells in RPMI-1640 complete medium.

2.4.8.4 Detection of sGFP expression by fluorescence microscopy

The activation of T hybridoma cells could be directly observed by the inverse fluorescence microscopy (AxioVert 200 M, Zeiss) by the expression of the super green fluorescent protein (sGFP). Briefly, after 16 hours of co-cultivation (Section 2.4.7), expression of sGFP could be detected at 498/516 nm emission with a combination of a CCD-camera (CoolSNAP-HQ, Roper Scientific), fluorescence lamp (HXP 120, Visitron) and different Zeiss objectives (5×, NA 0.15; ∞/0, Epiplan-NEOFLUAR; 10x, NA 0.45 Plan Apochromat; 20×, NA 0.4; ∞/0-1.5 Achroplan, Korr Ph2). A GFP-filter (excitation/emission at 472 (30)/520 (35) nm, Semrock, BrightLine) was adopted to detect the sGFP expression and Cy3-filter (excitation/emission: 545 (25)/605 (70) nm, Zeiss) was used to

counter-check the auto-fluorescence of T hybridoma cells. Light microscopy was performed with phase contrast illumination while the exposure times were 600 ms for the 5× and 20× objectives and 100 ms for the 10× objective. Images were taken in three channels (transmitted light illumination, sGFP fluorescence, and Cy3 fluorescence) by the software "MetaMorph V6.3r6" (Vistron, Puchheim, D) and edited with the software "ImageJ 1.51f" (Wayne Rasband, National Institutes of Health, USA).

2.4.8.5 Detection of IL-2 by ELISA

In addition to fluorescence microscopy, the activation of T hybridoma cells could also be indirectly detected by quantitative Enzyme-Linked Immunosorbent Assay (ELISA) for measurement of IL-2 in the cell supernatant. In this thesis, Mouse IL-2 ELISA Ready-SET-Go® kit (eBioscience) was employed, according to the manufacturer's introduction. About 100 µl of cell supernatant was taken to do the IL-2 measurement. A standard curve for IL-2 is performed with the concentrations between 5 pg/ml and 1000 pg/ml. The detection limit of the kit is 5 pg/ml or 0.25 pg/well.

2.4.9 **Flow Cytometry Analysis**

Flow cytometry is used to detect the cell surface markers and intracellular sGFP expression upon CD3 activation. Briefly, a cell suspension was prepared in PBS at a density of 10^5-10^7 cells/ml. After centrifugation at 4°C at 300× g for 5 minutes, the cell pellet was rinsed twice with 150 µl of FACS buffer (Table 2-3). Then the cell pellet was resuspended in 50 µl of FACS buffer containing diluted primary antibody and incubated in the darkness on ice for 30 minutes. Afterwards, cells were rinsed twice with FACS buffer and then incubated on ice with the secondary antibody solution for 20 minutes. Finally, the cell pellet was resuspended in FACS buffer containing dead cell counterstain (e.g., Topro-3) and then examined by the FACSCslibur flow cytometer with two excitation lasers for 488 nm and 633 nm. Data were collected and analyzed by the software FlowJo V10.0.

2.4.10 Identification of Single T Cells from CSF Specimens

2.4.10.1Workflow

The analysis of TCR repertoire from the blood and CSF specimens of MS patients is accomplished with the procedure illustrated in Figure 2-2.

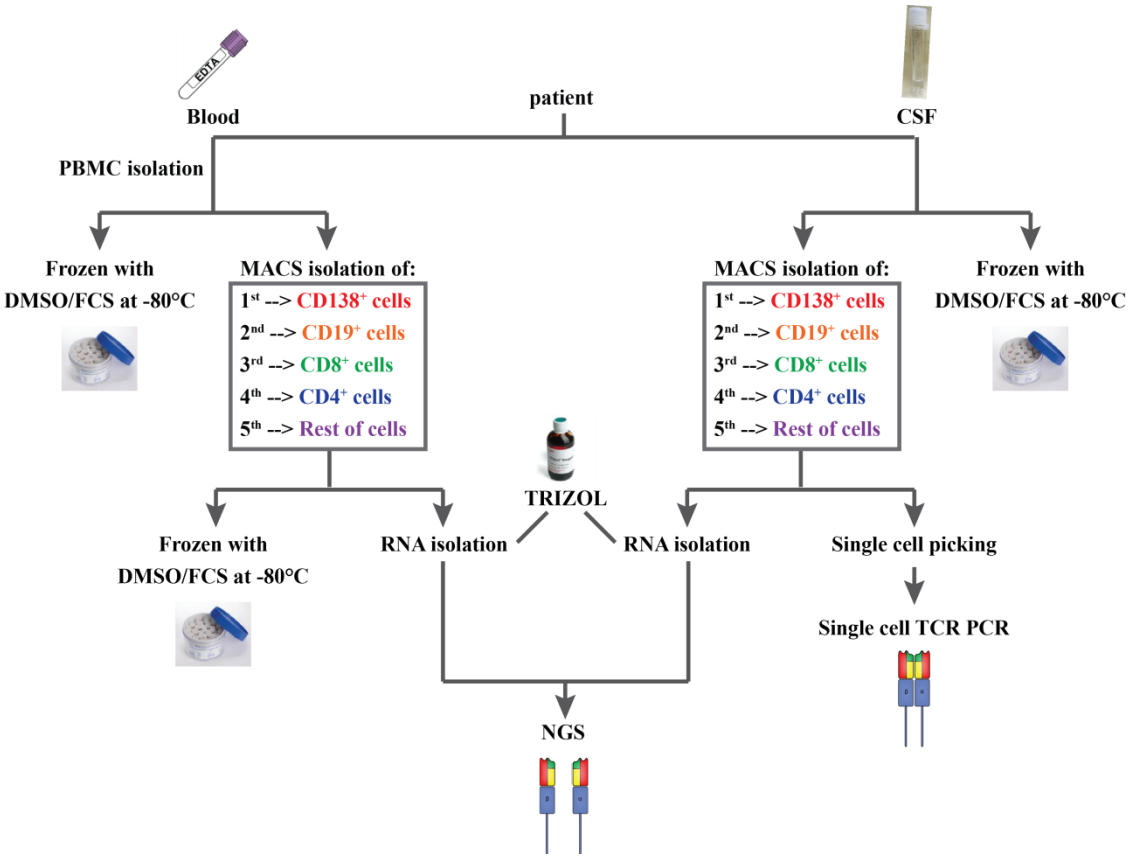

Figure 2-2: Workflow of TCR repertoire analysis from the blood and CSF samples from MS patients

After obtaining fresh 10 ml of blood and CSF samples from one MS patient, we immediately divided the blood and CSF samples into two parts: one part was instantly stored at -80°C in freezing medium; the other part was used for TCR/BCR analysis. This part performed in cooperation with Dr. Kathrin Held and Dr. Eduardo Beltrán. $CD138^+$ cells (plasma cells), $CD19^+$ cells (B cells), and $CD8^+$ and $CD4^+$ T cells were isolated by MACS® technology (Miltenyi Biotec). Subsequently, each cell population was also divided into two aliquots: one aliquot was employed for NGS; another aliquot was isolated under the microscope and then used for single cell αβ-TCR characterization.

2.4.10.2Initial processing of CSF specimens

CSF samples were centrifuged at 4°C at 300× g for 10 minutes, and the cell pellet was either processed with MACS isolation for T cell subsets (Section 2.4.10.3) or frozen in 1 ml of FCS which contained 10% DMSO (Section 2.4.3). For long-term storage, the cells should be kept at -80°C with a freezing medium for two days and then transferred into liquid nitrogen.

2.4.10.3Isolation of T-cell subsets

After centrifugation, the cells were used for isolation of the $CD4^+$/$CD8^+$ T cell subsets, using T Cell Isolation Kits (Miltenyi Biotec). Briefly, 1×10^7 cells were resuspended in 40 µl of MACS® buffer (Table 2-3) and mixed with 10 µl of $CD8^+$ T Cell Biotin-Antibody Cocktail. The cell suspension was incubated at 4°C for 5 minutes. In addition to 30 µl of MACS® buffer, we added another 20 µl of $CD8^+$ T Cell MicroBead Cocktail and incubated the cell suspension at 4°C for 10 minutes. Once the MACS® column was mounted on the magnetic separation device, the cell suspension was loaded onto the column, and the $CD8^+$ T cells were collected in the flow-through. After rinsing the column with 3 ml of MACS® buffer, 5 ml of MACS buffer was added onto the column and then the non-$CD8^+$ T cells were immediately flashed out by firmly pushing the plunger into the column. These non-$CD8^+$ T cells were used for the isolation of $CD4^+$ T cells, plasma cells ($CD138^+$) and B cell ($CD19^+$).

2.4.10.4Isolation of single T cells

The isolated T cells were diluted until averagely one cell in 2 µl of MACS buffer, which were observed clearly under the microscope. Single living T cells were isolated with a pipette, transferred into a PCR tube with 2 µl of MACS buffer, and immediately placed on dry ice. These individual T cells will be further used for single cell αβ-TCR characterization (Section 2.2.9).

2.5 Immunology-based Methods

2.5.1 Preparation of Tissue Cryosections

Human tissue blocks were taken from -80°C and placed in a Cryostat (CM3050 S, Leica) where 10 µm cryostat tissue sections were generated. Cryosections were placed on PET-membrane slides 1.0 (Zeiss) that were pretreated following these procedures: these slides were firstly baked at 180°C for 4-5 hours. Then they were rinsed with decontamination solutions and RNase-free DEPC-treated water. After 30 minutes of UV-irradiation, 100 µl of diluted Poly-Lysine solution was coated on the slides for 1 hour. Then the Poly-Lysine solution was diluted with DEPC-treated water and completely removed. Finally, the slides were dried at room temperature for 30 minutes in the presence of UV-irradiation. The preparation of slides was carried out in a DNase/RNase-free chamber. Once the human tissue blocks were cut and mounted correctly, the cryosections were stored at -80°C.

2.5.2 Immunofluorescence of the Immune Cells in Human Tissue

Immunofluorescence was used to detect the different immune cells in human tissues with commercial antibodies (Table 2-10). The general staining protocol was as followed: cryosections were fixed in 100% Acetone for 10 minutes and then blocked with 2% BSA (Sigma-Aldrich) in PBS for 20 minutes. Subsequently, cryosections were incubated with the diluted primary antibody for one hour. After rinsing with PBS, the cryosections were incubated with the diluted secondary antibody for 30 minutes. The antibodies had already been diluted in PBS with optimized ratios. After rinsing with PBS, cryosections were stained with DAPI for 5 minutes and then attached with a glass cover with the help of the fluorescent mounting medium (Dako). All the incubation steps were carried out in a humidified dark staining chamber. The isotype control antibody instead of primary antibody served as a negative control. An Axioplan 2 microscope (Zeiss) was employed to analyze the staining results of immune cells on human tissue cryosections.

2.6 Laser Capture Microdissection

Single activated $CD8^+$ T cells were isolated by laser capture microdissection (LCM) for further αβ-TCR characterization. Before cell isolation, the activated $CD8^+$ T cells should be visualized under the fluorescence microscopy using an optimized fluorescent staining method. Based on the immunofluorescence method described in Section 2.5.2, the improved protocol should be finished within 15 minutes. To avoid RNA degradation, monoclonal antibodies against CD8α and CD137 were used to stain the activated $CD8^+$ T cells on human brain cryosections. In addition, CD8α antibody was labeled with the fluorescence dye Cy3 using a Cy3™ Labeling Kit (Amersham). The details of this optimized method are described in Section 3.3.1.

Once covered with isopropanol, the cryosection was placed on P.A.L.M Axiovert 200 M microscope for single cell isolation. The apparatus consists of the fluorescence lamp HXP 120 (Visitron), the Microscopy Camera AxioCam MRm Rev.3 FireWire (Zeiss), the LD Plan-NEOFLUAR objective 40×/0.6 Korr, ∞/0-1.5 (Zeiss), the Robo Mover and the software "P.A.L.M. Robo Software V4.6" (P.A.L.M. Microlaser Technologies). Before the evaporation of isopropanol, single T cells were marked on the computer screen within 30 minutes. After isopropanol was completely evaporated, the single circled cells were isolated from dried cryosection by a RoboMover (Zeiss) and catapulted into a lid of PCR reaction tubes by laser pressure catapulting. The lid was coated with mineral oil to enhance the adhesion of cells. The RT reaction mix (Section 2.2.9.2) was immediately added to the tube since the single T cell was isolated. Then the cell sample was centrifuged at 20,800× g for 5 minutes. Finally, an RT reaction was subsequently performed at 50°C for 30 minutes.

In addition, the whole procedures including staining and microdissection were carried out in an independent, closed and UV-irradiated room to prevent the contaminations. The working areas and devices were rinsed with decontamination solutions before and after usage.

2.7 Characterization of Antigen Coding Plasmids from COS-7 cells

2.7.1 Isolation of Candidate COS-7 Cells by Micromanipulation

COS-7 cell line served as APC in this thesis. They are adherent cells, which were superposed with T hybridoma cells that stably express CD8, activated TCR and sGFP molecule under the control of NFAT promoter. The isolation of positive COS-7 cell was controlled by the manipulator monitor and observed through the MetaMorph® Microscopy Automation & Image Analysis Software. Briefly, once a cluster of green fluorescing T hybridoma cells was detected, the underlying COS-7 cell was aspirated into a customized glass capillary (beveled end, 14 µm inner diameters, +/- heat formed spike, +/- flexible material, BioMedical Instruments). The capillary was fixed on an LN25 Mini micromanipulator and connected to a mineral oil-filled pipe. The latter device was controlled by a CellTram Vario microinjector that allowed applying slight changes of pressure. The candidate COS-7 cell was absorbed in the capillary along with some microliters of culture medium in the dish and immediately expelled into a PCR tube that contained 7 µl of DEPC treated H_2O. Finally, the cell was spun down and further employed for the plasmid recovery PCR (Section 2.2.10).

2.7.2 Reconstruction of PCR Products into Expression Plasmids

The PCR products were inserted into an expression vector with directional TOPO TA cloning technology. The pcDNA™ 3.1 Directional TOPO® Expression Vector Kit (Invitrogen) was employed for DNA reconstruction, and the details of ligation mix are presented below:

Reagent	Volume (µl)	Final concentration
RNase-free H_2O	3.5	-
Salt Solution	1	0.2 M of NaCl, 0.01 M of $MgCl_2$
pcDNA™ 3.1 D/V5-His-TOPO® Vector (15 to 20 ng/µl)	0.5	7.5 to 10 ng
Diluted PCR-Product	1	1 ng
Total	6	

The ligation reaction was carried out at room temperature for 30 minutes and then placed overnight at 16°C. Once the PCR product was successfully ligated into a vector, the plasmids were then

precipitated in Ethanol as described in Section 2.2.7. Afterwards, the reconstructed plasmids were transformed into electrocompetent ElectroMAX™ DH10B™ T1 Phage-Resistant Competent Cells (Invitrogen) by electroporation (Section 2.3.6). Finally, the plasmids were amplified and isolated from 2 ml of the *E.coli* cultures (Section 2.2.2).

2.7.3 **Reactivation of T Hybridoma Cells**

The isolated plasmids were co-transfected with the plasmids coding for human HLAs into the COS-7 cells as introduced in Section 2.4.6. These co-transfected COS-7 cells were employed to examine the reactivation of T hybridoma cells. The antigen coding plasmids were enriched through several sub-pools of *E.coli* cultures (Section 2.7.4) if the activation was detected by the fluorescence microscopy. During the subpooling, it was necessary to examine the reactivation of T hybridoma cells to ensure that the obtained signal was increased due to enrichment. In addition, new software ZEN 2.0 (Zeiss) for the microscope was employed for searching the activated cells from the high cell numbers of samples quickly and efficiently. It can automatically record coordinates and take photos for each sample with different fluorescent lights.

2.7.4 **Antigen Coding Plasmids Enrichment by plasmid subpools**

If the reactivation of T hybridoma cells is detected under the fluorescence microscope as described in Section 2.7.3, the antigen coding plasmids will be identified in subpools of *E.coli* culture (Figure 2-3). Briefly, after the plasmids transformed into *E.coli* (ElectroMaxDH10B), the bacteria were grown in liquid LB^{amp} medium, and a small aliquot was plated out on LB^{amp} agar plates for an estimation of the initial clone number (e.g., 300,000) in Figure 2-3 (A). Usually, less than 1/1000 of antigen plasmids diluted with non-relevant bystander plasmids was observed. Thus, to identify the antigen coding plasmid from bystanders, the subpools of *E.coli* culturing with limited numbers of bacteria were generated (Figure 2-3, B). In the first round of *E.coli* subpools, 30 probes containing 1/10 (e.g., 30,000) of the original clone numbers of the same *E.coli* culture were added to a 96-well deep flat-bottom block with 1.25 ml of LB medium containing the appropriate antibiotics. Meanwhile, exact

numbers of *E.coli* was plated to estimate the real clone numbers. After incubation for 16 hours, 1 ml of cell suspension from the bulk *E.coli* culture was taken for plasmid isolation (Section 2.2.2). Then the reactivation assay from the 30 probes was subsequently carried out in the presence of antigen coding plasmids (Section 2.7.3). If the activated signal was received in one probe (Figure 2-3, #5), the second round of *E.coli* subpools containing another 30 probes began. The number of *E.coli* clones in each probe was 1/10 (e.g., 30,000) of clone numbers in the first round of *E.coli* subpools. The following procedure was as same as the one in the first round of *E.coli* subpools.

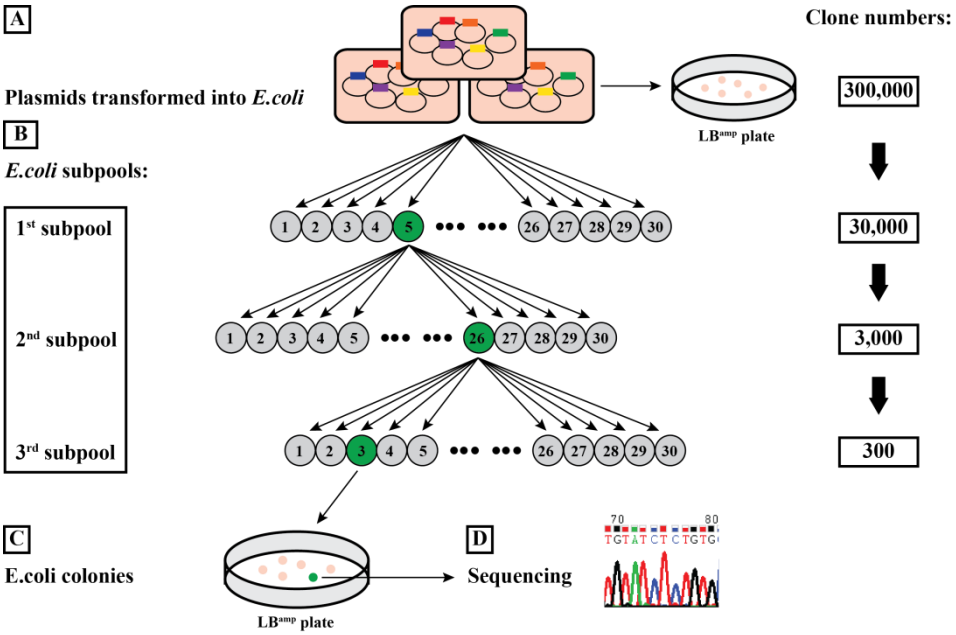

Figure 2-3: Workflow for the enrichment of positive *E.coli* clones in subpools

The characterization of antigen coding plasmids was accomplished in subpools of *E.coli* culture according to this scheme, and the explanation is given in detail in Section 2.7.4.

When the antigen coding sequence was present at a dilution of 1:300 or lower (Figure 2-3, 3rd subpool) in the final stage of antigen isolation, at least 300 clones of *E.coli* were cultured on LB plates containing the appropriate antibiotics overnight at 37°C (Figure 2-3, C). Then 30 connected colonies are marked as presented in Figure 2-4, isolated with autoclaved toothpicks and incubated in a volume of 20 ml LB medium with the appropriate antibiotics for 16 hours. Afterward, 2 ml of *E.coli* culture from each bacteria colony was taken for plasmids purification, and then reactivation assay was performed. Once the positive probe containing the antigen coding plasmids was determined, the 30

E.coli colonies were separately incubated in 3 ml of LB medium with the appropriate antibiotics overnight at 37°C. Each bacteria colony containing the same plasmids was examined by final reactivation assay. Finally, the antigen coding plasmid from the potentially tested *E.coli* subpool was successfully identified, isolated and sequenced (Figure 2-3, D).

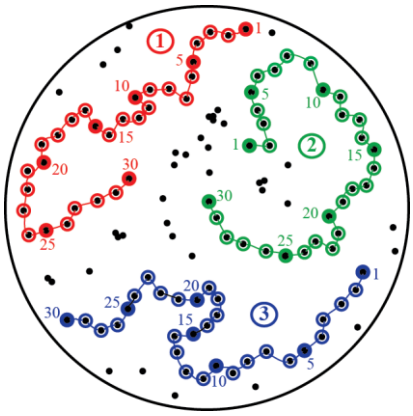

Figure 2-4: Streets of 30 bacteria colonies were marked on LB^{amp} agar plate

About 300 different clones identified in a positive pool were plated on LB^{amp} agar plates after several rounds of *E.coli* subpools. Each plate had at least 90 colonies. Subsequently, lines with different colors (①-③) connected 30 single colonies, and then these colonies were picked separately and sorted individually into subpools.

3 Results

3.1 Immunofluorescence of the Immune Cells on Human Tissue Cryosection

T or B lymphocytes are considered to be the principal effector cells in the pathogenesis of MS. However, many other types of immune cells such as DCs, macrophages, and NK cells may also cross the BBB, infiltrate into the lesions, and attack the CNS structures in the process of MS. They may further serve as the antigen presenting cells (APCs) to present the self-antigens to the autoaggressive T cells or B cells in an immune reaction.

Table 3-1: Detection of different immune cells with the specific antibodies

√√: Specific staining of the target cells. √: Faint staining of the target cells and unspecific staining. ×: No staining of target cells but unspecific staining. **Bold font**: Two antibodies were verified specifically to stain the activated $CD8^+$ T cells on the brain sections by the optimized rapid immunostaining method.

Cell Marker	Antibody	Isotype/Clone ID	Tonsil	Brain
T cell	CD3	IgG/Polyclonal	√√	√√
$CD8^+$ T cell	**CD8*α***	**IgG1/LT8**	√√	√√
	CD8β	IgG2a/2ST8.5H7	√√	√√
		IgG1/5F2	√√	√
		IgG2a/F-5	×	×
Activated cell	CD69	IgG1/FN50	√√	√√
	CD134	IgG1/ACT35	√√	×
		IgG1/7H163	√	×
		IgG2a/443318	×	×
		IgG2a/H-10	×	×
		IgG2a/W4-3	√√	√
	CD137	IgG/Polyclonal	×	×
		IgG1/BBK-2	√√	√√
NK cell	CD57	IgM/HNK-1	×	×
Dendritic cell	CD83	IgG1/HB15e	√√	√√
Macrophage	CD68	IgG1/EBM11	√√	√√
		IgG1/KP1	√√	√√
		IgG3/PG-M1	√√	×

It is still unknown what the functions of the immune cells in the MS lesions are and how this is related to the pathogenesis of MS. Here, we employed the immunofluorescence staining to visualize the immune cells on frozen brain sections of MS patients. It is of great interest to figure out the relationship between the $CD8^+$ T cells and the other immune cells in the MS brain lesions. However, many commercial antibodies were designed for the application of the paraffin sections, and only a few

of them could be used for the frozen sections, in particular for the human brain. In the awareness of the disadvantages, we firstly examined the antibody candidates on the frozen tonsil sections from the donors. Only the antibodies that stained well on tonsil could be used for frozen brain sections from MS patients. We list six types of immune cells and different antibodies that were tested here (Table 3-1). Immunofluorescence staining reveals these target cells on tonsil and brain tissues, which are presented in Figure 3-1 to 3-3. In addition, the isotype controls of these antibodies testing on tonsil and brain sections are summarized in supplementary data (Figure 5-1 to 5-3).

Previous research discovered that clonally expanded $CD8^+$ T cells were detected both at perivascular and intraparenchymal sites of the brain from MS patient FE (Babbe et al., 2000). Here, we attempted to validate this result and detect $CD8^+$ T cells in brain tissues from MS patient FE. Figure 3-1 shows that the T cells and its subset-$CD8^+$ T cells were specifically detected on human tonsil (A1-A3) and MS brain (B1-B3) sections by four commercial antibodies. However, the $CD8^+$ T cells could not be detected by another antibody (Clone F-5, A5 and B5) against CD8 β-chain. Conversely, the unspecific staining was discovered in the isotype control of this antibody (Figure 5-1, A5 and B5). Therefore, the staining results demonstrate that there are many T cells infiltrated in the brain lesions of MS patient FE, expecially the $CD8^+$ T cells, which is in accordance with the previous discovery (Babbe et al., 2000).

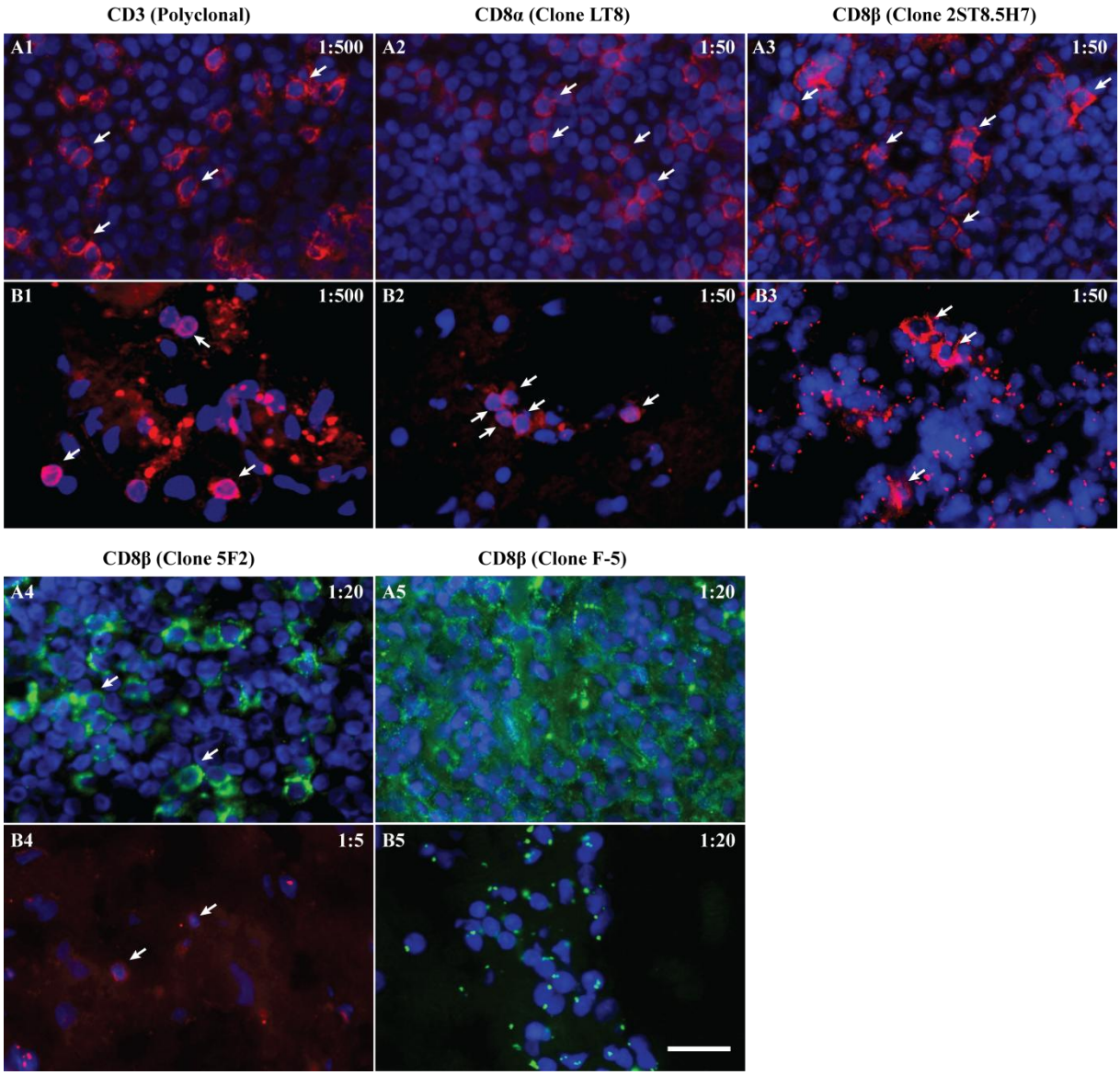

Figure 3-1: Immunofluorescence staining of immune cells in tonsil and brain tissues. (Part 1)

The $CD8^+$ T cells were detected on human tonsil section **(A)** and MS brain sections **(B)** by different commercial antibodies. All nuclei were stained with DAPI (blue). Red and green dyes were used to visualize the $CD8^+$ T cells. The names of antibodies (Clone ID) are written on the top of each image, and the working dilution ratios are labeled on each picture. The specific staining of $CD8^+$ T cells is marked with the solid arrow. Scale bar=20 µm.

In brain lesions of MS patients, the activated $CD8^+$ T cells are more likely to be the dominators of inflammatory demyelination (Dornmair et al., 2003). These activated cells might be the clonally expanded $CD8^+$ T cells. Here, we could use a T cell activation marker to identify the activated $CD8^+$ T cells in MS brain tissue morphologically. We examined several antibody candidates against T cell activation markers, such as CD69, CD134, and CD137 (Table 3-1). CD69 is the earliest glycoprotein appeared on the inducible cell surface during the activation of T lymphocytes and NK cells (Ziegler et al., 1994). The tested antibody against CD69 specifically detected its target cells both on tonsil and brain sections (Figure 3-2, A1 and B1). Furthermore, CD134 and CD137, as the other stimulatory checkpoint molecules, are up-regulated on the most recently antigen-activated T cells within inflammatory lesions (Anderson et al., 2012; Carboni et al., 2003). In the five anti-CD134 antibodies, two antibodies did not detect their target cells on tonsil and brain sections (Figure 3-2, A4, A5, B4, and B5). However, the activated T cells were specifically detected by the other three anti-CD134 antibodies on tonsil sections (Figure 3-2, A2, A3, and A6). Unfortunately, the former two antibodies stained other targets on brain sections (Figure 3-2, B2 and B3). The shape of these cells suggests that they might be neurons or astrocytes. For the two tested antibodies against CD137, only one antibody specifically stained its target cells both on tonsil and on brain sections (Figure 3-2, A8 and B8), but another one had unspecific staining in the isotype controls (Figure 5-2, A7 and B7).

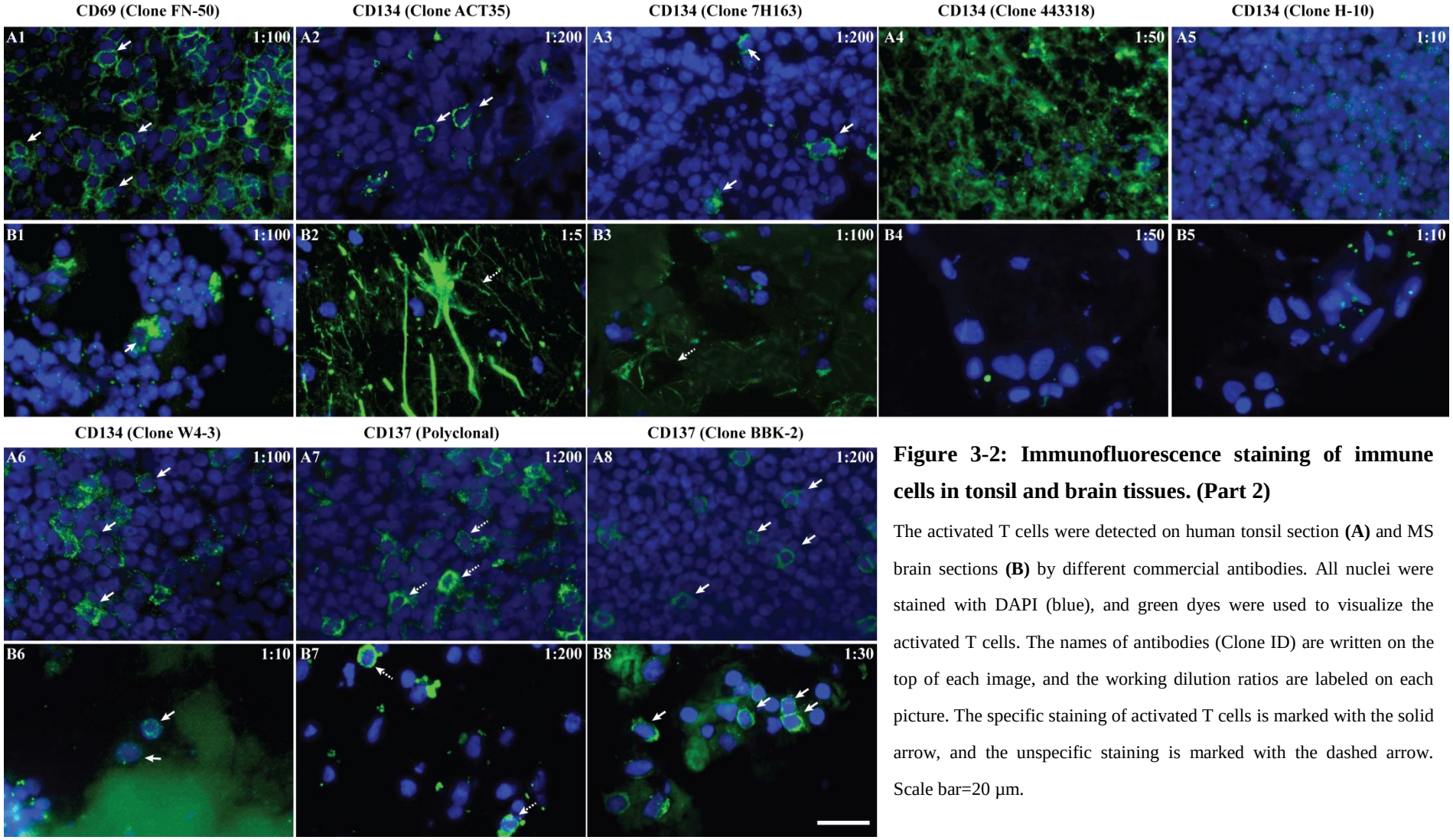

Figure 3-2: Immunofluorescence staining of immune cells in tonsil and brain tissues. (Part 2)

The activated T cells were detected on human tonsil section **(A)** and MS brain sections **(B)** by different commercial antibodies. All nuclei were stained with DAPI (blue), and green dyes were used to visualize the activated T cells. The names of antibodies (Clone ID) are written on the top of each image, and the working dilution ratios are labeled on each picture. The specific staining of activated T cells is marked with the solid arrow, and the unspecific staining is marked with the dashed arrow. Scale bar=20 µm.

Moreover, we tested several antibodies against the cell surface markers CD57, CD83, and CD68 for the natural killer cells, dendritic cells and macrophages (Table 3-1). The staining results show us that the NK cells were not detected by the monoclonal antibody (mAb) against CD57 (Clone HNK-1) either on tonsil or brain sections (Figure 3-3, A1-B1), because the unspecific staining was also observed in the isotype controls of the antibody (Figure 5-3, A1 and B1). Furthermore, three commercial antibodies against CD83 and CD68 specifically detected their target cells in tonsil and brain tissues, especially in the perivascular space of the brain tissue (Figure 3-3, A2-A4 and B2-B4), but another anti-CD68 antibody (Clone PG-M1) could not stain its target cells on brain sections (Figure 3-3, B5).

In conclusion, the activated $CD8^+$ T cells could be specifically detected by the anti-CD8α antibody (Clone LT8, 1:50 dillution) and the anti-CD137 antibody (Clone BBK-2, 1:200 dillution) on frozen brain sections. These visiable T cells later were isolated by laser microdissection and used for single cell αβ-TCR characterization. In addition, dendritic cells and macrophages were also detected in the brain lesions of MS patient FE. It demonstrates that except T lmphocytes, other immune cells might be infiltrated in the CNS lesions of MS patients during MS progress, which needs more evidences in the future.

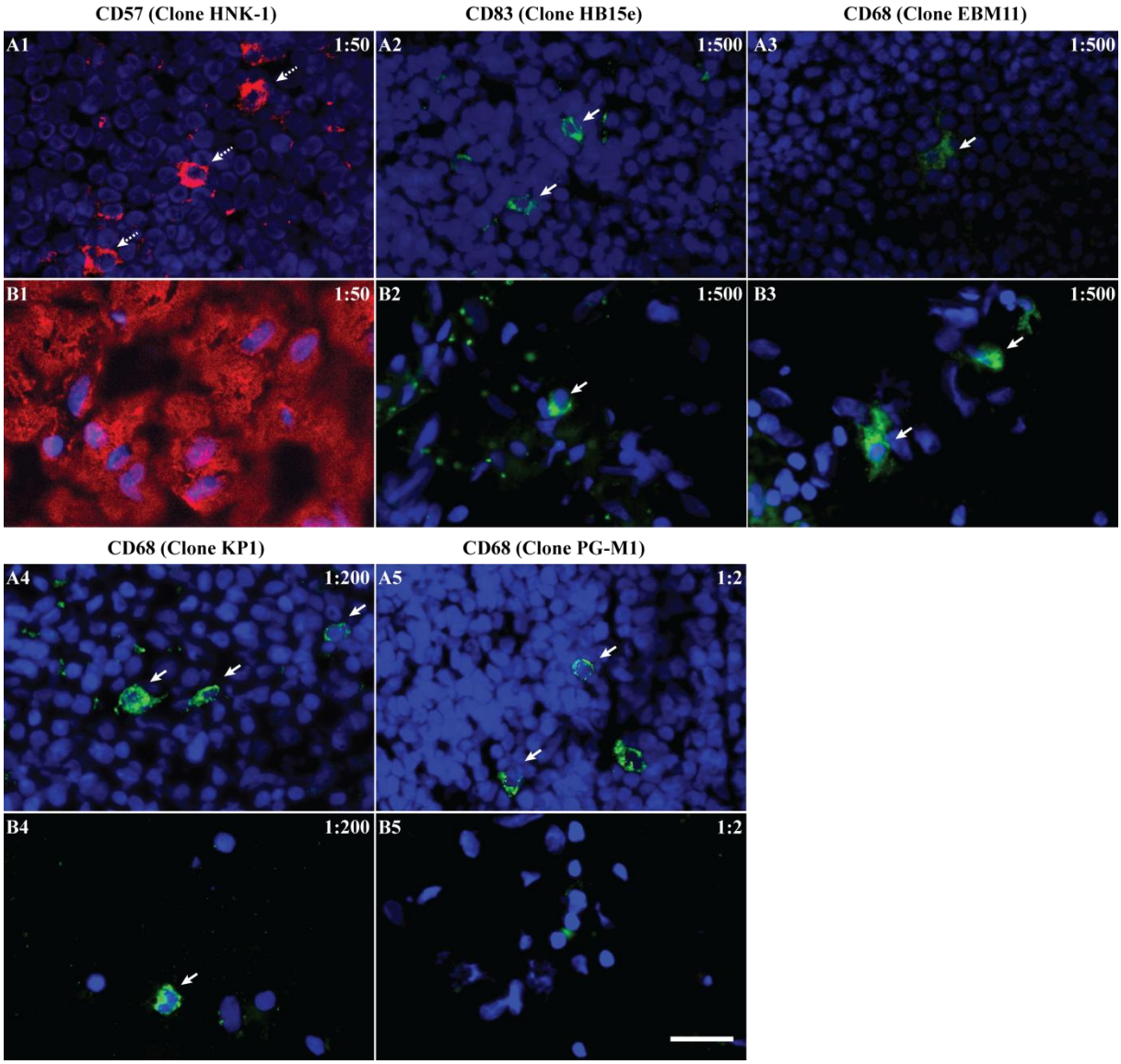

Figure 3-3: Immunofluorescence staining of immune cells in tonsil and brain tissues. (Part 3)

The NK cells, dendritic cells and macrophages were detected on human tonsil section **(A)** and MS brain sections **(B)** by different commercial antibodies. All nuclei were stained with DAPI (blue). Red and green dyes were used to visualize the NK cells, dendritic cells and macrophages. The names of antibodies (Clone ID) are written on the top of each image, and the working dilution ratios are labeled on each picture. The specific staining of NK cells, dendritic cells and macrophages is marked with the solid arrow, and the unspecific staining is marked with the dashed arrow. Scale bar=20 µm.

3.2 Morphological Identification of Activated CD8$^+$ T Cells in the Lesion of MS Brain

During the thesis, some brain tissue blocks from MS patient FE were available to investigate the distribution of CD8$^+$ T cells in the lesions. In the previous analysis of the brain tissue blocks by Anna G. Niedl, block #12 contains higher numbers of CD8$^+$ T cells than other blocks, especially in the meninges, perivascular and parenchymal spaces. However, it was still unknown whether these CD8$^+$ T cells were activated and proliferated to the clonally expanded CD8$^+$ T cells or not.

The monoclonal antibodies LT8 against CD8a and BBK-2 against CD137 specifically detected their targets on frozen brain sections without unspecific staining background (Section 3.1). Therefore, we employed the two antibodies to identify the activated CD8$^+$ T cells in the different brain blocks of MS patient FE. Before staining, the purified monoclonal antibody anti-CD8α was labeled with the fluorescent dye by the Cy3 mAb Labelling kit (Amersham). After the fluorescence staining as described in Section 2.5.2, we detected the activated CD8$^+$ T cells under the fluorescence microscope. The numbers of the activated CD8$^+$ T cells in the different blocks were calculated by the software "ImageJ 1.48i".

Figure 3-4 presents the distribution of the activated CD8$^+$ T cells in three brain blocks (#2, #6, and #12). Block #2 has the least numbers of CD8$^+$ T cells as well as the lowest numbers of activated CD8$^+$ T cells (CD137-positive) amongst the brain tissue blocks. Another two blocks (#6 and #12) have more CD8$^+$ T cells, some of which are also demonstrated to be CD137-positive. Many clusters of activated CD8$^+$ T cells were found in the perivascular space of brain blocks (#6 and #12 with red frame). These activated CD8$^+$ T cells were composed of several T-cell clusters that are presented in Figure 3-5. In block #2, the T cell clusters were rarely detected, but only single activated CD8$^+$ T cells showed up in this part of MS brain, where obviously no inflammation occurred. On the contrary, many CD8$^+$ T cell clusters were observed in block #6 and #12, most of which were activated (CD137-positive). We assume that these two brain tissue blocks might be the parts of MS lesions, which were infiltrated by inflammatory CD8$^+$ T lymphocytes. Thus, these T cells will subsequently be isolated by laser

microdissection to identify the paired αβ-TCRs in the single cell level. The expanded TCR clones identified from the brain lesions might belong to the auto-aggressive $CD8^+$ T cells underlying the pathogenesis of MS.

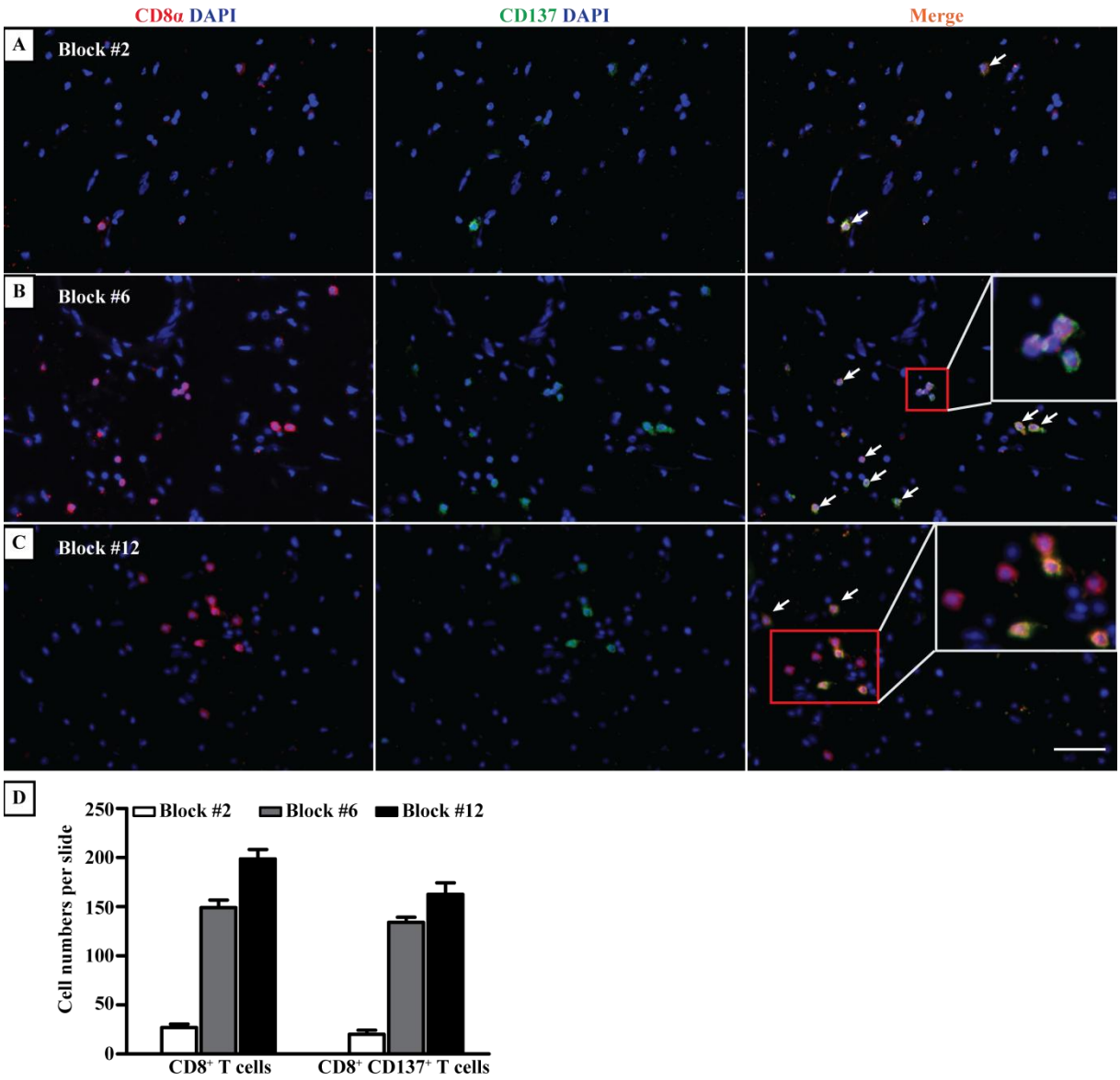

Figure 3-4: Identification of activated $CD8^+$ T cells in different brain blocks of MS patient FE

8-10 µm of cryosections from frozen brain biopsies block #2 **(A)**, #6 **(B)** and #12 **(C)** were employed for the fluorescence staining. **Left panel:** $CD8^+$ T cells were stained with anti-CD8α-Cy3 antibody (red). **Middle panel:** activated T cells were stained with anti-CD137 antibody as well as the Alexa Fluor® 488-labeled secondary antibody anti-mouse IgG (H+L) (green). **Right panel:** Double-positive cells for CD8α and CD137 were merged (yellow). All nuclei were stained with DAPI (blue). The cluster of activated $CD8^+$ T cells is framed out. **(D)** The comparison of the numbers of $CD8^+$ T cells and activated $CD8^+$ T cells per slide were plotted for each brain blocks. Red frame: activated $CD8^+$ T cell clusters; white arrows: activated $CD8^+$ T cells. Scale bars=50 µm.

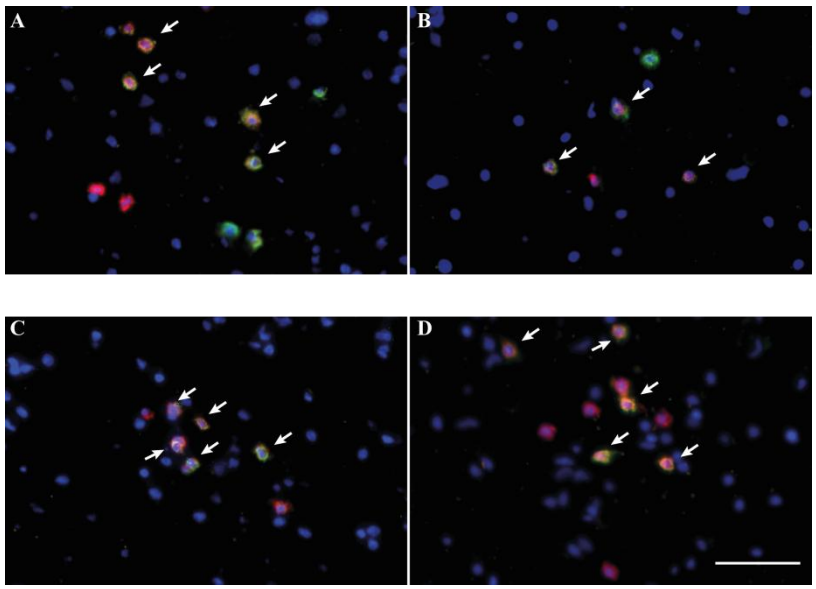

Figure 3-5: Clusters of activated CD8$^+$ T cells infiltrated in the MS brain tissue

8-10 µm of cryosections from brain block #12 of MS patient FE were stained with primary antibodies anti-CD8α-Cy3 (red) and anti-CD137 as well as the secondary antibody anti-mouse IgG (H+L)-Alexa Fluor® 488 (green). All nuclei were stained with DAPI (blue). The double-positive cells were appeared in yellow and indicated by arrows. **(A-D)** Four clusters of activated CD8$^+$ T cells were detected by fluorescence microscopy. Subsequently, single activated CD8$^+$ T cells in the clusters were isolated by laser microdissection for the characterization of paired αβ-TCRs. Scale bars=50 µm.

In the spaces of brain tissue where T-cell clusters were found, most of the activated CD8$^+$ T cells were detected to contact tightly to another cells (Figure 3-6). The contact site between the activated CD8$^+$ T cell and its contacting cell was clearly discovered under the confocal microscope (Figure 3-6, D1-D3). In the future, it will be interesting to figure out the cell types of the contacting cells and the relationship with the activated CD8$^+$ T cells that were contacted.

In summary, we successfully identified the activated CD8$^+$ T cells in the different brain tissue blocks of MS patient FE, and also found that these T cells showed up in clusters in the MS lesions. To characterize expanded TCR clones of these activated CD8$^+$ T cells, single T cells will be isolated to do the amplifications of TCR α- and β-chains. In addition, many activated CD8$^+$ T cells in the lesions were found to contact another cells that might be their targets expressing the MS-related antigens. This hypothesis will be verified in the future.

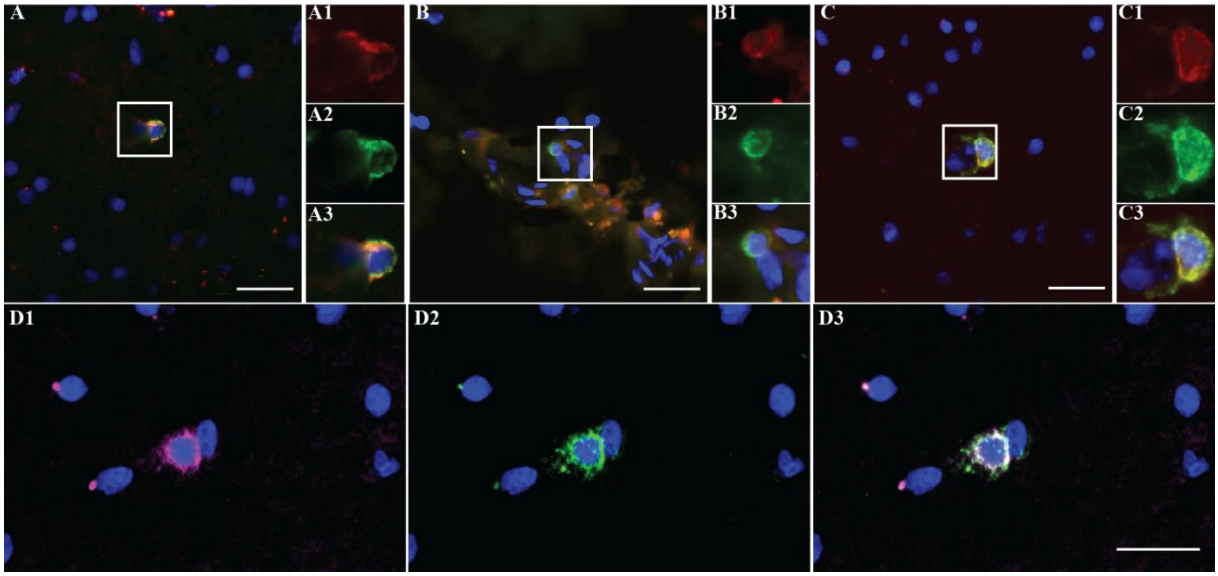

Figure 3-6: Detection of the activated CD8$^+$ T cells in directly contact with another cells in the MS brain tissue

8-10 µm of cryosections from frozen brain biopsy of MS patient FE were stained with the primary antibodies anti-CD8α-Cy3 (**A1-D1**, red) and anti-CD137 as well as the secondary antibody anti-mouse IgG (H+L)-Alexa Fluor® 488 (**A2-D2**, green). The double-positive cells appeared in yellow (**A3-D3**). All nuclei were stained with DAPI (blue). The activated CD8$^+$ cells contacted another cell are framed out (**A-C**). The confocal microscopy was used to get better quality of images for activated CD8$^+$ T cell and its contacting cell (**D1-D3**). Observation at higher magnification is both shown in the red channel and green channel. Scale bars=20 µm.

3.3 Identification of Matching TCR α- and β-Chains from MS Patients

MS is a relapsing inflammatory autoimmune disorder and characterized by repeated inflammatory infiltration of the CNS. Progressive demyelination together with axonal loss causes the chronic disability of human body (Hohlfeld and Wekerle, 2001). CD8$^+$ T cells prevail and conduct the direct attack on CNS tissue structure in all infiltrating cell populations (Hohlfeld et al., 2016). Therefore, characterization of TCR molecules initiating from autoaggressive CD8$^+$ T cells may bring further insightful opinions into the pathogenesis of MS. In addition, MS is initiated by the migration of pathogenic T cells from the peripheral blood over the BBB to the CNS. The brain-infiltrating CD8$^+$ T cells were demonstrated to persist as clonal expansions in the CSF and blood of MS patient (Skulina et al., 2004). Therefore, identification of clonally expanded pathogenic T cells is vital for understanding the pathogenesis of MS.

A technology to characterize the matching TCR α- and β-chains of single T cells was established earlier (Kim et al., 2012; Seitz et al., 2006). Here, this unique technology was optimized to generate the matching TCR α- and β-chains of the putatively pathogenic T cells from MS patients. Firstly, an approach of rapid immunostaining was improved for better distinguishing the single activated $CD8^+$ T cells from bystander T cells in MS brain tissues (Section 3.3.1). Secondly, the different effective treatments on brain tissues were explored for minimizing the RNA degradation (Section 3.3.2). Thirdly, the approach of amplifying the αβ-TCRs of single T cells was improved to obtain a high yield of the matching TCR α- and β-chains (Section 3.3.3). Fourthly, several TCR β-chains of autoaggressive $CD8^+$ T cells were identified from the frozen brain biopsies of MS patients (Section 3.3.4). Lastly, TCR α/β chains of migrated T cells were generated from the CSF of MS patients (Section 3.3.5).

3.3.1 Rapid Immunostaining of Single $CD8^+$ T Cells for Microdissection

MS patient FE is characterized by large $CD8^+$ T-cell populations infiltrated in the brain lesions (Babbe et al., 2000). Biopsy samples are necessary to characterize these MS-related $CD8^+$ T cells by the current technologies (Kim et al., 2012; Seitz et al., 2006). The single activated $CD8^+$ T cells have to meet three criteria before LCM: Firstly, T-cell appearance (relatively round, 8-20 μm in diameters) is displayed with the cell's morphology. Secondly, the T cells of interest carry the CD8 molecules on the surface along with the activation markers (such as CD69, CD134, and CD137). Lastly, the single isolated T cells still contain enough intact mRNA for subsequent TCR characterization. Immunostaining of activated $CD8^+$ T cells on frozen sections was described previously (Kim et al., 2012), but needs to be optimized. This study is dedicated to establishing a reliable protocol for rapid immunostaining of the single activated $CD8^+$ T cells from MS brain biopsies and improving the accuracy of isolating single T cells for subsequent TCR analysis.

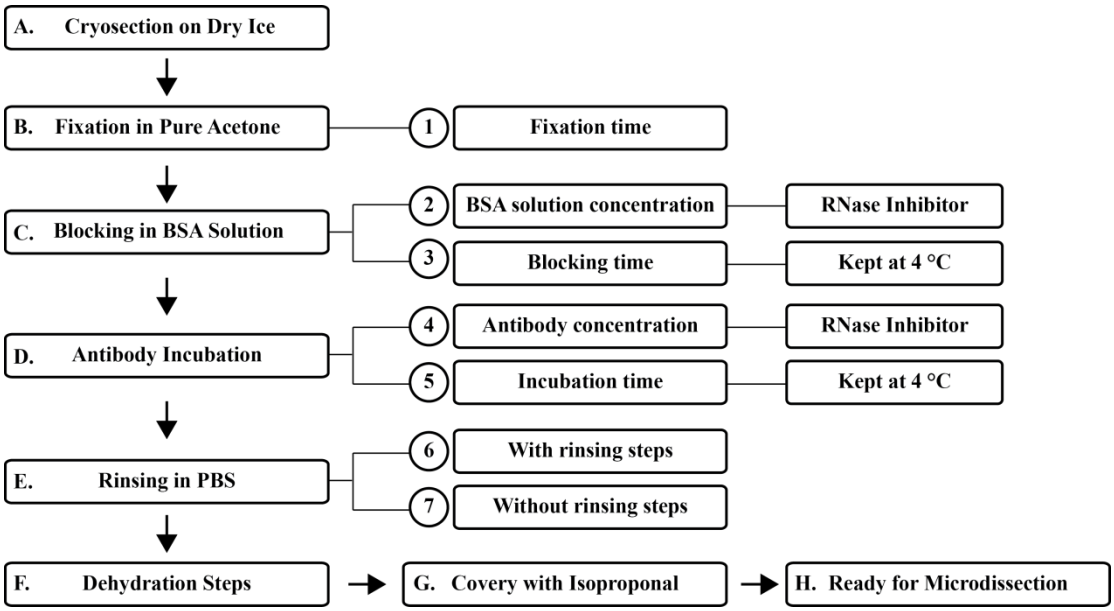

Figure 3-7: Steps and examinations within the rapid immunostaining method

The immunostaining includes these steps (**A-H**). **①:** Different fixation periods with Acetone were tested. **②-③:** Various BSA concentration and blocking time were examined. **④-⑤:** The concentrations of antibodies against CD8α, CD137 and mouse IgG (H+L) as well as the incubation time were tested. **⑥-⑦:** The staining procedure including the rinsing steps or not was examined. In addition, we appended three additional conditions to the rapid immunostaining protocol to minimize RNA degradation: Firstly, the staining temperature was sustained at 4°C. Secondly, RNase Inhibitor was used in the dilution of BSA and antibodies. Lastly, the dehydration steps (**F**) proceeded after staining.

The steps and examination points within the rapid immunostaining protocol are summarized in the scheme shown in Figure 3-7. These tests were carried out in five crucial steps. Firstly, the fixation time was optimized (Figure 3-7, ①). Secondly, the relationship between the concentration of BSA solution and the blocking time was investigated (Figure 3-7, ②-③). Thirdly, the different antibodies' concentrations and incubation times were tested (Figure 3-7, ④-⑤). Fourthly, the staining protocols with and without rinsing steps were also compared (Figure 3-7, ⑥-⑦). Lastly, considering minimizing RNA degradation, we compared the results obtained from the rapid immunostaining protocol at 4°C and room temperature. Table 3-2 summarizes the staining results obtained from the five different conditions above and scored in score of 5.

Table 3-2: Summary of staining results obtained from different conditions

1: no staining, 2: faint staining, 3: weak staining, 4: acceptable staining, 5: strong staining.

A. Staining results obtained with different fixation time

Fixative	10 s	1 min	5 min	10 min
100% Acetone	4	4	5	5
Without fixation	1	1	1	1

B. **Staining results from different concentration of BSA and blocking time**

Block Reagent	Concentration	30 s	2 min	5 min	10 min
BSA	1:50	1	1	3	5
	1:20	1	2	3	5
	1:10	1	4	4	5

C. Staining results of different concentration of antibodies and incubation periods

Anti-	Concentration	2 min	3 min	5 min	10 min
Human CD8α-Cy3	1:50	3	4	5	5
Human CD137	1:100	1	1	2	3
	1:50	1	2	3	3
	1:5	2	3	4	5
Mouse IgG (H+L)-Alexa Fluor® 488	1:1000	1	1	1	2
	1:100	2	2	3	4
	1:20	4	4	5	5

D. Staining results of different staining temperatures

Temperature	10 min	15 min	20 min	30 min
4°C	4	3	3	2
Room temperature	5	5	5	5

E. Staining results with or without rinse steps

Step	10 s	30 s	1 min	2 min
Rinsing with PBS solution	4	4	5	5
Without rinse steps			4	

If the tissue sections were not fixed initially, the detection of staining was impossible. Fixation of tissue sections with acetone for ten seconds or one minute was a little weaker than for five or ten minutes, with no difference between ten seconds and one minute (Table 3-2, A). Slides were immersed in acetone ten times rather than applying them by drops because the acetone is highly volatile, and drops may wash cells out of slides by surface tension (Salem et al., 2003). Blocking the tissue with 10% BSA solution for 2 minutes, were comparable to those obtained from blocking for longer times (Table 3-2, B). Less than one minute of blocking resulted in no staining absolutely. Unfortunately, the weak staining by blocking with lower concentrations of BSA solutions (such as 2% and 5%) for less than 5 minutes did not reveal reliable results.

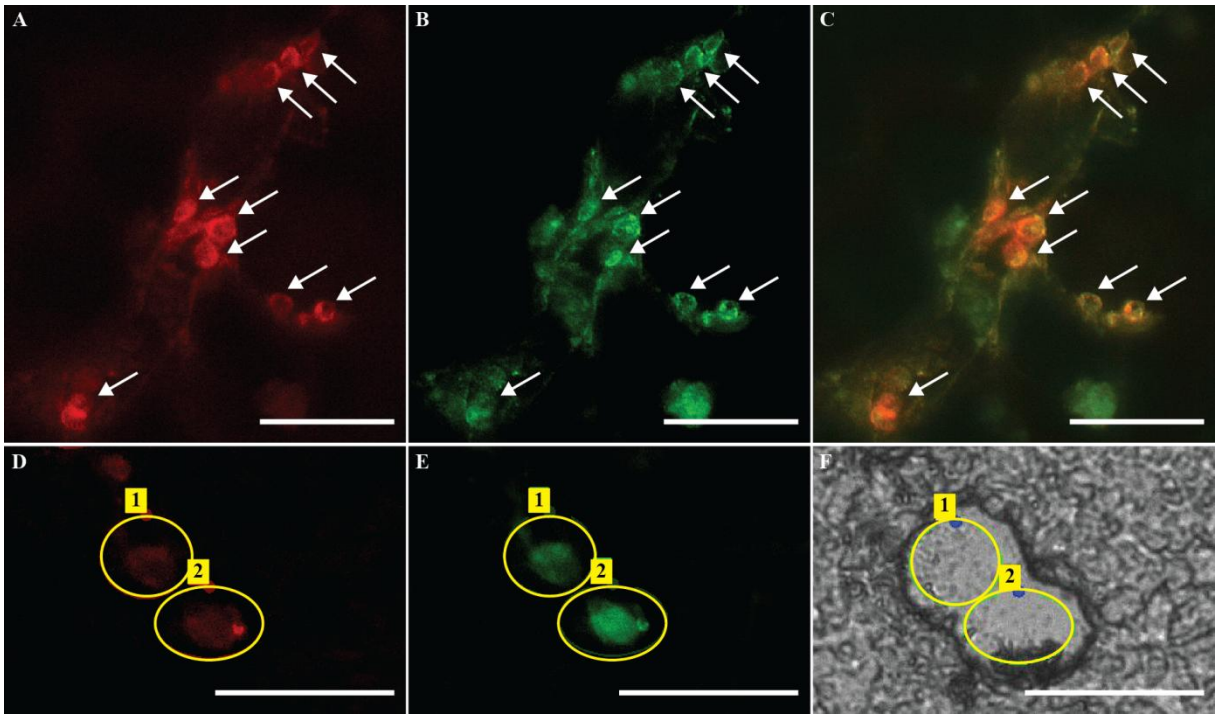

Figure 3-8: Pathogenic CD8$^+$ T cells located in the MS brain and isolated by laser microdissection

8 µl cryosections of a frozen biopsy sample (block #12) from the MS patient FE were stained with Cy3-labeled anti-CD8α (red, 1:50) and anti-CD137 (1:5) primary antibodies as well as Alexa Fluor® 488-labeled anti-mouse IgG (H+L) (green, 1:20) secondary antibody. **(A-C)** Detection of activated CD8$^+$ T cells (white arrows) that were double-positive **(C)** for CD8 **(A)** and CD137 **(B)**. **(D-F)** Laser microdissection of single T cells was co-stained for CD8α (red, **D**) and CD137 (green, **E**). The single activated CD8$^+$ T cells (cell element #1, 2 and so on) were dissected within the yellow circles and then captured directly into the cap of a PCR tube for subsequent TCR analysis. After laser microdissection (**F**), the corresponding image of the tissue from transmitted channel is presented. Scale bars=25 µm.

Results obtained from incubating brain sections with antibodies anti-CD8α-Cy3 (1:50), anti-CD137 (1:5) and anti-mouse IgG (H+L)-Alexa Fluor® 488 (1:20) for 3, 5, and 2 minutes, respectively, were comparable to those acquired from incubation with lower concentrated antibodies for longer times (Table 3-2, C). In addition, results obtained from the staining at 4°C were slightly weaker than those obtained from the staining at the room temperature, but the former ones were acceptable staining for microdissection (Table 3-2, D). There was no significant difference in staining results with or without rinsing steps (Table 3-2, E). Therefore, using the improved rapid immunostaining method we obtained the same results on frozen brain sections as fluorescence staining with the long protocol (Section 3.2).

In summary, we tested the influence of different conditions to the staining results on frozen brain sections. The repaid immunostaining method was successfully optimized to visualize the activated, i.e. double-stained $CD8\alpha^+/CD137^+$ single T cells in a limited time before laser microdissection. A sample of isolation of single activated $CD8^+$ T cells by laser microdissection from the brain biopsies of MS patients are shown in Figure 3-8.

3.3.2 Effective Treatments on Tissue to Minimize the Degradation of RNA Quality

RNA quality is crucial for subsequent TCR analysis. The decay of RNA transcripts is mainly infected by the environmental elements like temperature, chemicals, RNases and so on. The degradation of RNA mostly happened in the treatment of MS brain cryosections, even though the completely staining period was shortened to 12 minutes (Section 3.3.1). The brain biopsy samples of MS patient FE and RF were used for the measurement of RNA quality as described in Section 2.2.4. The assessment of RNA integrity in brain tissues before and after staining is shown in Figure 3-9.

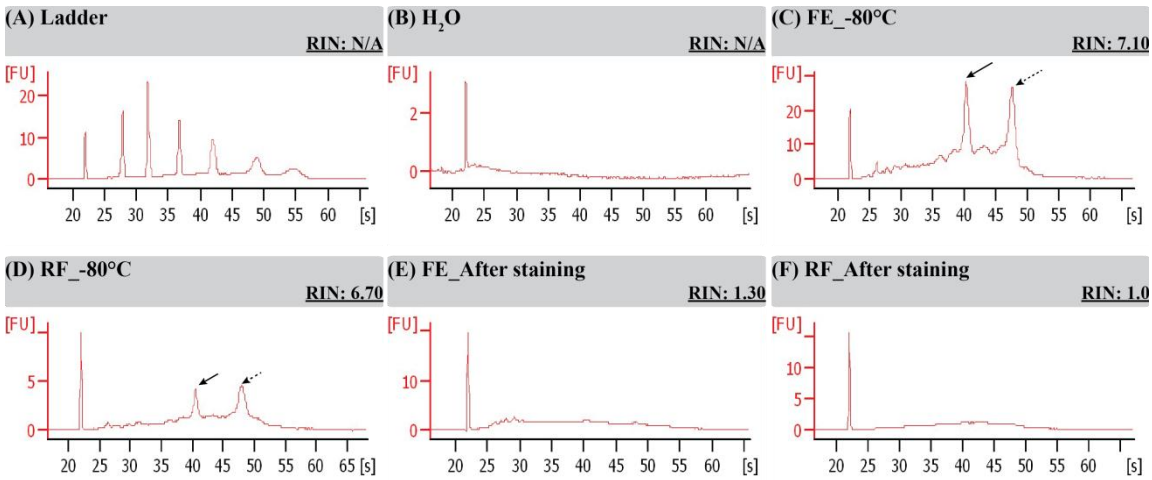

Figure 3-9: Comparison of RNA qualities in brain tissues before and after fluorescence staining

The RNA quality in tissue blocks of the brain biopsies from MS patients FE and RF were determined by the Agilent 2100 bioanalyzer. Densitometry plot shows RNA signals in runtime (s) against fluorescence intensity with relative fluorescence units (FU). Note the different scales of the Y-axes. RIN values represent standardization of RNA quality control. **(A-B)** The positive and negative controls of the experiment. **(C-D)** Initial RNA qualities of brain biopsies from MS patients FE and RF. **(E-F)** The RNA quality after fluorescent staining procedure. Solid arrow: 18S rRNA; dashed arrow: 28S rRNA.

The densitometry plots present that the fresh brain biopsy samples stored at -80°C both had the high RNA integrity numbers (RIN) of 7.60 and 6.70 with two peaks at the signals of 18S and 28S rRNA

(Figure 3-9, C-D, arrows), respectively. However, weak signals of 18S and 28S rRNA were detected from the same brain biopsy samples after the fluorescence staining. The RNAs were almost decayed according to the low RINs with 1.30 and 1.0, respectively (Figure 3-9, E-F).

Therefore, except for using the improved rapid immunostaining (Section 3.3.1) instead of the general fluorescence staining (Section 2.5.2), some other conditions were included to minimize RNA degradation. Firstly, RNases inhibitor[2] was added to the blocking solution, diluted antibodies, and rinsing solution. Secondly, instead of preparing the blocking solution with the BSA-1[3] powder, 10% of the BSA-2[4] solution was used as the blocking reagent, which is a commercial product without RNase/DNase. Thirdly, the slides were kept on a cold metal block during the staining to maintain the temperature of slides at 4°C. Lastly, to get rid of the water within the tissues completely, we used a series of ethanol with different concentration gradients and xylene solution to deal with the slides before laser microdissection. These steps are called dehydration. The frozen sections of tonsil were used to test these conditions above, and the results are presented in Figure 3-10.

The untreated RNA (Figure 3-10, A) from fresh tonsil biopsy stored at -80°C was examined with high quality (RIN=5.30) and visible signals of 18S and 28S rRNA (two peaks marked with arrows). The untreated RNA sample stored on dry ice served as the positive control in our study. After subsequent fluorescence staining, RNA was mostly decayed (Figure 3-10, B), but faint signals of 18S and 28S rRNA were detected in addition of RNases inhibitor (Figure 3-10, C). It indicates that the amount of RNase inhibitor is not enough to minimize RNA degradation. However, the RNA quality after the fluorescence staining performed at 4°C was comparable to that at room temperature (Figure 3-10, D).

[2] RNases inhibitor: protector RNase inhibitor (40 U/µl, Roche)

[3] BSA-1: the powder of Bovine Serum Albumin (Sigma-Aldrich)

[4] BSA-2: the solution of Bovine Serum Albumin (Protease/DNase/RNase free, 20 mg/ml in H_2O, Sigma-Aldrich)

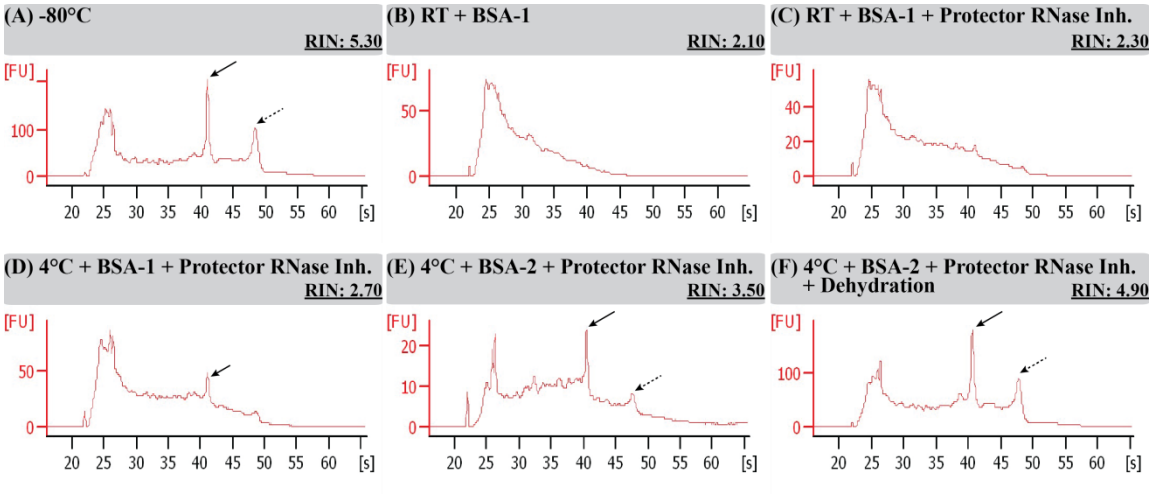

Figure 3-10: Comparison of RNA qualities in tonsil tissues with different treatments

RNA quality was examined after different treatments of tonsil tissues by the Agilent 2100 bioanalyzer. Densitometry plot shows RNA signals in runtime (s) against fluorescence intensity with relative fluorescence units (FU). Note the different scales of the Y-axes. RIN values represent standardization of RNA quality control. **(A)** Untreated RNA stored on dry ice served as positive control. **(B)** RNA quality after fluorescent staining without any treatment served as negative control. **(C)** RNA quality after fluorescent staining with Protector RNase Inhibitor. **(D)** RNA quality after fluorescent staining at 4°C with Protector RNase Inhibitor. **(E)** RNA quality after fluorescent staining at 4°C with BSA-2 and Protector RNase Inhibitor. **(F)** RNA quality after fluorescent staining at 4°C with BSA-2, Protector RNase Inhibitor and the dehydration steps (Xylene). Solid arrow: 18S rRNA; dashed arrow: 28S rRNA.

As complete RNA degradation was observed in the stained sections (Figure 3-10, B), it is hypothesized that BSA-1 solution might contain RNases. However, BSA-2 solution (10%) is a Protease/DNase free, liquid BSA purchased from Sigma-Aldrich. The RNA sample treated with BSA-2 solution yielded a RIN value of 3.50 and detectable signals of 18S and 28S rRNA (Figure 3-10, E). Even though RNases inhibitor could delay the RNA degradation, the water contained in the tissues might speed up the decay of RNA. The RNA samples obtained from dehydrated sections yielded a good RIN value of 4.90 and strong signals of 18S and 28S rRNA (Figure 3-10, F). The RNA quality after these treatments is much close to the original RNA quality from fresh biopsies stored at -80°C (Figure 3-10, A). The dehydration takes the water completely out of tissue sections and stops RNases further to decompose RNAs.

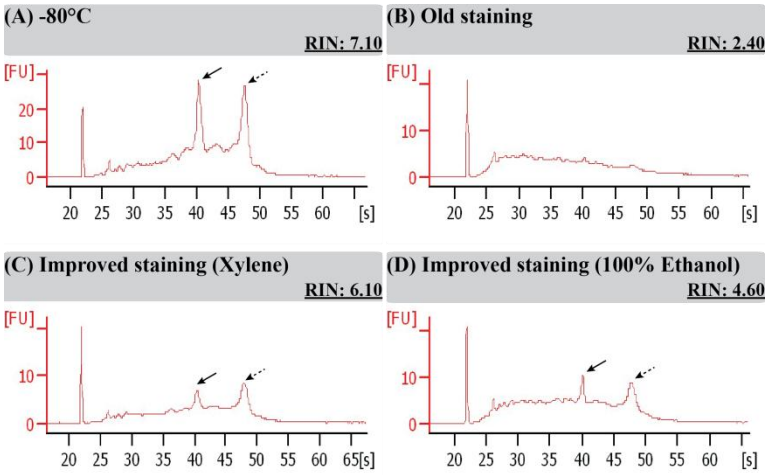

Figure 3-11: Minimization of RNA degradation on brain biopsy with the improved rapid immunostaining

RNA quality of brain biopsy (Block #9) from MS patient FE was examined before and after rapid immunostaining by the Agilent 2100 bioanalyzer. Densitometry plot shows RNA signals in runtime (s) against fluorescence intensity with relative fluorescence units (FU). Note the different scales of the Y-axes. RIN values represent standardization of RNA quality control. **(A)** Untreated RNA stored on dry ice served as positive control. **(B)** RNA quality after fluorescent staining without any treatment served as negative control. **(C)** RNA quality after the improved staining was dehydrated with Xylene solution in the last step. **(D)** RNA quality after the improved staining was dehydrated with 100% Ethanol in the last step. Solid arrow: 18S rRNA; dashed arrow: 28S rRNA.

Due to the high RNA quality of tonsil (Figure 3-10, F) after treatment with the optimized staining method, we measured the RNA quality of brain tissue sections from MS patient FE (Block #9) after the same treatment as mentioned above. Meanwhile, 100% ethanol solution instead of Xylene solution in the dehydration steps was also examined. The assessment of RNA qualities in brain tissues is shown in Figure 3-11. Compared to the RNA quality before fluorescence staining (RIN=7.10, A), the degradation of RNA is actually slowed down after the treatment of improved staining and the dehydration (Figure 3-11, C-D). The strong signals of 18S and 28S rRNA were detected after the improved staining either with dehydration of Xylene solution or with 100% Ethanol (C-D, arrows). However, the value of RIN with dehydration of Xylene solution (RIN=6.10) is much higher than the treatment with 100% Ethanol (RIN=4.60) in the dehydration steps.

In summary, for the subsequent laser microdissection experiments the addition of RNases inhibitor to each staining solutions and dehydration included in the optimized staining protocol is necessary. The

commercial blocking solution (BSA-2) and the staining temperature (4°C) are essential for the minimization of RNA degradation. During the following one hour of microdissection, the RNA quality is preserved well enough for subsequent TCR analysis.

3.3.3 **Optimization of the Unbiased PCR Technology to Identify Paired TCR α- and β-Chains**

Brain tissue specimens from MS patients FE and RF were employed for identification of the single activated $CD8^+$ T cells by staining with antibodies against CD8α and CD137. The double positive single T cells ($CD8^+CD137^+$) were isolated by laser microdissection and analyzed by the multiplex RT-PCR-based approach to amplify the αβ-TCRs of single T cells (Kim et al., 2012). Here, this unbiased technology was optimized for higher yield of TCR α- and β-chains. The strategically steps and optimization are shown in Figure 3-12. Single T cells from peripheral blood of a healthy donor were used to examine these changes within the unbiased PCR protocol. DEPC-treated water instead of DNA sample served as negative control.

The TCR α- and β-chains are named in accordance with IMGT® nomenclature (Lefranc et al., 2009; Lefranc and Lefranc, 2001), except for the variable regions of the TCR chains, which are specially designated according to Arden et al. (Arden et al., 1995).

3.3.3.1 Different PCR thermal cyclers

To enhance the accuracy of PCR, we compared the unbiased TCR amplification with three different PCR thermal cyclers. A new PCR thermal cycler (Mastercycler® pro, Eppendorf) and another two old cyclers (Mastercycler® Gradient Thermal Cycler from Eppendorf and GeneAmp PCR System 9600 from Perkin Elmer) were included in the comparison. There is no difference on the yield of TCR β-chains amongst the PCR thermal cyclers (data not shown). However, based on the principles of timesaving and preventing the evaporation of PCR master mix, we chose the Mastercycler® pro PCR thermal cycler for subsequent PCR experiments.

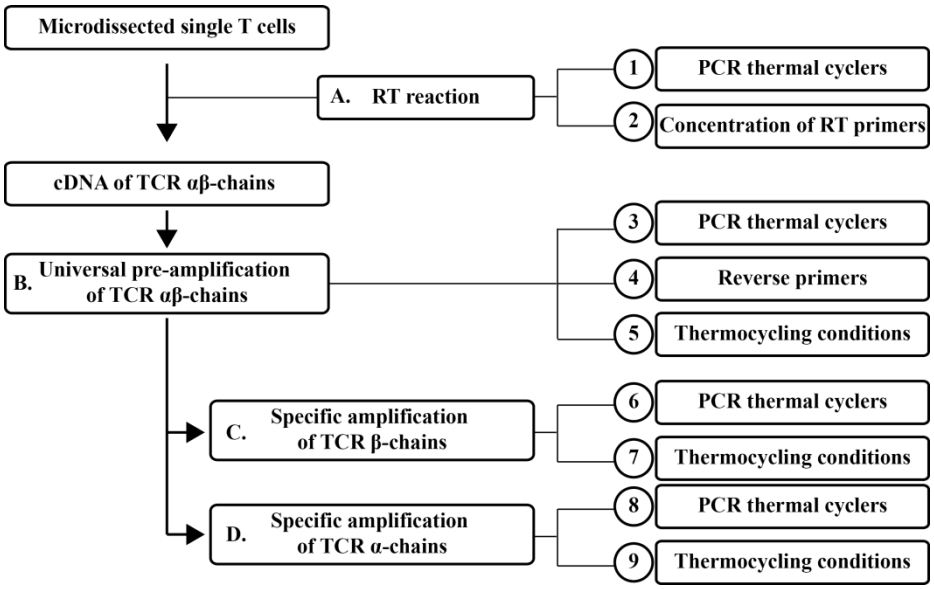

Figure 3-12: Strategically steps and optimization to identify paired TCR α- and β-chains from dissected tissue-infiltrating T cells

(A) RT reaction was employed to prepare cDNA of TCR molecules. In this step, we examined the reaction performed in different PCR thermal cycles (①) and the concentrations of primers (②) used in the reaction **(B)** Touchdown PCR was employed to pre-amplify the TCR α- and β-chains. In this step, we examined the reaction performed in different PCR thermal cyclers (③), different reverse primers (④) and the Thermocycling conditions (⑤) involved in the reaction. **(C-D)** The TCR α- and β-chains were separately amplified with two PCRs. In these two steps, we both examined the reactions performed in different PCR thermal cyclers (⑥, ⑧) and the Thermocycling conditions (⑦, ⑨) involved in the responses.

3.3.3.2 Different concentrations of RT primers

Two primers (Cβ-RT-2 and Cα-RT-imp) are involved in the reaction for preparation the cDNA of TCR α- and β-chains, respectively. In the original protocol, the final concentration of RT-primers might have been too high to obtain high yield of TCR β-chains finally. Thus, we reduced the amount of RT-primers in order to improve the output of PCR. To avoid further RNA degradation, we added RNases inhibitor to the reaction. The RT reaction is described in Section 2.2.9.2, and the TCR β-chains obtained from two concentrations are given in Table 3-3. Three TCR β-chains (9%) have been achieved from 32 single T cell samples with the high concentration of primers (Table 3-3, #1-#3). However, with the low concentration of primers, TCR β-chains were double yielded from the same T cells (Table 3-3, #1-#5). In addition, two identical TCR β-chains (BV6S2-GRGGGF-BJ2.5) were found with a low concentration of primers. The high amount of primers might increase unspecific PCR

products, such as primer dimers and short oligonucleotides. Therefore, the low concentration of RT primers will be used for subsequent unbiased PCR experiments.

Table 3-3: TCR β-chains obtained from unbiased PCR protocol with various concentrations of RT primers

In the unbiased PCR protocol, we examined the high (0.6 µM) and low (0.3 µM) concentrations of primers involved in RT reaction. All the TCR β-chains (#1-#5) were obtained with the low concentrations of primers, except for the first three sequences (#1-#3) that were obtained with the high concentrations of primers. ‡Two identical TCR β-chains (BV6S2-GRGGGF-BJ2.5) were found. Blue: amino acid sequence, red: V region, black: n(D)n, green: J region. N=numbers of the single T cells.

Cell Nr.	TCR β-chains	Sequence n(D)n													(N=32)
			C	A	S	S	Y	S	I	G	T	G	R	R	Q	
#1	BV 13S2a-BJ 2.5	5'-	TGT	GCC	AGC	AGT	TAC	TCG	ATT	GGG	ACT	GGG	CGG	AGG	CAA	- 3'
			C	A	S	G	T	R	D	T	D	T	Q	Y	F	
#2	BV 8S3-BJ 2.3	5'-	TGT	GCT	AGT	GGT	ACC	CGG	GAC	ACA	GAT	ACG	CAG	TAT	TTT	- 3'
			C	A	S	S	L	G	R	G	X	X	S	K	R	
#3	BV 6S2-BJ 2.5	5'-	TGT	GCC	AGC	AGC	TTA	GGG	CGA	GGA	GNN	NNN	TCC	AAG	AGA	- 3'
			C	A	S	S	L	G	R	G	G	G	F	Q	E	
#4	BV 6S2-BJ 2.5‡	5'-	TGT	GCC	AGC	AGC	TTA	GGG	CGA	GGC	GGG	GGG	TTC	CAA	GAG	- 3'
			R	A	S	S	L	G	R	G	G	X	I	Q	E	
#5	BV 6S5-BJ 2.5	5'-	CGC	GCC	AGC	AGC	TTA	GGG	CGA	GGA	GGG	NGA	ATC	CAA	GAG	- 3'

3.3.3.3 Design of different reverse primers for TCR β-chains

In the pre-amplification of TCR α/β chains, multiple primer sets are included to produce different sized amplicons. Multiple primer sets were designed for the "V-segments" of TCR α/β chains, which are named as Vβ primer pools and Vα-for-out primer pools (Table 2-5 to Table 2-6). Two reverse primers (Cα-out and Cβ-out) were designated for the constant regions of TCR α/β chains. However, the binding site of primer Cβ-out (5'-TGGTCGGGGWAGAAGCCTGTG-3') overlaps to that of primer Cβ-RT-2 (5'-GWAGAAGCCTGTGGCC-3') involved in the RT reaction. The low yield of the PCR products might be arised by mispriming during PCR, which verified that the primer Cβ-out has no additional complementary regions within the template DNA. In addition, all primers involved in this reaction have the similar melting temperature (T_m=60°C), except for the primer Cβ-out (T_m=68°C). T_m can also be known as the annealing temperature (T_a), at which the primers start to bind template DNA during PCR. Too high T_a might produce insufficient hybridization of the primer-DNA template and result in low yield of PCR products. Moreover, closely matched T_m of primers leads to

maximize the yield of PCR products. The difference of 5°C or more between forward and reverse primers may result in no amplification or non-specific products. Therefore, a new primer Cβ-mid4 is designed, (5'-TGGGTGTGGGAGATCTCTG-3', T_m=60°C), which locates at the inner fragment of "C-segments" of TCR β-chains. The pre-amplification of TCR chains is described in Section 2.2.9.3, and the TCR β-chains obtained from two branches are shown in Table 3-4. Only one TCR β-chain (6%) was obtained from 16 single T cell samples using the reverse primer Cβ-out (Table 3-4, #1). However, nine TCR β-chains (56%) were obtained from same numbers of single T cell samples with the reverse primer Cβ-mid4 (Table 3-4, #1-#9). The high yield of productive TCR β-chains was achieved from the unbiased PCR with the newly designed primer Cβ-mid4. Thus, the newly designed reverse primer (Cβ-mid4) is much more efficient for pre-amplify the TCR chains than the former primer (Cβ-out). We therefore will employ the primer (Cβ-mid4) for subsequent TCR analysis.

Table 3-4: TCR β-chains obtained from unbiased PCR protocol with various reverse Cβ primers

In the unbiased PCR protocol, we examined the two different reverse primers (Cβ-out and Cβ-mid4) involved in the pre-amplification of TCR chains. The TCR β-chains (#2-#9) were obtained with the primer Cβ-mid4. The first sequence (#1) was obtained with the primer Cβ-out. Blue: amino acid sequence, red: V region, black: n(D)n, green: J region. N=numbers of the single T cells.

Cell Nr.	TCR β-chains	Sequence n(D)n													(N=16)
			C	A	S	S	P	V	G	G	I	E	A	F	F
#1	BV 6S2-BJ 1.1	5'-	TGT	GCC	AGC	AGC	CCC	GTT	GGG	GGC	ATA	GAA	GCT	TTC	TTT - 3'
			C	A	S	S	T	G	R	R	S	S	Y		
#2	BV 13S3-BJ 2.7	5'-	TGT	GCC	AGC	AGC	ACG	GGA	CGC	CGG	AGC	TCC	TAC - 3'		
			C	A	S	S	Y	G	E	N	T	I			
#3	BV 6S4-BJ 1.3	5'-	TGT	GCC	AGC	AGC	TAC	GGG	GAA	AAC	ACC	ATA - 3'			
			C	A	W	S	P	Q	F	N	T	G			
#4	BV 20S1-BJ 2.2	5'-	TGT	GCC	TGG	AGT	CCC	CAG	TTC	AAC	ACC	GGG - 3'			
			C	A	S	S	L	G	R	I	P	S	H	G	Y
#5	BV 8S1/8S2-BJ 1.2	5'-	TGT	GCC	AGC	AGC	CTA	GGA	CGC	ATA	CCG	AGC	CAT	GGC	TAC - 3'
			C	A	S	S	I	R	A	P	L	A	K	N	
#6	BV 17S1-BJ 2.4	5'-	TGT	GCC	AGT	AGT	ATT	CGG	GCG	CCT	CTA	GCC	AAA	AAC - 3'	
			C	A	I	S	G	S	G	G	T	G	M	G	Q
#7	BV 12S1-BJ 1.5	5'-	TGT	GCC	ATC	AGT	GGC	AGC	GGC	GGT	ACA	GGG	ATG	GGT	CAG - 3'
			C	A	S	S	Q	D	A	L	A	V	E	T	Q
#8	BV 9S1-BJ 2.5	5'-	TGT	GCC	AGC	AGC	CAA	GAT	GCG	CTA	GCG	GTA	GAG	ACC	CAG - 3'
			C	A	S	N	P	T	R	S	A	D			
#9	BV 6S5-BJ 2.3	5'-	TGT	GCC	AGC	AAC	CCA	ACC	CGG	AGC	GCA	GAT - 3'			

3.3.3.4 Different thermocycling conditions to pre-amplify TCR chains

The unbiased amplification of TCR chains is achieved by a multiplex RT-PCR-based method to analyze the matching i.e. paired αβ-TCR chains of single human T cells (Kim et al., 2012). During the pre-amplification of paired αβ-TCRs, nine degenerate primers (Vβ1-Vβ9) together with 24 degenerate primers (Vα-for-out) (Seitz et al., 2006) were designed to cover the entire "V-segments" of functional TCR α- and β-chains (Table 2-5 to Table 2-6). The average of T_m for all the degenerate primers is 61°C, and the optimum T_a is determined by the gradient PCR. In the previous setup by Kim et al., two annealing temperatures (60°C and 53°C) each with 10 and 30 cycles were employed for the TCR amplification. To this point, we tested some modification, which are shown in Table 3-5 (A). Except for the modified conditions, the pre-amplification of TCR chains is performed as described in Section 2.2.9.3. The TCR β-chains obtained from the unbiased PCR protocol with the different thermocycling conditions are displayed in Table 3-5 (B).

Following the previous setup by Kim et al., we obtained two TCR β-chains (12.5%) from 16 cell samples, together with many non-specific products that may be caused by the low annealing temperature (53°C). We improved the annealing temperatures (58°C and 56°C) and adjusted the PCR cycles according to the nucleotides sizes of different TCR α- and β-chains (Table 3-5, A). Then eight functional TCR β-chains (50%) were acquired from the same numbers of T cell samples. In addition, we also optimized the DNA elongating temperature (72°C) for the best activity of Taq polymerase. Therefore, the optimized thermocycling conditions will be used in the pre-amplification of the paired αβ-TCRs in the future.

Table 3-5: TCR β-chains obtained from unbiased PCR protocol with different thermocycling conditions

(A) In the unbiased PCR protocol, we modified the thermocycling conditions for pre-amplification of the paired αβ-TCRs. **(B)** All the TCR β-chains (#1-#8) were obtained with optimized thermocycling conditions, except for the first two sequences (#1-#2) that were achieved with the original PCR setup (Kim et al., 2012). Blue: amino acid sequence, red: V region, black: n(D)n, green: J region. N=numbers of the single T cells.

(A)

Conditions	**Original**	**Modified**
Annealing temperature (°C)	60 → 53	61→58→56
Elongating temperature (°C)	68	72
Numbers of cycles	10× 30×	4× 4× 10×

(B)

Cell Nr.	**TCR β-chains**	**Sequence n(D)n**	**(N=16)**
		C A S S L V G S G R S T D	
#1	BV 6S4-BJJ 2.3	5'- TGT GCC AGC AGC TTA GTT GGG AGC GGG AGA AGC ACA GAT - 3'	
		C A S T Q G W G D T E A F	
#2	BV 8S1/8S2-BJ 1.1	5'- TGT GCC AGC ACC CAA GGG TGG GGA GAT ACT GAA GCT TTC - 3'	
		C A S S L D R T G G E E T	
#3	BV 21S3-BJ 2.5	5'- TGT GCC AGC AGC TTA GAT CGC ACA GGG GGC GAA GAG ACC - 3'	
		C A S S P I G G D Y G Y T	
#4	BV 7S1-BJ 1.2	5'- TGC GCC AGC AGC CCC ATC GGG GGG GAC TAT GGC TAC ACC - 3'	
		C A S R Q G R D I Q	
#5	BV 8S1/8S2-BJ 2.4	5'- TGT GCC AGC AGA CAG GGG CGG GAC ATT CAG - 3'	
		C A S S T R Q Q T N T	
#6	BV 21S2-BJ 1.1	5'- TGT GCC AGC AGC ACC CGA CAG CAG ACG AAC ACT - 3'	
		C A S S W G E K L F	
#7	BV 14S1-BJ 1.4	5'- TGT GCC AGC AGT TGG GGG GAA AAA CTG TTT - 3'	
		C A T S D P R T D G N T	
#8	BV 15S1-BJ 1.3	5'- TGT GCC ACC AGT GAC CCA AGG ACT GAT GGA AAC ACC - 3'	

3.3.3.5 Specific amplification of TCR α- and β-chains

The pre-amplification PCR products served as templates to amplify the TCR β-chains by anchor PCR and the corresponding α-chains by nested PCR (Kim et al., 2012). The anchored PCR includes two steps according to the previous protocol. Firstly, the pre-amplification PCR products are introduced to a run-off reaction using the nine anchored primers ($VP1^{+}$-$VP9^{+}$), at the 5' end of which a unique oligonucleotide sequence (5'-ACAGCACGACTTCCAAGACTCA-3', T_m=66°C) is connected. Secondly, the unique sequence (UP) serves as the forward primer together with a nested primer (Cβ-in, T_m=60°C) are used to amplify the TCR β-chain rearrangement. However, we did not obtain a high yield with this PCR setup (Kim et al., 2012). Four problems were in our concern. Firstly, non-specific products might be caused by the run-off reaction. Secondly, the two primers (UP and Cβ-in) have

different T_m values, which compromise the PCR efficiency. Thirdly, the PCR cycles are not enough for the addition of anchor sequences to the V-segments of TCR β chains. Lastly, the annealing temperature (53°C) is not high enough to avoid the non-specific PCR products.

Table 3-6: TCR β-chains obtained from unbiased PCR protocol with different PCR setups

(A) PCR setups were modified for the amplification of TCR β-chains. **(B)** All the TCR β-chains (#1-#16) were obtained with optimized PCR setup, except for the first sequence (#1) that was achieved with the original PCR setup (Kim et al., 2012). Blue: amino acid sequence, red: V region, black: n(D)n, green: J region. N=numbers of the single T cells.

(A)

Conditions	Original	Modified
Anchor primer	UP (T_m=66°C)	UP_{new} (T_m=60°C)
Anchored VP primer	$VP1^+$-$VP9^+$	$VP1^+{}_{new}$-$VP9^+{}_{new}$
Reverse primer	-	Cβ-in (T_m=60°C)
Cycling program	Run-off reaction	Anchor PCR
Annealing temperature (°C)	53	56
Elongating temperature (°C)	68	72
Numbers of cycles	1×	30×

(B)

Cell Nr.	TCR β-chains	Sequence n(D)n													(N=16)
			C	A	S	R	S	V	K	G	I	G	S	E	Q	
#1	BV 7S1-BJ 2.1	5'-	TGC	GCC	AGC	AGG	AGC	GTA	AAG	GGT	ATA	GGA	TCT	GAG	CAG	- 3'
			C	A	S	S	L	D	S	R	A	S	T	D	T	
#2	BV 13S1-BJ 2.1	5'-	TGT	GCC	AGC	AGT	CTG	GAC	AGC	CGA	GCT	AGC	ACA	GAT	ACG	- 3'
			C	A	S	S	Y	S	P	A	H	E	Q	F	F	
#3	BV 21S3-BJ 2.7	5'-	TGT	GCC	AGC	AGT	TAC	TCC	CCG	GCC	CAT	GAG	CAG	TTC	TTC	- 3'
			C	A	S	R	S	G	L	A	G	G	D	E	Q	
#4	BV 21S3-BJ 2.7	5'-	TGT	GCC	AGC	AGA	TCC	GGA	CTA	GCG	GGG	GGG	GAC	GAG	CAG	- 3'
			C	A	S	S	Y	S	P	E	G	G	N	T	Q	
#5	BV 13S2-BJ 2.3	5'-	TGT	GCC	AGC	AGT	TAC	TCC	CCG	GAA	GGG	GGG	AAT	ACG	CAG	- 3'
			C	A	S	S	L	A	I	Y	S	N	Q	P	Q	
#6	BV 6S2-BJ 1.5	5'-	TGT	GCC	AGC	AGC	TTA	GCC	ATT	TAT	AGC	AAT	CAG	CCC	CAG	- 3'
			C	A	S	S	A	L	G	G	Q	E	T	Q	Y	
#7	BV 14S1-BJ 2.5	5'-	TGT	GCC	AGC	AGT	GCG	CTG	GGG	GGC	CAA	GAG	ACC	CAG	TAC	- 3'
			C	A	S	S	L	I	A	G	D	G	E	T	Q	
#8	BV 8S1/8S2-BJ 2.5	5'-	TGT	GCC	AGC	AGT	TTA	ATA	GCG	GGA	GAC	GGG	GAG	ACC	CAG	- 3'
			C	A	S	S	L	Q	L	G	D	Y	G	Y	T	
#9	BV 14S1-BJ 1.2	5'-	TGT	GCC	AGC	AGT	TTA	CAA	CTG	GGA	GAC	TAT	GGC	TAC	ACC	- 3'
			C	A	S	R	S	V	K	G	I	G	S	E	Q	
#10	BV 7S1-BJ 2.1	5'-	TGC	GCC	AGC	AGG	AGC	GTA	AAG	GGT	ATA	GGA	TCT	GAG	CAG	- 3'
			C	A	W	T	K	L	G	V	G	Y	T	F		
#11	BV 20S1-BJ 1.2	5'-	TGT	GCC	TGG	ACC	AAG	TTG	GGG	GTT	GGC	TAC	ACC	TTC	- 3'	
			C	A	S	S	L	G	G	T	G	G	N	E	Q	
#12	BV 21S3-BJ 2.7	5'-	TGT	GCC	AGC	AGC	TTA	GGA	GGG	ACA	GGG	GGC	AAC	GAG	CAG	- 3'
			C	A	S	S	P	P	A	T	N	T	G	E	L	
#13	BV 6S4-BJ 2.2	5'-	TGT	GCC	AGC	AGC	CCC	CCA	GCT	ACG	AAC	ACC	GGG	GAG	CTG	- 3'
			C	A	S	S	P	P	A	T	N	T	G	E	L	
#14	BV 6S8-BJ 2.2	5'-	TGT	GCC	AGC	AGC	CCC	CCA	GCT	ACG	AAC	ACC	GGG	GAG	CTG	- 3'
			C	A	S	S	P	G	A	G	S	A	E	A	F	
#15	BV 7S2-BJ 1.1	5'-	TGC	GCC	AGC	AGC	CCG	GGG	GCA	GGG	AGC	GCT	GAA	GCT	TTC	- 3'
			C	A	S	S	P	D	I	P	D	T	Q	Y	F	
#16	BV 18S1-BJ 2.3	5'-	TGT	GCC	AGC	TCC	CCA	GAC	ATC	CCA	GAT	ACG	CAG	TAT	TTT	- 3'

In aware of the disadvantages, a new anchor (UP_{new}, Table 2-5) is designed, which is modified from the original anchor primer (UP) and has 20 oligonucleotides (5'-AGCACGACTTCCAAGACTCA-3', T_m=60°C). We used the modified Vβ primers[5] ($VP1^{+}_{new}$ to $VP9^{+}_{new}$) and Cβ-in primer in an anchored PCR instead of run-off reaction. In addition, the annealing temperatures and PCR cycles are improved as presented in Table 3-6 (A) for higher yield of TCR β-chains. Thus, the TCR-β chains obtained from unbiased PCR protocol with two different PCR setups for amplification of TCR β-chains are shown in Table 3-6 (B). Except for the modification mentioned above, the amplification of TCR β-chains is performed as described in Section 2.2.9.4. From the sequencing results, we obtained one TCR β-chain (6%) from 16 single T cell samples using the original PCR setup (Table 3-6, #1). However, with the optimized PCR setup, we got 16 TCR β-chains (100%) from the same numbers of T cell samples (Table 3-6, #1-#16). Therefore, the optimized PCR setup will be employed for subsequent TCR analysis.

Table 3-7: TCR α-chains obtained from the nested PCRs with different PCR setups

(A) In the nested PCRs, we tried two different PCR setups to avoid non-specific products. However, no difference of PCR products was observed from different setups. **(B)** Five TCR α-chains were achieved from 16 single dissected T cells with different PCR setups. Blue: amino acid sequence, red: V region, black: n(D)n, green: J region. N=numbers of the single T cells.

(A)

Conditions	**Original**	**Modified #01**	**Modified #02**
Annealing temperature (°C)	61→58→56→53	61→58→56	61→58
Numbers of cycles	4× 4× 4× 40×	4× 4× 30×	10× 20×

(B)

Cell Nr.	**TCR α-chains**	**Sequence n(D)n**										**(N=16)**
			C	**A**	**A**	**P**	**I**	**I**	**Q**	**G**	**A**	
#1	AV 28S1-AJ 54	**5'-**	TGT	GCT	GCG	CCT	ATA	ATT	CAG	GGA	GCC	**- 3'**
			C	**L**	**L**	**Y**	**S**	**N**	**S**	**N**	**S**	
#2	AV 31-AJ 41	**5'-**	TGT	CTT	CTG	TAC	TCG	AAC	TCA	AAT	TCC	**- 3'**
			C	**A**	**L**	**G**	**D**	**A**	**R**	**L**	**M**	
#3	AV 5S1-AJ 31	**5'-**	TGT	GCT	CTA	GGA	GAT	GCC	AGA	CTC	ATG	**- 3'**
			C	**A**	**T**	**A**	**S**	**I**	**S**	**N**	**D**	
#4	AV 3S1-AJ 20	**5'-**	TCT	GTG	CTA	CGG	CTA	GCA	TTT	CTA	ACG	**- 3'**
			C	**A**	**V**	**Q**	**X**	**A**	**N**	**A**	**G**	
#5	AV 30S1-AJ 39	**5'-**	TGT	GCT	GTG	CAG	GNA	GCT	AAT	GCA	GGC	**- 3'**

[5] The modified Vβ primers were formed with the addition of an oligonucleotide (UP_{new}) at the 5' end of Vβ primers.

When the rearranged sequence of a productive TCR β-chain was obtained, we amplify the corresponding α-chain from the pre-amplification PCR products with five parallel nested PCRs (Seitz et al., 2006). Five Vα-for-in primer sets designed for the "V-segments" of TCR α-chains together with a reverse primer Cα-rev-in are subjected to nested PCRs (Table 2-7). Because of the non-specific products shown in the PCR results, we introduced some modifications to the PCR setup (Table 3-7, A) to get a higher yield of TCR α-chains. We compared the different PCR setups using the single dissected T cells from tonsil sections. Except for the modifications, the nested PCRs are performed as described in Section 2.2.9.5. However, there is no difference of PCR results between the original PCR setup and modifications (data not shown). The TCR α-chains obtained from the nested PCRs are indicated in Table 3-7 (B).

In summary, the method for specific amplification of TCR β-chains is optimized. Higher yield of TCR β-chains was obtained with the improved protocol compared to the former one. This optimized method will be used to unbiased amplify the TCR β-chains of single T cells from blood, CSF and tissues of MS patients. However, so far there is no effective way to optimize the protocol for specific amplification of TCR α-chains, which needs more investigation in the future.

3.3.4 Identification of TCR β-chains from Single $CD8^+$ T Cells Infiltrating in the MS Brain

The brain tissue blocks from MS patients FE (blocks #6, #9, and #12) and RF (block #B) were employed for identification of auto-aggressive $CD8^+$ T cells. In the previous investigation as described in Section 3.2, these brain tissue blocks contain many infiltrated $CD8^+$ T cells. Here, we used the modified rapid immunostaining method (Section 3.3.1) to visualize the activated $CD8^+$ T cells with the antibodies against CD8α and CD137. When the single T cells were successfully isolated by laser microdissection, the optimized unbiased multiplex RT-PCR-based approach (Section 3.3.3) was employed to identify the paired αβ-TCRs.

We have successfully isolated 182 single activated $CD8^+$ T cells from MS patient FE and 387 from RB (Table 3-8, A). Totally, 569 single activated $CD8^+$ T cells were used for subsequent TCR analysis. The

information of TCR β-chains obtained from these single T cells is presented in Table 3-8, B. In the brain tissue blocks of MS patient FE, we obtained four unique TCR β-chains from 182 single $CD8^+$ T cells. Three TCR β-chains contain same V-regions (BV 8S1/8S2) and J-regions (BJ 1.1), but different CDR3 regions. Moreover, one β-chain (BV8S1/8S2-QGWGD-BJ1.1) was detected four times in MS patients FE and one time in MS patient RF, which might be a DNA cross-contamination from patient FE. Moreover, two unique TCR β-chains were identified from MS patient RF. These TCR β-chains were differed from the earlier discovered β-chains. There are no contamination from the former discovered sequences. Unfortunately, we could not recover the corresponding α-chains even by the improved method. Compared to the high yield from single T cells from blood (Section 3.3.3), the low yield of αβ-TCRs from MS brain biopsies is mainly caused by the RNA degradation of the brain biopsies.

Table 3-8: TCR β-chains obtained from the single dissected T cells using the improved unbiased PCR approach

(A) The numbers of single activated $CD8^+$ T cells were isolated from different brain tissue blocks of MS patients FE and RF. These single T cells were immediately used for TCR analysis. **(B)** The sequences and the frequency of TCR β-chains were obtained from these dissected T cells by the improved unbiased PCR approach. Blue: amino acid sequence; red: V region, black: n(D)n, green: J region. N=numbers of the single T cells.

(A)

Block	Numbers of cells
FE Block #6	122
FE Block #12	34
FE Block #9	26
RF Block #B	387
Total	569

(B)

Frequency	Tissue	TCR β-chains	Sequence n(D)n											(N=569)
				C	**A**	**S**	**S**	**E**	**G**	**A**	**G**	**E**	**H**	**N**	
2	FE	BV 22S1-BJ 2.1	**5'-**	TGT	GCC	AGC	AGT	GAA	GGG	GCG	GGA	GAA	CAC	AAT	**- 3'**
				C	**A**	**S**	**S**	**L**	**G**	**L**	**R**	**A**	**E**	**A**	
2	FE	BV 8S1/8S2-BJ 1.1	**5'-**	TGT	GCC	AGC	AGC	CTG	GGA	CTC	CGA	GCT	GAA	GCT	**- 3'**
				C	**A**	**S**	**S**	**F**	**G**	**T**	**E**	**A**	**F**	**F**	
3	FE	BV 8S1/8S2-BJ 1.1	**5'-**	TGT	GCC	AGC	AGT	TTT	GGC	ACT	GAA	GCT	TTC	TTT	**- 3'**
				C	**A**	**S**	**T**	**Q**	**G**	**W**	**G**	**D**	**T**	**E**	
4	FE/RF	BV 8S1/8S2-BJ 1.1	**5'-**	TGT	GCC	AGC	ACC	CAA	GGG	TGG	GGA	GAT	ACT	GAA	**- 3'**
				C	**A**	**S**	**S**	**P**	**G**	**Q**	**G**	**Q**	**E**	**T**	
1	RF	BV 6S2-BJ 2.5	**5'-**	TGT	GCC	AGC	AGC	CCA	GGA	CAG	GGC	CAA	GAG	ACC	**- 3'**
				C	**A**	**S**	**G**	**Y**	**I**	**S**	**A**	**T**	**E**	**A**	
1	RF	BV 8S3-BJ 1.1	**5'-**	TGT	GCT	AGT	GGT	TAT	ATC	TCG	GCT	ACT	GAA	GCT	**- 3'**

In conclusion, using the improved RT-PCR technology, we identified 13 specific TCR β-chains from the single activated $CD8^+$ T cells in the brain tissues of MS patients. However, the corresponding α-chains failed to be amplified from the tissue, which needs more investigation in the future.

3.3.5 Characterization of Paired αβ-TCRs from Single T Cells of the MS CSF Specimens

Considering the degraded RNA involved in the frozen brain tissues of MS patients, we could not easily recover the paired αβ-TCRs with damaged RNAs. However, fresh CSF specimens obtained from MS patients could be the other choice for TCR analysis independent from the RNA degradation. The clonally expanded T cells persisted in the CSF of MS patient for several years might be the auto-aggressive T cells initiating the occurrence of MS (Skulina et al., 2004).

Table 3-9: TCR chains obtained from single T cells of the MS CSF specimens

Single isolated $CD4^+$ (**A**) and $CD8^+$ T cells (**B**) from the CSF specimens of different patients (the first column) were employed for TCR analyzation. TCR-α: TCR α-chain. TCR-β: TCR β-chain. TCR-αβ: Matched αβ-TCRs. TCR-ααβ: TCRs, which are composed of two α-chains and one β-chain. Cell Nr.: numbers of single T cells used for TCR analysis. Red: no functional TCRs were found in these patients with limited numbers of single T cells.

	A. $CD4^+$ T cell					B. $CD8^+$ T cell				
Patient ID	**TCR-α**	**TCR-β**	**TCR-αβ**	**TCR-ααβ**	**Cell Nr.**	**TCR-α**	**TCR-β**	**TCR-αβ**	**TCR-ααβ**	**Cell Nr.**
CIS #01	4	5	3	0	24	0	6	0	0	24
CIS #02	19	9	3	3	40	15	9	3	4	40
CIS #04	0	6	0	0	96	1	36	1	0	88
RIS #01	9	7	2	2	40	2	4	0	1	32
RIS #02	8	11	4	1	24	3	4	3	0	24
RIS #03	9	4	1	2	28	3	1	0	0	16
MP #01	77	35	9	10	80	34	17	7	3	40
MP #02	9	4	1	1	48	5	3	1	2	48
TWIN #2.1	5	3	1	2	32	4	3	2	1	32
TWIN #2.2	29	12	2	5	32	8	3	0	1	32
TWIN #4.2	5	2	1	0	24	2	1	0	1	13
NMDA #01	25	9	3	1	48	5	2	0	1	24

Once the fresh CSF specimens were obtained, we followed the protocol as described in Section 2.4.10 to isolate the single T cell populations ($CD4^+$/$CD8^+$). Then the single T cells were used for the analysis of paired TCR α- and β-chains by the optimized TCR amplification approach (Section 3.3.3). We discovered many TCR α-chains and β-chains from the CSF samples of MS patients (Table 3-9). Because of some technological obstacles (Section 4.2.3.3), we could not recover all the paired αβ-

TCRs from the limited T cell numbers (Table 3-9, CIS #01, CIS #04 and RIS #03). In addition, due to the high sensitivity of this method, we enabled detect dual TCRs (Padovan et al., 1993) on the single cell level, which express one β-chain in combination with two different α-chains in the $CD4^+$ and $CD8^+$ T cell subsets.

As described in Section 2.4.10, one part of the CSF specimens was employed for the analysis of paired TCR α- and β-chains, and the other part was used for NGS[6] to figure out the clonally expanded α-chains and β-chains. The identical sequences for TCR α- and β-chains obtained from the single cell analysis and NGS are shown in Table 3-10. In sample CIS #02, we discovered 5 identical α-chains and 3 identical β-chains. These TCR sequences might belong to the clonally expanded T cells in the CSF of MS patients.

Table 3-10: Identical TCR α- and β-chains obtained from single cell analysis and NGS

The single T cell subsets ($CD4^+$/$CD8^+$) were isolated from the CSF specimens of MS patients. The CSF specimens were divided into two parts for identification of the TCR α- and β-chains on the single cell level and by NGS. **(A)** Identical TCR α-chains were detected with the two methods. **(B)** Identical TCR β-chains were recovered with the two approaches.

(A) TCR α-chains

Patient #	Subset		Sequence	
CIS #02	$CD8^+$	AV 23S1	- CAVPTSGTYKYIF	- AJ 40
	$CD8^+$	AV 2S1	- CAGSRDDKIIF	- AJ 30
	$CD8^+$	AV 7S2	- CAVPTQAGTALIF	- AJ 15
	$CD8^+$	AV 7S2	- CAVRGGYYSSASKIIF	- AJ 3
	$CD8^+$	AV 7S2	- CAVTSASGGSYIPTF	- AJ 6
MP #01	$CD8^+$	AV 24S1	- CVVSASGTDKLIF	- AJ 34
	$CD8^+$	AV 15S1	- CADLYGGSQGNLIF	- AJ 42
TWIN #02	$CD4^+$	AV 4S1	- CLVGGNTGTASKLTF	- AJ 44

(B) TCR β-chains

Patient #	Subset		Sequence	
CIS #02	$CD4^+$	BV 12S1	- CAIRTRSNYGYTF	- BJ 1.2
	$CD8^+$	BV 14S1	- CASSLMWNTEAFF	- BJ 1.1
	$CD8^+$	BV 12S2	- CASSEDNQETQYF	- BJ 2.5
CIS #04	$CD8^+$	BV 13S3	- CASPLPPGNEQFF	- BJ 2.1
MP #01	$CD8^+$	BV 8S1/8S2	- CASSFGTEAFF	- BJ 1.1
	$CD8^+$	BV 8S1/8S2	- CASSLAREPQHF	- BJ 1.5
MP #02	$CD8^+$	BV 8S1	- CASSTLAVNTEAFF	- BJ 1.1
TWIN #02	$CD8^+$	BV 8S1	- CASSTTSGASTDTQYF	- BJ 2.3

[6] NGS was accomplished in cooperation with Dr. Kathrin Held and Dr. Eduardo Beltran.

Even though the clonally expanded T cells were not found yet in the CSF specimens of MS patients, several α- and β-chains were frequently detected (Table 3-11). In sample TWIN #02, three TCR α-chains were detected twice, and three TCR β-chains were found twice or three times. Furthermore, there were several TCR α- and β-chains discovered twice or three times in the CSF specimens of the other four MS patients. In addition, two TCR β-chains (BV 8.1/8.2-CASSFGTEAFF-BJ 1.1 and BV 8.1-CASSTLAVNTEAFF-BJ 1.1) were detected by NGS as well.

Table 3-11: Frequency of TCR α- and β-chains discovered from different MS patients

The single T cell subsets ($CD4^+$/$CD8^+$) were isolated from the CSF specimens of MS patients for identification of the TCR α- and β-chains on the single cell level. **(A)** The TCR α-chains were frequently detected in three CSF samples of MS patients. **(B)** The TCR β-chains were frequently detected in four CSF specimens of MS patients. Frequency indicates the number of times that a specific sequence is recovered.

(A) TCR α-chains

Patient #	Subset		Sequence		Frequency
MP #01	$CD4^+$	AV 1S4	- CAVRSDGQKLLF	- AJ 16	2
TWIN #02	$CD4^+$	AV 16S1	- CAVRDGSSYKLIF	- AJ 12	2
	$CD8^+$	AV 11S1	- CAVDPKTHGSSNTGKLIF	- AJ 37	2
	$CD8^+$	AV 16S1	- CAVRDRGSSNTGKLIF	- AJ 37	2
RIS #01	$CD4^+$	AV 22S1	- CALLRSNDYKLSF	- AJ 20	2

(B) TCR β-chains

Patient #	Subset		Sequence		Frequency
CIS #04	$CD8^+$	BV 6S4	- CASSSLNTEAFF	- BJ 1.1	2
	$CD8^+$	BV 6S2	- CASSLGTSYTGELFF	- BJ 2.2	3
MP #01	$CD8^+$	BV 8S1/8S2	- CASSFGTEAFF	- BJ 1.1	2
MP #02	$CD8^+$	BV 8S1	- CASSTLAVNTEAFF	- BJ 1.1	2
TWIN #02	$CD8^+$	BV 6S3	- CASSLNGISSYEQYF	- BJ 2.7	3
	$CD4^+$	BV 8S1	- CASSLMAPNTEAFF	- BJ 1.1	2
	$CD4^+$	BV 8S1	- CASSARTTNYGYTF	- BJ 1.2	2

Except for the detection of paired TCR α- and β-chains from single T cells, it is important to figure out the clonally expanded TCR transcript repertoire (Vβ, Jβ, Vα, and Jα). We investigated the frequency of these TCR transcript repertoires in 11 CSF specimens from MS patients. The analyzed results are summarized in Figure 3-13. In the Vβ and Jβ transcripts, two V_β (BV 6S2 and BV 8S1) were detected more than 25 times and two Jβ (BJ 1.1 and BJ 2.1) were even discovered 35 times in these CSF specimens. Furthermore, these transcripts mentioned above are also shown in most of the MS patients (Figure 3-13, B). In addition, one Vα (AV 9S2) and J_α (AJ 23) were found more than 10 times in these

TCR sequences. The latter one is shown in 7 MS patients. These transcript repertoires above might belong to the TCRs of clonally expanded T cells persisting in the CSF of MS patients. It brings a new insight to establish a database containing the MS-related TCR repertoires for the MS patients in the future.

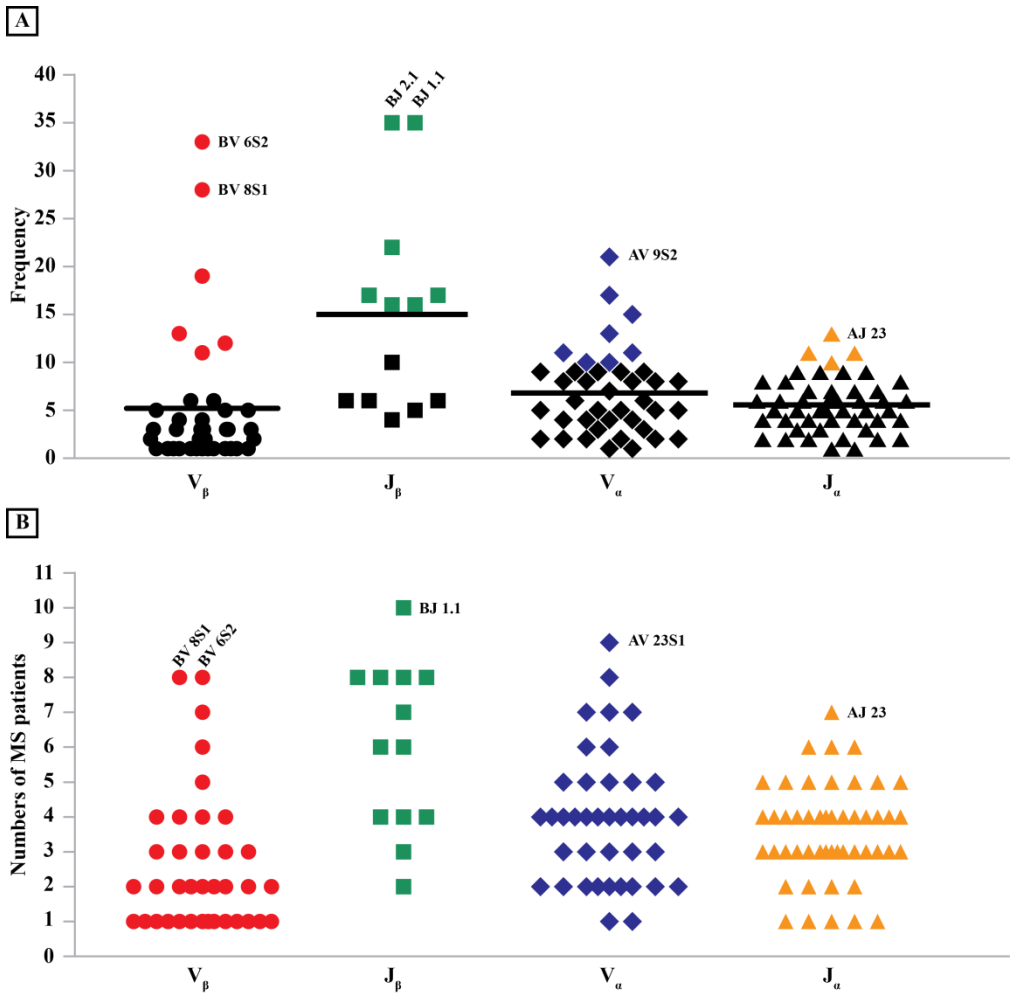

Figure 3-13: TCR α and β transcripts obtained from single CSF T cells of MS patients

The single T cells isolated from CSF specimens of MS patients were employed to recover the TCR α- and β-chains using the optimized unbiased PCR approach. **(A)** The frequency of TCR transcripts was calculated from the CSF specimens of all the MS patients. **(B)** The frequency of the CSF specimens was calculated for the detected TCR transcripts. The red dot represents the Vβ transcripts. Green square represents the Jβ transcripts. Blue diamond represents the Vα transcripts. Orange triangle represents the Jα transcripts. The most detected TCR transcripts are named. Vβ: variable region of β-chain, Jβ: jointing region of β-chain, Vα: variable region of α-chain, Jα: Jointing region of α-chain.

In the 11 CSF specimens, we totally obtained 37 Vβ, 113 Jβ, 40 Vα, and 49 Jα transcripts using the optimized unbiased RT-PCR method. The distribution of these TCR transcripts in the MS patients is

shown in Figure 3-14. The aim is to investigate the correlation between the TCR transcripts and the pathogenesis of MS. The Vβ transcripts are averagely distributed in each MS patient. However, one Jβ (BJ 1.1) was detected in 10 MS patients expect for the MS patient RIS #01, which is also included in many TCR β-chains (Figure 3-13, A). In addition, almost all the Vα and Jα transcripts were detected in MS patient MP #01 (Figure 3-14, B-C), which indicates that the TCR α-chains are polyclonal compared to the TCR β-chains. With the limited specimens, it is hard to figure out the clonally expanded T cells in MS patient #01.

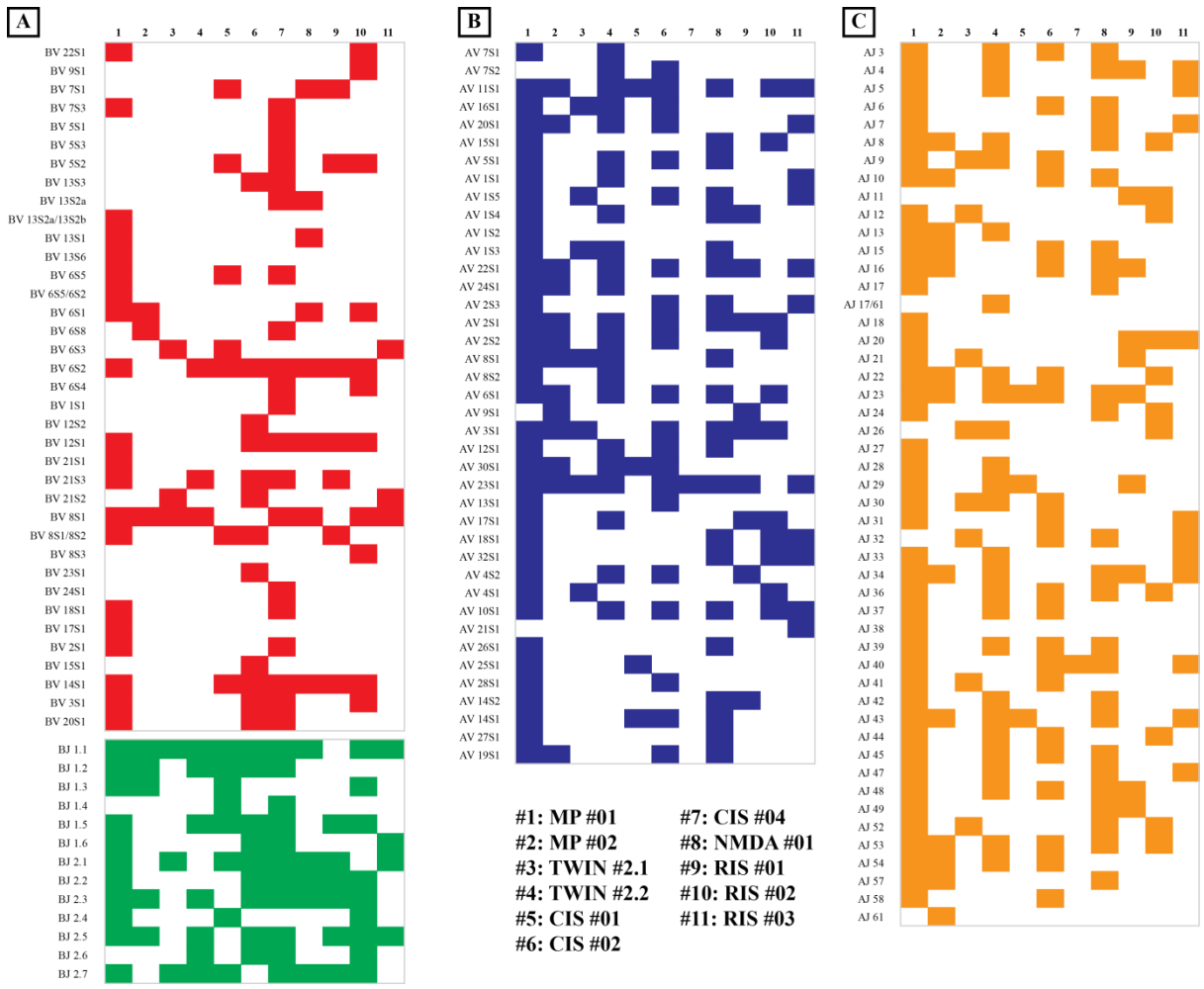

Figure 3-14: Distribution of TCR α and β transcripts obtained from single CSF T cells of MS patients

The single T cells isolated from CSF specimens of MS patients were employed for recover the TCR α- and β-chains using the optimized unbiased PCR approach. We totally achieved 37 Vβ transcripts, 113 Jβ transcripts, 40 Vα transcripts and 49 Jα transcripts from 11 CSF specimens of MS patients (#1-#11). **(A-C)** We examined the distribution of these TCR transcripts in different MS patients. Red represents the Vβ transcripts. Green represents the Jβ transcripts. Blue represents the Vα transcripts. Orange represents the Jα transcripts.

In summary, high yield of TCR α- and β-chains from single T cells were obtained in the CSF samples of MS patients using the optimized RT-PCR technology. Even if the clonally expanded αβ-TCRs failed to be identified from the limited numbers of single T cells, some TCR transcripts were indeed detected frequently both in the TCR clones and in the MS patients. These transcripts might indeed be consisted in the clonally expanded TCRs of disease-related T-cell populations, which need more investigation in the future.

3.4 Resurrection of Disease-Related $CD8^+$ T cells *in vitro*

In the section, we introduced two other recombinant diseased-related TCRs to identify the target antigens. One TCR is the well-investigated standard TCR JM22 model (Gotch et al., 1987; Stewart-Jones et al., 2003), which is specific for *HLA-A*02101* (HLA-A2) and recognizes the presenting peptide, such as the amino acids 58-66 of the influenza matrix protein (flu (58-66)). The other TCR (BV1-BJ2.3-AV7.2-AJ24.2) was done from the brain biopsy sample of the MS patient FE, which owns the identical TCR β-chain and the same V_α gene segments with other three detected αβ-TCRs (Figure 1-4). In the previous work, these two reconstructed αβ-TCRs are ligated into an expression vector and then transfected to the T hybridoma cell line $58\alpha^-\beta^-$ that is deficient of endogenous TCRs (Blank et al., 1993). Subsequently, the stably transfected cells were employed in the thesis for the antigen search. COS-7 cell line and autologous Epstein-Barr virus transformed B (EBV-B) cell lines from patients served as the APCs to express the patient-related HLA molecules and present the candidate peptide libraries (PECP library). COS-7-A2 cell line, stably expressing the human HLA-A2 molecules, is used to present the antigens to the reconstructed T hybridoma cells 58-JM22 (Siewert et al., 2012). The EBV-B cell lines, generated from the patients' blood, express HLA alleles of the patients and present the autologous antigens to specific T cells.

Before antigen screening with the candidate peptide libraries, the cell lines used to be characterized. Firstly, we analyzed the two stable transfected T hybridoma cell lines for stably expressing murine CD3, the patient-specific αβ-TCRs, and CD8 molecules additionally with NFAT-sGFP upon cell

activation (Section 3.4.1). Secondly, the T hybridoma cells must be activated by CD3-cross-linking (Section 3.4.2).

3.4.1 Expression of Recombinant TCRs and Co-Receptor CD8 *in vitro*

58-JM22 T hybridoma cell line was created and re-cloned by Katherina Siewert (Siewert et al., 2012). 58-FE-BV1-BJ2.3-AV7.2-AJ24.2 T hybridoma cell line was established in our lab and subcloned by Latika Bhonsle. When I got these two T-cell clones, I immediately examined the expressions of recombinant TCRs (JM22 and BV1-BJ2.3-AV7.2-AJ24.2) and the co-receptor CD8 molecules. As described in Section 2.4.9, 1.5×10^6 cells were stained with the particular antibodies (Table 2-11). Then flow cytometry was used to examine the expression of these molecules mentioned above. The testing results are shown in Figure 3-15.

The FACS results indicate that all molecules are stably expressed on the surfaces of 58-JM22 T hybridoma cells (Figure 3-15, A). Due to the unavailable commercial antibody against AV10.1 TCR α-chains of JM22, we may ascertain the mRNA level expression by the application of an RT-PCR (Data not shown). However, the expression of human CD8 β-chain on the 58-FE-BV1-BJ2.3-AV7.2-AJ24.2 T hybridoma cells is only 18.3%, while all other molecules including murine CD3ε, human CD8α, and human TCR αβ-chains were highly detected (Figure 3-15, B). The affinity between CD8 and Class I MHC molecules facilitates the TCR to bind the target cell closely during the antigen-specific T cell activation. Therefore, we have to increase the expression of CD8 β-chain on the 58-FE-BV1-BJ2.3-AV7.2-AJ24.2 T hybridoma cells.

The genes for human CD8 α- and β-chains are connected by an IRES sequence in the expression vector (Siewert et al., 2012). However, the reason for low expression of CD8 β-chain during the plasmid replication was unknown so far. Fortunately, there were still few numbers of cells expressing CD8 β-chains (Figure 3-15, B). It is conceivable to enrich and produce these hCD8β-positive cells by MACS® technology according to the manufacturer's introduction. After cell separation and cultivation, the expression of CD8 β-chains on the 58-FE-BV1-BJ2.3-AV7.2-AJ24.2 T hybridoma cells was

examined by flow cytometry (Figure 3-16). Compared to the percentage of hCD8β-positive cells before cell separation, more than 99% cells are capable of stable expression of human CD8β after cell separation.

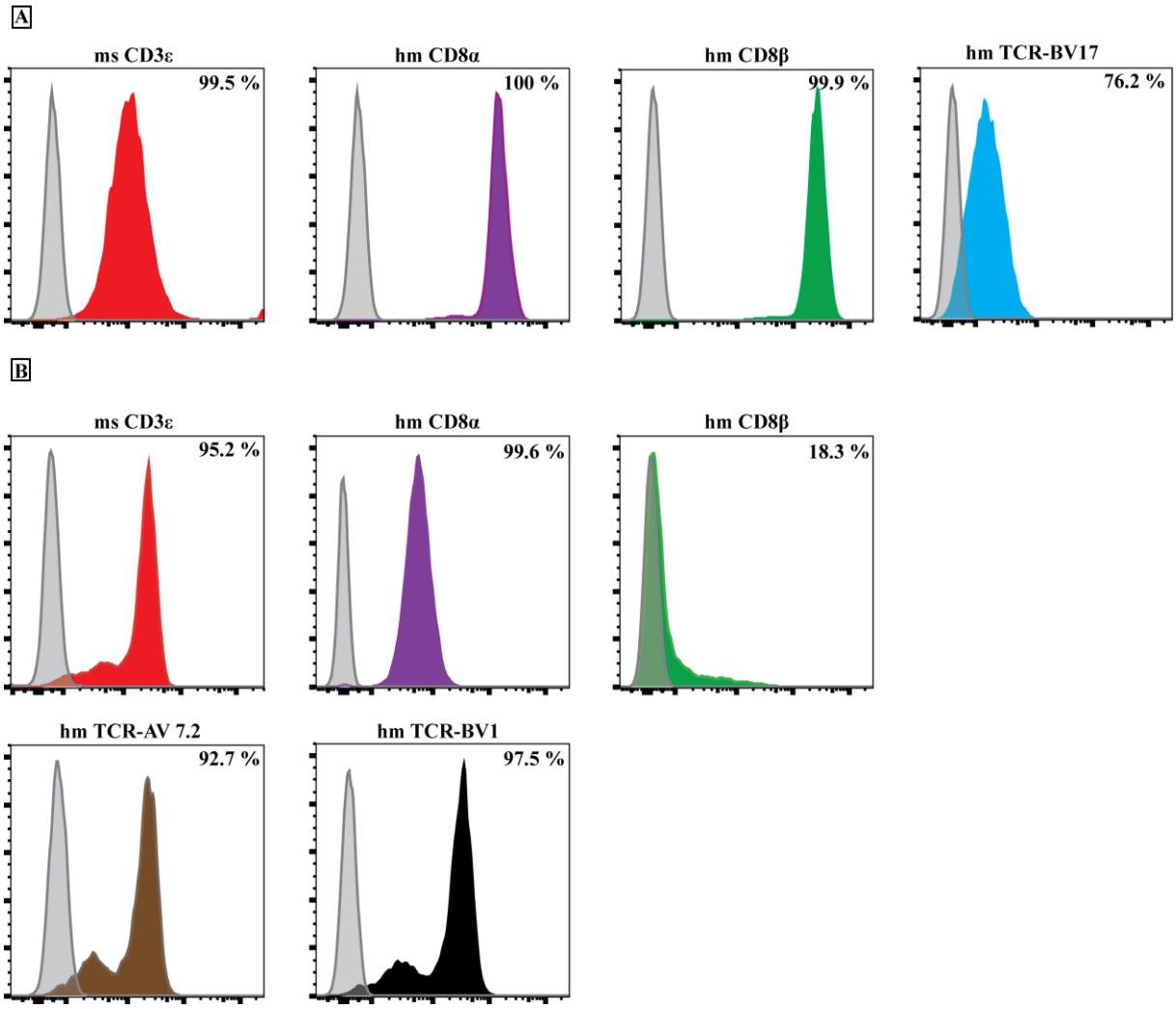

Figure 3-15: Expression of recombinant TCRs and co-receptor CD8 molecules before subcloning

The inherent murine CD3 (ms CD3, red) and the human CD8 molecule (hm CD8, α: purple, β: green) were expressed on the surface of both 58-JM22 **(A)** and 58-FE-BV1-BJ2.3-AV7.2-AJ24.2 **(B)** T hybridoma cell lines. Two recombinant TCRs were examined with the expressions of human BV17 TCR β-chains (hm TCR-BV17, blue) for 58 JM22 cells and human AV7.2 TCR α-chains (hm TCR-AV7.2, brown) as well as the human BV1 TCR β-chains (hm TCR-BV1, black) for 58-FE-BV1-BJ2.3-AV7.2-AJ24.2 cells. The isotype control of each antibody is presented with a gray shaded curve in Flow cytometry. The percentage of the expression of each molecule is labeled on each flow chart. Ms: mouse; hm: human.

In conclusion, before antigen search, the expression of recombinant TCRs and other important molecules in two stable transfected T hybridoma cells were examined and optimized. Then the two cell lines are ready for subsequent target antigen screening experiments.

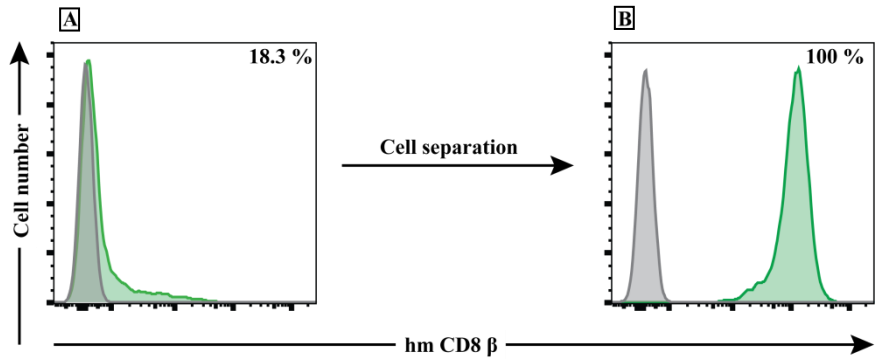

Figure 3-16: Expression of CD8β in 58-FE-BV1-BJ2.3-AV7.2-AJ24.2 T hybridoma cells before and after separation

MACS® technology was employed to separate and enrich the cells containing the plasmid LPC-hCD8α-IRES-hCD8β. The expressions of hCD8β (green curve) on the surface of cells before **(A)** and after **(B)** separation were detected by Flow cytometry. The isotype control of the antibody is presented with a gray shaded curve.

3.4.2 TCR Activation *in vitro* by CD3 Cross-linking

The two T hybridoma cell lines were co-transfected with pcDNA-NFAT-sGFP that encoded for sGFP under the control of the NFAT promoter. The green signal could be detected by a fluorescence microscopy, once the T cells are activated by specific antigens. As described in Section 2.4.8.1, T cell activation could be stimulated *in vitro* by a specific antibody against murine CD3e. sGFP expression was detected by the following three readout methods: fluorescence microscopy, flow cytometry and IL-2 secretion measurement. The examination results are shown in Figure 3-17. The two cell lines could be activated *in vitro* by CD3 cross-linking (Figure 3-17, A1, A2, B1, and B2). In addition, the IL-2 secretion upon TCR activation was also detected in the supernatant (Figure 3-17, A3 and B3).

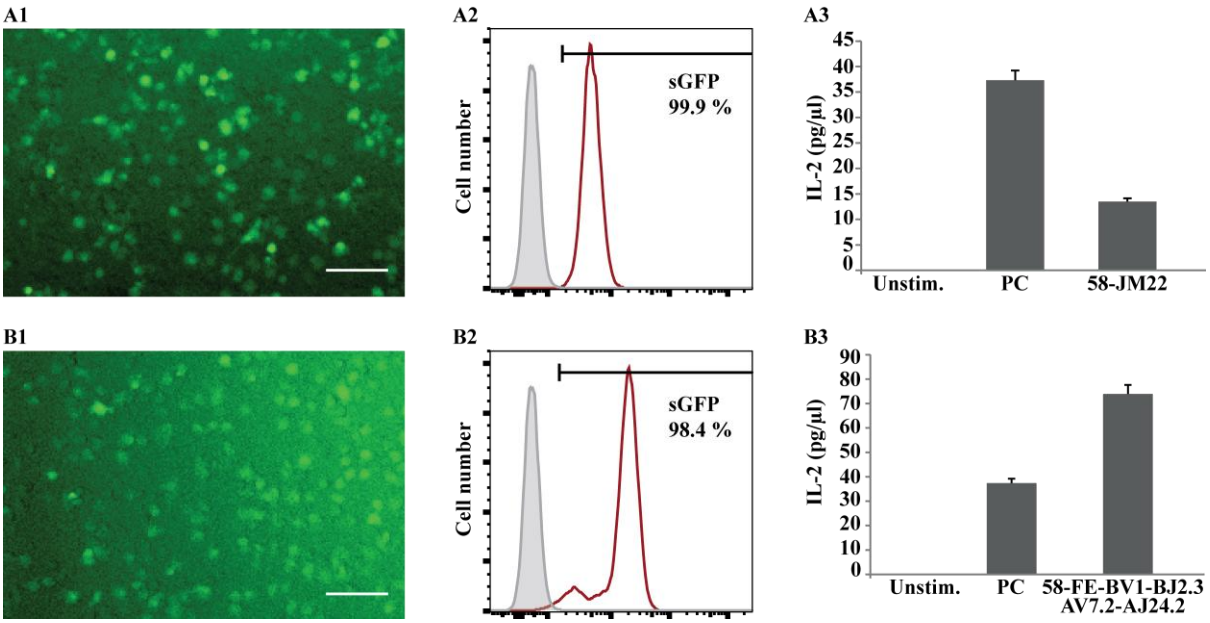

Figure 3-17: TCR activation *in vitro* by CD3 cross-linking

The activation of 58-JM22 **(A)** and 58-FE-BV1-BJ2.3-AV7.2-AJ24.2 **(B)** T hybridoma cells by CD3 cross-linking was examined by the following three readout ways. **(A1-B1)** Upon the NFAT-sGFP production in the activated cells, the green signals were directly detected by fluorescence microscopy. Almost 80% of activated T hybridoma cells directly discerned by the fluorescence channel were NFAT-sGFP$^+$ cells. **(A2-B2)** These stimulated T cells (red curve) were examined by Flow cytometry. The gray curves correspond to the unstimulated T hybridoma cells as negative control. **(A3-B3)** In the supernatant of these stimulated T cells, the secretion of IL-2 was measured by ELISA. The IL-2 secretion of unstimulated (Unstim) T cells served as negative control, and the transfected T hybridoma cells (IP2-8S1) was used as positive control (PC). Scale bar=50 µm.

Before target antigen screening, we did investigate the autologous or EBV antigens for the MS-related TCR BV1-BJ2.3-AV7.2-AJ24.2. The EBV-transducted B cells (EBV-B-FE) derived from MS patient FE served as APCs (Section 2.4.8.2). Unfortunately, the MS-related T hybridoma cells could not be activated, i.e. the signals with autologous APC were not distinguishable from signals of the negative control (Data not shown). It indicates that the target antigens of the MS-derived TCR are neither ubiquitously expressed autologous proteins nor EBV proteins.

In summary, before antigen search, the two stable transfected T hybridoma cell lines could be activated by CD3 cross-linking, which are suitable for the following experiments of antigen search.

3.5 Identification of Specific Antigens of Recombinant TCRs

Since the MS-derived TCRs failed to recognize the autologous and EBV antigens, it was required to apply an unbiased method to search the specific target antigens. In combination with the plasmid-encoded combinatorial peptide (PECP) libraries and the NFAT-sGFP TCR activation, we successfully established a prominent technology to apply the antigen search (Siewert et al., 2012). This technology allows us to screen ~10^9 possible peptide antigens and is available to process and present the proper antigen to the TCR. Importantly, we could isolate the correct antigen-presenting cells and screen the specific antigenic peptide finally.

3.5.1 PECP Libraries Employed for Antigen Unbiased Search

$CD8^+$ T cells recognize the MHC class I restricted antigenic peptides that usually contain 8-10 amino acids. In the previous study, five mimotopes of antigens were successfully characterized from a PECP library ($A2^{269}$), which could activate TCR JM22 co-cultured with *HLA-A*0201* expressed COS-7 cells (Siewert et al., 2012). These mimotopes are shown to be nonapeptides with similar amino acids to the flu (58-66) peptide from the influenza matrix protein. Based on the applicable unbiased technology, we characterized other mimotopes from the $A2^{269}$ library, which are recognized by TCR JM22.

Likewise, the TCR BV1-BJ2.3-AV7.2-AJ24.2 was derived from autoaggressive $CD8^+$ T cells in the brain lesions of MS patient FE who was examined to be homozygous for only three HLA alleles of *HLA-A*0101, -B*0801* and *-C*0701*. To investigate the specific antigens of TCR BV1-BJ2.3-AV7.2-AJ24.2, we synthesized three PECP libraries ($A1^{39}$, $B8^{359}$, and $C7^9$) specifically for these HLAs. In addition, due to the Vα7.2 genes belongs to the semi-variable TCRs of the MAIT cells that recognize MR1-restricted antigens, the TCR BV1-BJ2.3-AV7.2-AJ24.2 might be possessed by the MAIT cells (Figure 1-4). Despite the identical Vα7.2 genes and longer CDR3 regions of α-chain, there is no direct evidence so far to tell the MS-derived TCR belonging to $CD8^+$ T cells or MAIT cells. Thus, except for the three PECP libraries mentioned above, a universal PECP library (N27) was created to investigate

the potential antigenic peptide recognized by the MAIT cells. The nucleotides of nonamer insert and the total clone numbers for these PECP libraries are presented in Table 3-12. Except N27 library containing nine random amino acids, all the other PECP libraries comprise conserved amino acid residues or "anchor positions" specifically binding to the MHC class I molecules.

Table 3-12: PECP library employed for antigen search

The five-nonamer residues all start with a guiding Kozak sequence, the start codon (ATG) and all end with the stop codon (TGA). 9 positions of amino acid are performed with the random amino acid (X) except the fixed anchor positions (red). In the cDNA sequences depicted in red, "N" represents the presence of any of the four (adenine, cytosine, thymidine and guanidine) residues while a "K" residue corresponds to a guanine or thymidine residue. $A1^{39}$: PECP library containing nonapeptides anchored at positions 3 and 9 by an Aspartic acid (D) and Tyrosine (Y) residue. $A2^{269}$: PECP library containing nonapeptides anchored at positions 2, 6 and 9 by an Isoleucine (I), Tyrosine (V) and Leucine (L) residue. $B8^{359}$: PECP library containing nonapeptides anchored at positions 3, 5 and 9 by a Lysine (K), Lysine or Arginine(R) and Leucine (L) residue respectively. $C7^{9}$: PECP library containing nonapeptides anchored at position 9 with a Lysine (K) residue. N27: PECP library containing nine random amino acids. *These libraries are established by Katherina Siewert and Latika Bhonsle, respectively.

		Nonamer insert								
PECP library ID*	**Total clones**	**1**	**2**	**3**	**4**	**5**	**6**	**7**	**8**	**9**
$A1^{39}$	80×10^6	X	X	D	X	X	X	X	X	Y
		NNK	NNK	GAC	NNK	NNK	NNK	NNK	NNK	TAT
$A2^{269}$	17×10^6	X	I	X	X	X	V	X	X	L
		NNK	ATC	NNK	NNK	NNK	GTG	NNK	NNK	CTA
$B8^{359}$	70×10^6	X	X	K	X	K/R	X	X	X	L
		NNK	NNK	AAA	NNK	ARG	NNK	NNK	NNK	CTN
$C7^{9}$	110×10^6	X	X	X	X	X	X	X	X	K
		NNK	NNK	NNK	NNK	NNK	NNK	NNK	NNK	AAR
N27	95×10^6	X	X	X	X	X	X	X	X	X
		NNK	NNK	NNK	NNK	NNK	NNK	NNK	NNK	NNK

3.5.2 Reduction of T-cell Spontaneous Activation by Re-cloning

Not all positive signals, i.e. green ($sGFP^+$) TCR-transfected T hybridoma cells, indicate TCR activation, as T cells might turn green by spontaneous self-activation (Section 1.7). During the antigen search, spontaneous activation may be detected both in negative controls and in antigen-screening samples. If the T hybridoma cells contain a high content of clones that were spontaneously activated, we re-cloned the cells as described in Section 2.4.4. Activation of 58-FE-BV1-BJ2.3-AV7.2-AJ24.2 T hybridoma cells with and without CD3 stimulation was examined by Flow cytometry (Figure 3-18). The chosen cell clone should meet two criteria: (i) Rare spontaneous activation was detectable without the antigen recognition. (ii) In the presence of the antigenic stimuli, the chosen T cell clone responded

as the strongest signal that was clearly observed by fluorescence microscope or Flow cytometry. Before cell re-cloning, we detected 4.78% false positives in the 58-FE-BV1-BJ2.3-AV7.2-AJ24.2 T hybridoma cells without CD3 stimulation (Figure 3-18, A). After re-cloning for the cell line, we got the best cell clone (Figure 3-18, B) that had ~0.014% of false positives (right panel) and strongest activation signals upon CD3 stimulation (left panel). Consequently, the best cell clone was increased to a certain number and stored in liquid nitrogen for subsequent antigen search of TCR BV1-BJ2.3-AV7.2-AJ24.2.

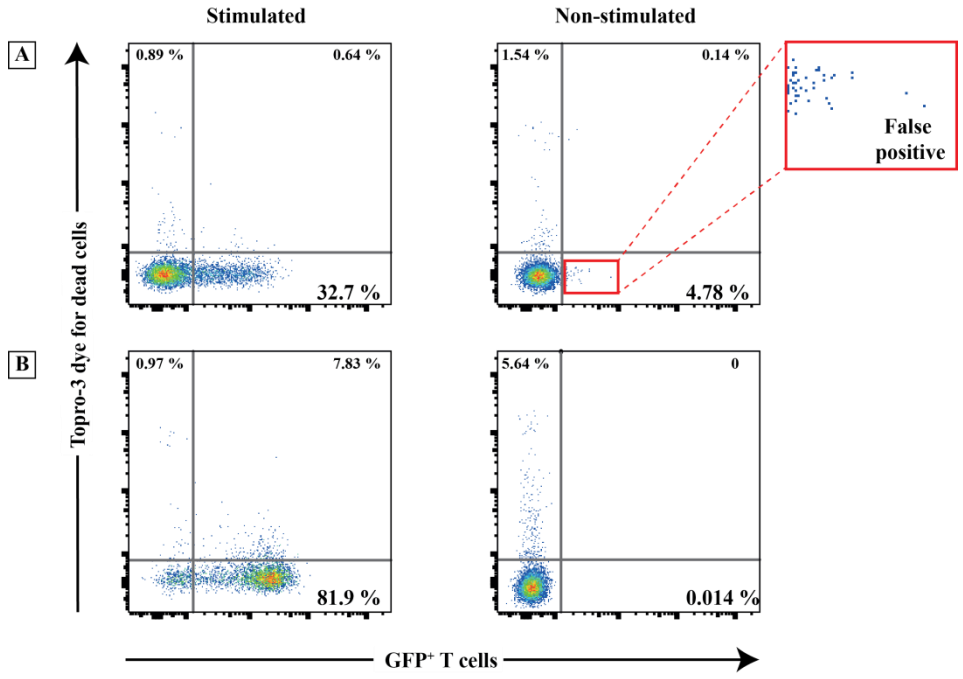

Figure 3-18: Spontaneous activation of TCR BV1-BJ2.3-AV7.2-AJ24.2 reduced by cell re-cloning

The activation response (by sGFP expression) of 58-FE-BV1-BJ2.3-AV7.2-AJ24.2 T hybridoma cells with or without CD3 stimulation was measured by flow cytometry. **(A)** High false positive is shown in the spontaneous activation of T cells before re-cloning. **(B)** The best cell clone presents hypo-stimulated response and less false activation after re-cloning. The scatter plots are divided into four quadrants based on the negative control (data not shown). The upon two quadrants contain the population of the dead cells that were stained with the Topro-3 dye, and the lower right quadrant includes the portion of the $sGFP^+$ cell populations that were count and further analyzed.

3.5.3 Search of Positive APCs upon TCR Activation

3.5.3.1 Antigen search for TCR JM22

TCR JM22 recognizes antigens presented by the HLA-A2 restricted APCs. Here, the COS-7-A2 cell line served as APCs, which was verified for stable expression of HLA-A2 on the cell surface before antigen search (Figure 3-19). As described in Section 2.7, 58-JM22 T hybridoma cells were co-cultured with the COS-7-A2 cells that were transfected with the $A2^{269}$ library for 16 hours. After 16 hours co-cultivation, we examined the samples and searched for T cells that have turned green. The green T cells ($sGFP^{+}$) were observed under the fluorescence microscope (Figure 3-20).

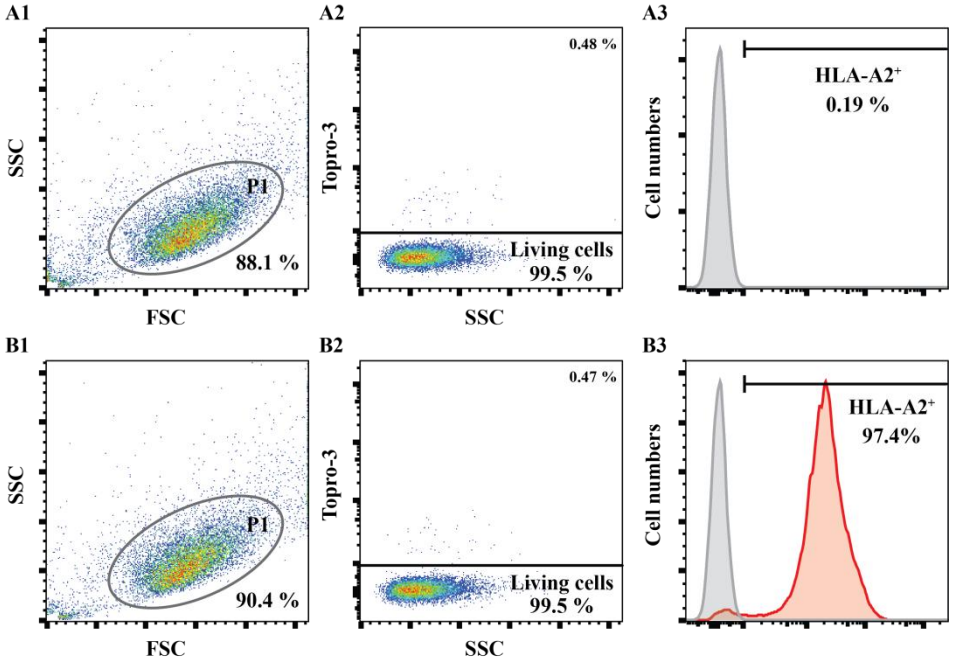

Figure 3-19: Expression of HLA-A2 in the stably transfected COS-7-A2 cell line

Stable transfected COS-A2 cells were stained either with the isotype control IgG2b-PE **(A1-A3)** or with the antibody anti-HLA-A2-PE **(B1-B3)** as well as the fluorescent dye (Topro-3) for dead cells. **(A1-B1)** Gate P1 represents the population of COS-7-A2 cells. **(A2-B2)** The living COS-7-A2 cells are subsequently selected from gate P1. **(A3-B3)** The $HLA\text{-}A2^{+}$ cells are subsequently selected from the living COS-7-A2 cells. **(B3)** $HLA\text{-}A2^{-}$ (gray) and $HLA\text{-}A2^{+}$ (red) expressions are overlaid in COS-7-A2 cells. SSC: Side scatters, FCS: Forward scatters.

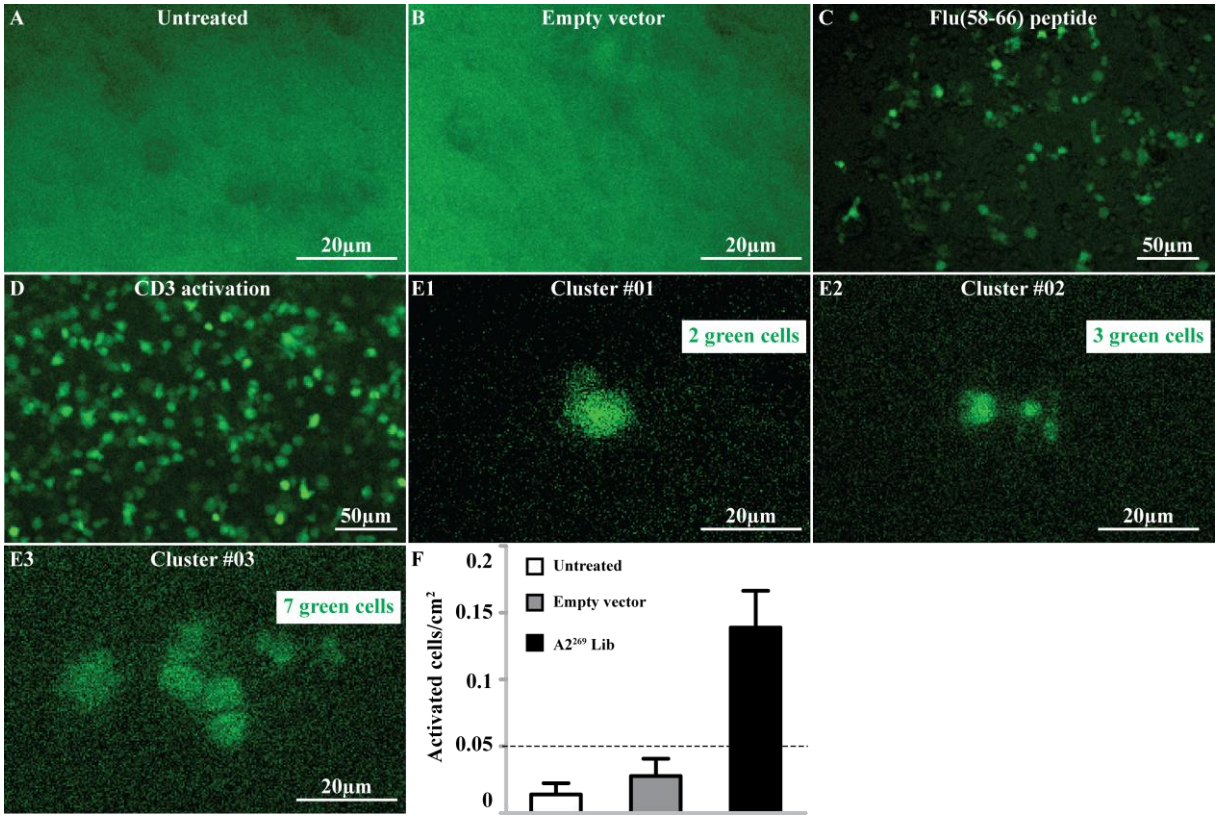

Figure 3-20: TCR JM22 activation by $A2^{269}$ library

The sGFP expression of T hybridoma cells that were co-cultured with different treated COS-7-A2 cells was observed under the fluorescence microscope. After transfection, the T hybridoma cells were added and analyzed at the time point of 48 and 72 hours post transfection. **(A-B)** Un-transfected COS-7-A2 cells and transfected with empty vector served as negative controls. **(C)** COS-7-A2 cells treated with Flu (58-66) peptide served as positive control. **(D)** T hybridoma cells were activated by CD3 cross-linking. **(E1-E3)** Clusters of activated T hybridoma cells were detected with the transfection of $A2^{269}$ Lib. The number of $sGFP^+$ cells is labeled in green. **(F)** Activated (GFP^+) cells (counted per cm^2) in response to different treated COS-7-A2 cells are calculated and shown in a histogram. $A2^{269}$ Lib: *HLA-A*0201* matched nonapeptide library. The size of scale bar is labeled on each image.

Un-transfected COS-7-A2 cells and transfected with empty vector served as the negative controls (Figure 3-20, A-B). The aim is to distinguish library-dependent activation of T cells from background activation. The threshold value of activated T cells per cm^2 is set at 0.05 in Figure 3-20 (F, dashed line). Therefore, higher numbers of activated T cells were detected with $A2^{269}$ Lib, compared to negative controls. Three cell clusters of JM22 T hybridoma cells were detected in the activation assays. The clusters are shown in Figure 3-20 (E1-E3), which contain 2, 3, or 7 activated T cells. Obviously, Cluster #03 with 7 activated T cells was the most promising activation of TCR JM22 and COS-7 cell underneath might express the particular antigen. In addition, flu (58-66) peptide and CD3 cross-

linking served as positive controls to ensure the activated efficiency of 58-JM22 T hybridoma cells (Figure 3-20, C-D). Later, the single positive APCs are isolated by micromanipulation for the recovery of the antigen coding plasmid. An example of APC isolation using a microcapillary is presented in Figure 3-21.

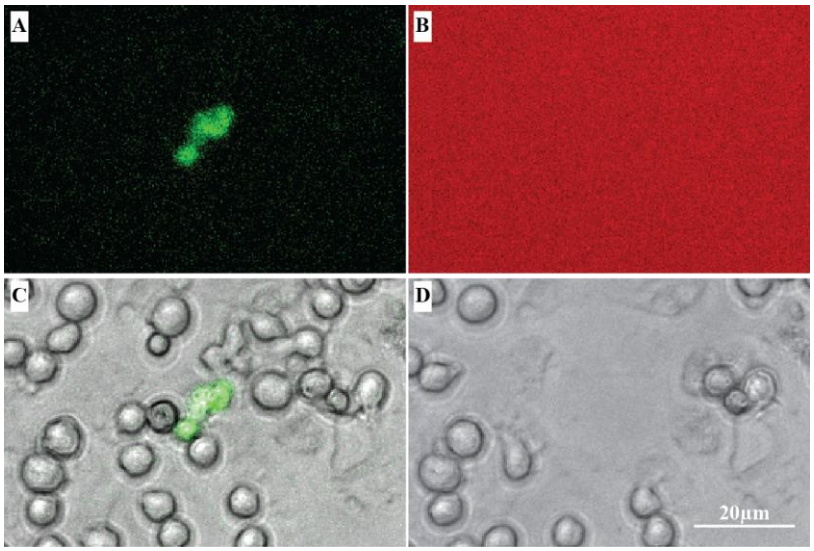

Figure 3-21: Micromanipulation of the COS-7 cell beneath the activated T hybridoma cells

T hybridoma cells were co-cultured with COS-7 cells that co-transfected with the patient related HLA alleles and the restricted PECP libraries. After 16 hours of co-culturing, the activated T cells were detected under the fluorescence microscope, and the positive COS-7 cells underneath were isolated using a micromanipulator. **(A-C)** The activated T cell cluster is detectable in green with FITC light and composited with the image in transmitted channel, yet undetectable with Cy3 light. **(D)** Image shows the same area after the isolation of COS-7 cells by a microcapillary (microcapillary not in the image). Scare bar=20 µm.

In conclusion, the numbers of positive APCs recognized by TCR JM22 is summarized in Table 3-13 (A). In the total areas of investigation (172.8 cm^2), 35 activated T cells by $A2^{269}$ library were detected under the fluorescence microscope. Meanwhile, 24 positive APCs underneath were immediately isolated for the recovery of the antigen coding plasmids. In these activated T cells, 5 clusters (N=2 + N≥3) were discovered, and the COS-7 cells underneath might express the specific antigen(s).

Table 3-13: Summary of APCs isolation in different antigen libraries recognized by two transfected T hybridoma cell lines

Co-cultivation of COS-7 cells and T hybridoma cells was performed on BD Falcon® cell culture dishes. At least 3 biological replicates proceed with the same investigated areas in the negative controls. N represents the numbers of activated T cells ($sGFP^+$) included in one cluster.

A. Activation of 58-JM22 T hybridoma cells

PECP Library	HLA-	Areas of Investigation (cm^2)	Activated T cells	Isolated APCs	Clusters (Areas of Investigation, cm^2)		
					N=1	N=2	N≥3
$A2^{269}$ Lib	A*0201	172.8	35	24	19 (134.4)	3 (9.6)	2 (28.8)

B. Activation of 58-FE-BV1-BJ2.3-AV7.2-AJ24.2 T hybridoma cells

PECP Library	HLA-	Areas of Investigation (cm^2)	Activated T cells	Isolated APCs	Clusters (Areas of Investigation, cm^2)	
					N=2	N≥3
$A1^{39}$ Lib	A*0101	115.2	1	0	0	0
$B8^{359}$ Lib	B*0801	115.2	4	2	2 (115.2)	0
$C7^{9}$ Lib	C*0701	192	31	14	11 (76.8)	3 (38.4)
$A1^{39}$, $B8^{359}$ and $C7^{9}$ Lib	A*0101, B*0801 and C*0701	336	19	5	1 (115.2)	4 (38.4)
N27 Lib	MR1	432	29	10	3 (48)	7 (105.6)

3.5.3.2 Antigen search for TCR BV1-BJ2.3-AV7.2-AJ24.2

TCR BV1-BJ2.3-AV7.2-AJ24.2 was identified from the $CD8^+$ T cells in the brain lesion of MS patient FE, but the HLA restriction was not ascertained. MS patient FE possesses the three alleles *HLA-A*0101*, *HLA-B*0801*, *HLA-C*0701*, because he is homozygous for the HLA class I gene locus. Here, we had to screen each HLA-matched PECP library (e.g., $A1^{39}$ Lib, $B8^{359}$ Lib, and $C7^{9}$ Lib) that expressed on the APCs bonding to each HLA allele (e.g., *HLA-A*0101*, *HLA-B*0801*, and *HLA-C*0701*).

In contrast to the cell line COS-7-A2 that was stably transfected with human *HLA-A*0201*, it was not possible to establish the stable transfected COS-7 cell lines expressing the different HLA alleles restricted for MS patient FE. So we had to co-transfect the plasmids encoding each HLA allele (e.g., *HLA-A*0101*, *HLA-B*0801*, and *HLA-C*0701*) and matched PECP library (e.g., $A1^{39}$ Lib, $B8^{359}$ Lib, and $C7^{9}$ Lib) into COS-7 cells. In addition, as mentioned in Section 1.5.3, it is uncertain whether TCR BV1-BJ2.3-AV7.2-AJ24.2 might be a MAIT cell or not. Therefore, it should also be examined whether this TCR might be activated by MR1 restricted N27 library or not. After 16 hour of co-culturing, the activation of TCR BV1-BJ2.3-AV7.2-AJ24.2 by different PECP library was detected under the fluorescence microscope (Figure 3-22).

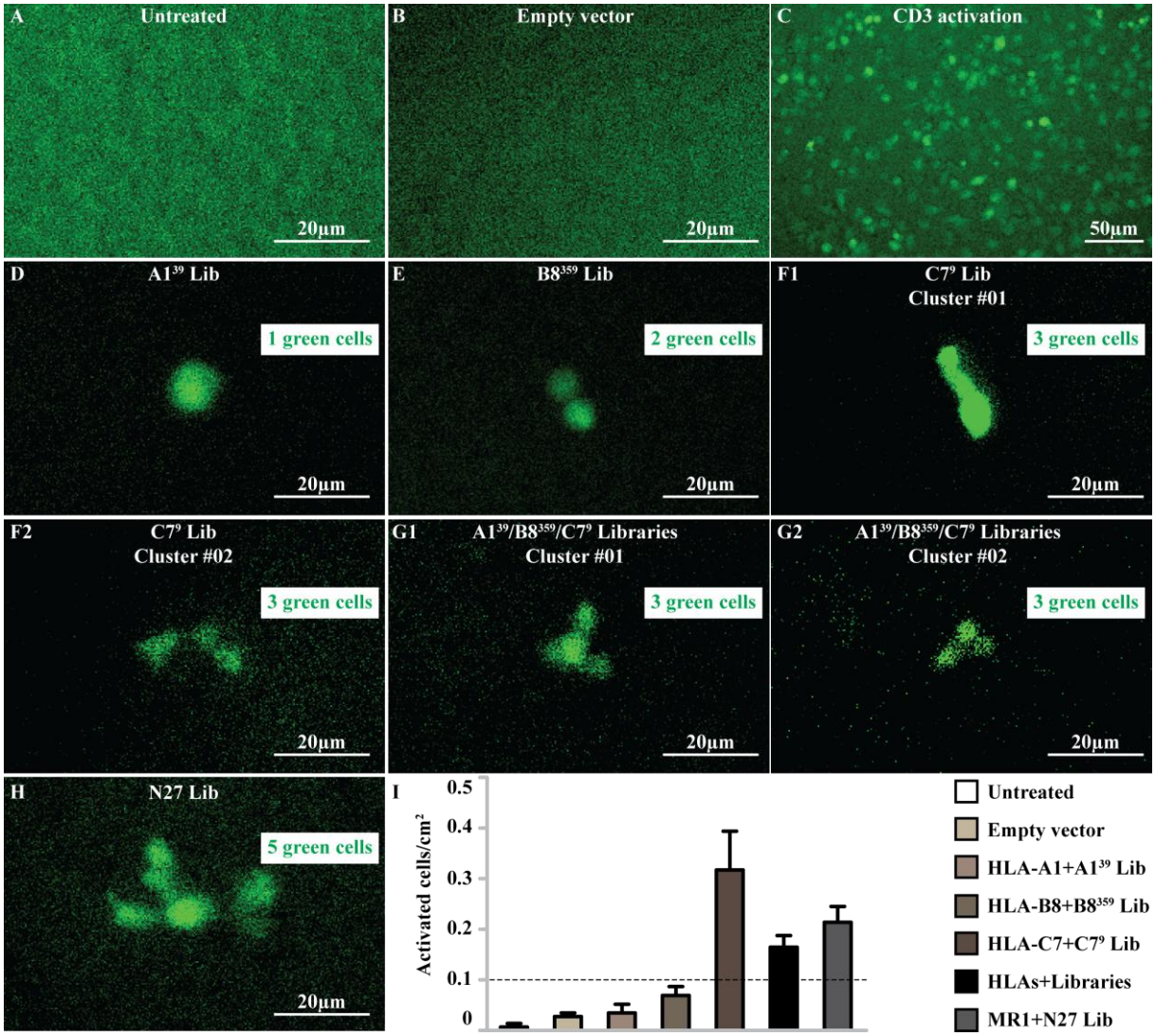

Figure 3-22: TCR BV1-BJ2.3-AV7.2-AJ24.2 activation by PECP libraries presented by different MHC molecules

Activated 58-FE-BV1-BJ2.3-AV7.2-AJ24.2 T hybridoma cells ($sGFP^+$) were observed in co-culturing with untransfected COS-7 cells **(A)**, COS-7 cells transfected with empty vector **(B)**, *HLA-A*0101* matched $A1^{39}$ Lib **(D)**, *HLB-A*0801* matched $B8^{359}$ Lib **(E)**, *HLA-C*0701*matched $C7^9$ Lib **(F1-F2)**, all HLA alleles (*HLA-A*0101*, *HLB-A*0801* and *HLA-C*0701*) matched PECP libraries **(G1-G2)** and MR1 matched N27 Lib **(H)**. The number of $sGFP^+$ cells is labeled in green on each image. **(I)** A column of GFP^+ cells (counted per cm^2) is in response to the PECP libraries presented by different MHC molecules. The activation by CD3 cross-linking **(C)** served as positive control. The three MHC class I alleles of the patient FE (only three alleles, as he is homozygous) and MR1 were tested and this experiment was repeated more than five times. HLA: human leukocyte antigen. MR1: MHC class I related molecule-1. $A1^{39}$ Lib: *HLA-A*0101* matched nonapeptide library. $B8^{359}$ Lib: *HLA-B*0801* matched nonapeptide library. $C7^9$ Lib: *HLA-C*0701* matched nonapeptide library. N27 Lib: Randomized nonapeptide library. The size of scale bar is labeled on each image.

In Figure 3-22 (A-C), un-transfected COS-7 cells and transfected with empty vector served as negative controls, and the activation of T cells by CD3 cross-linking served as positive control. For $A1^{39}$ and $B8^{359}$ libraries, only one or two green T cells were detected (Figure 3-22, D-E). However, higher numbers of green T cells were observed in the samples with the $C7^{9}$ library, which also are summarized in Table 3-13 (B). In the total areas of investigation (192 cm^2), 31 green T cells were detected and included in 14 activated T-cell clusters (N=2 + N≥3). Two clusters consisted of 3 green T cells were detected in the samples transfected with *HLA-C*0701* restricted $C7^{9}$ library (Figure 3-22, F1-F2). Furthermore, in a pool of PECP libraries ($A1^{39}$ + $B8^{359}$ + $C7^{9}$), activated T-cell clusters were also detected (Figure 3-22, G1-G2). In the areas of investigation (336 cm^2), five activated T-cell clusters (N=2 + N≥3) containing 19 green T cells were observed in the samples transfected with a pool of PECP libraries (Table 3-13, B). Combining the results from the activation assays for different PECP libraries above, we assume that the potential antigenic peptide might be contained in the $C7^{9}$ library.

In addition, in the MR1 restricted N27 library, one big cluster with five green T cells ($sGFP^{+}$) was detected (Figure 3-22, H). Totally 29 green T cells in 10 clusters (N=2 + N≥3) were observed in 432 cm^2 of investigation (Table 3-13, B). If the threshold value of activated T cells per cm^2 is set at 0.1, higher numbers of activated T cells were found in the samples transfected with $C7^{9}$ library compared to the MR1 restricted N27 library (Figure 3-22, I).

In summary, the samples transfected with *HLA-C*0701* restricted $C7^{9}$ library were consistently detected with more activated T cells than the other two HLA class I molecules (*HLA-A*0101* and *HLA-B*0801*). However, some activated T cells were also detected in the samples transfected with MR1 restricted N27 library. These observations indicate that either *HLA-C*0701* or MR1 might be the appropriate antigen-presenting partner for TCR BV1-BJ2.3-AV7.2-AJ24.2. To make sure which one is the "real" antigen-presenting partner for the TCR, positive APCs underneath are isolated for recovery of the antigen coding plasmids (Section 3.5.4). Reactivation assays are carried out to re-check these

recovered plasmids that might contain the target antigens for TCR BV1-BJ2.3-AV7.2-AJ24.2 (Section 3.5.5).

3.5.4 Recovery of Antigen Coding Plasmids from Single Positive APCs

Once 31 positive COS-7 cells were successfully isolated in the antigen search for TCR BV1-BJ2.3-AV7.2-AJ24.2, the plasmids were immediately recovered as described in Section 2.2.10. The PCR products were stored at -20 °C until the plasmid reconstruction. After amplification, PCR products (about 150 bp) were examined by gel electrophoresis (Figure 3-23). From the pictures of the agarose gel, no or faint bands were detected in three samples from *HLA-C*0701* restricted $C7^{9}$ Library (Lane 8, 12 and 13) and two samples from MR1 restricted N27 Library (Lane 30 and 31). Except for the five PCR products above, rest of PCR products were successfully amplified. No PCR products might be caused either by the invalid amplification or by the failure of capturing the correct COS-7 cell.

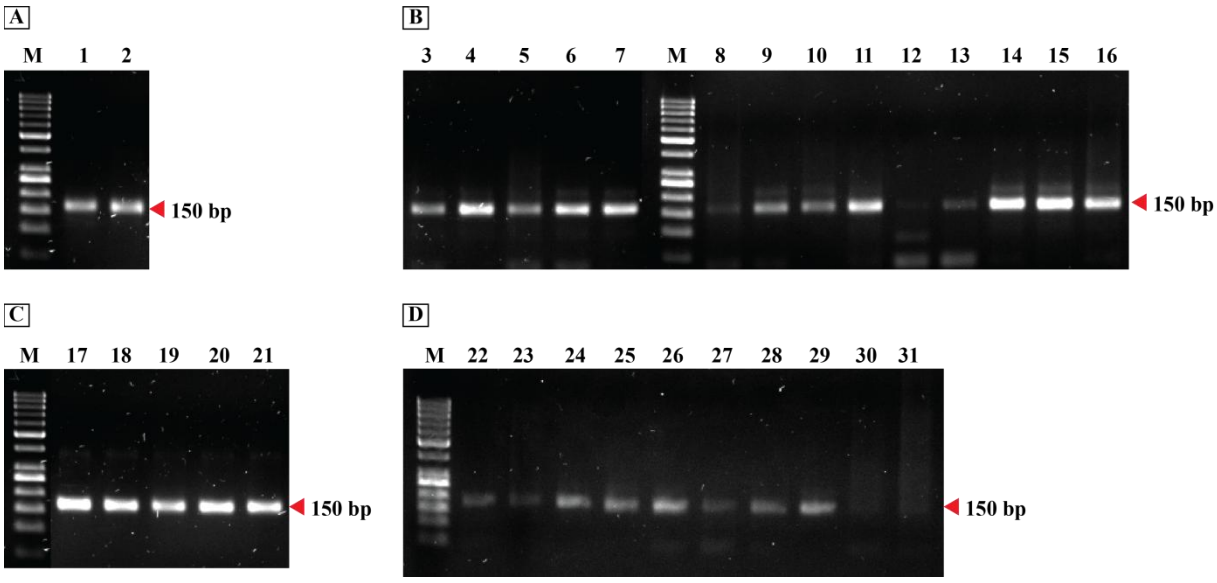

Figure 3-23: Detection of plasmid recovery PCR products by gel electrophoresis

During the antigen search for TCR BV1-BJ2.3-AV7.2-AJ24.2, single positive COS-7 cells were isolated and amplified to recover the antigen coding nucleotides inserted in the expression plasmids. 10 µl of each PCR product was analyzed by gel electrophoresis. **(A)** Lanes 1-2 represent the library inserts from $B8^{359}$ Lib. **(B)** Lanes 3-16 represent the library inserts from $C7^{9}$ Lib. **(C)** Lanes 17-21 represent the library inserts from the mixture of $A1^{39}$, $B8^{359}$, and $C7^{9}$ libraries. **(D)** Lanes 22-31 represent the library inserts from N27 Lib. A 50 bp size ladder (M) is used for size comparison.

In summary, amongst 31 isolated APCs, 29 of them were successfully amplified, which could be reconstructed into the expression vector for the reactivation assay (Section 3.5.5). These plasmids might contain the antigen coding plasmid specifically for TCR BV1-BJ2.3-AV7.2-AJ24.2.

3.5.5 TCR Reactivation by Antigen Pools Isolated from Single APCs

Once reconstructed *in vitro* and replicated through *E.coli* cultivation, these plasmids were re-transfected into the COS-7 cells to testify the reactivation of the recombinant TCRs as described in Section 2.7.3. When reactivation was verified in these plasmids, the promising plasmids were further divided into several smaller subpools to identify the antigen coding plasmid as described in Figure 2-3. Reactivation assays of TCR were performed in each round of subpools of *E.coli* culture until the antigen coding plasmid was identified. During the subpools, activation signals should be enlarged gradually.

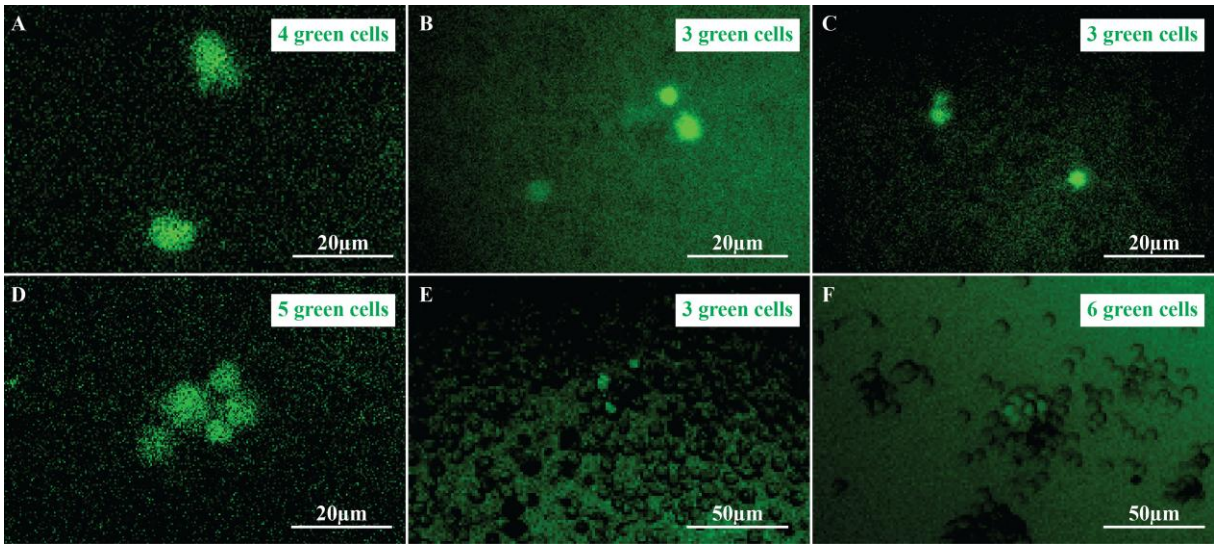

Figure 3-24: Reactivation of TCR JM22 by antigen pools isolated from single APCs

In each round of subpools for enrichment of antigen coding plasmid, reactivation assay was performed to check the antigen-coding plasmid in the 30 probes of subpools. The expression of GFP^+ T cells was detected under the fluorescence microscope. **(A)** The activated T cells were detected in co-culturing with COS-7-A2 cells that transfected with $A2^{269}$ library. The COS-7-A2 cell underneath was isolated and used for the plasmid recovery. **(B-D)** After the plasmid reconstruction, three clusters were detected in the reactivation of TCR JM22. **(E-F)** In the first round of subpools, the plasmids were divided into 30 probes and two clusters were detected in one of these probes. The number of $sGFP^+$ cells (green) and the scale bar (white) both are labeled on each image. Each round of reactivation was repeated with three independent experiments.

During the antigen search for TCR JM22, one cluster of four activated T cells was detected, and the COS-7-A2 cell underneath was isolated for recovery of the antigen coding plasmid. Once the plasmids were reconstructed and replicated, reactivation assay and enrichment of antigen coding plasmid by subpools of *E.coli* culture were carried out. Clusters of green activated JM22 T hybridoma cells were detected in reactivation assays (Figure 3-24). Unfortunately, after two rounds of subpools of *E.coli* culture, the activation signals could not reproduced in three independent experiments. In addition, it was also tried to isolate the positive APCs that were transfected with the plasmids. However, no activated T cells were found in these re-picking experiments.

Table 3-14: Reactivation of TCR BV1-BJ2.3-AV7.2-AJ24.2 by antigen pools isolated from single APCs

The COS-7 cells beneath the activated T cells were isolated and used for the plasmid recovery. The reconstructed plasmids and the corresponding HLAs were co-transfected into COS-7 cells, which employed for the reactivation of TCR BV1-BJ2.3-AV7.2-AJ24.2. The expression of $sGFP^+$ cells was detected by the fluorescence microscope. The reactivation was repeated with three independent experiments. Five plasmids (Bold) that have a strong reaction to TCR activation will be used for enrichment of antigen coding plasmid by subpools.

PECP library	HLA-	Plasmid ID	Initial clones	Areas of Investigation (cm^2)	Activated T cells	Clusters
$A1^{39}$ Lib	A*0101	# A-01	-	-	-	-
$B8^{359}$ Lib	B*0801	# B-01	5,000	12	0	0
		# B-02	8,000	12	0	0
$C7^{9}$ Lib	C*0701	# C-01	7,000	12	0	0
		# C-02	6,000	12	2	1
		# C-03	17,000	12	3	1
		# C-04	9,000	12	2	1
		# C-05	12,000	12	4	1
		# C-06	1,000	12	3	1
		# C-07	28,000	12	3	1
		# C-08	19,000	12	4	2
		# C-09	13,000	12	12	4
		# C-10	15,000	12	9	4
		# C-11	43,000	12	15	6
		# C-12	20,000	12	7	3
		# C-13	17,000	12	14	5
$A1^{39}$ $B8^{359}$ $C7^{9}$	A*0101 B*0801 C*0701	# ABC-01	8,000	16	2	1
		# ABC-02	17,000	16	2	1
		# ABC-03	18,000	16	6	3
		# ABC-04	9,000	16	4	2
		# ABC-05	9,000	16	4	2
N27	MR1	# N-01	31,000	12	0	0
		# N-02	25,000	12	0	0
		# N-03	18,000	12	0	0
		# N-04	31,000	12	4	1

During antigen search for TCR BV1-BJ2.3-AV7.2-AJ24.2, 29 positive APCs were successfully isolated, and the plasmids were recovered and reconstructed *in vitro* as mentioned in Section 3.5.4. Similar to TCR JM22, reactivation assay was repeated with three independent experiments, and the results are summarized in Table 3-14. Briefly, no activation signals were re-detected in two recovered plasmids from $B8^{359}$ library. On the contrary, higher reactivation signals were detected in five recovered plasmids (# C-09 to # C-13) from $C7^{9}$ library. Several green T-cell clusters were observed in these five plasmids, which indicate that they are the most probable ones to contain the antigen coding plasmid. Thus, these plasmids will be used for enrichment of antigen coding plasmid by subpools of *E.coli* culture. In addition, no or few activated T cells were re-detected with the four reconstructed plasmids (# N01 to # N-04) from MR1 restricted N27 library. Therefore, the results of reactivation assays indicate that TCR BV1-BJ2.3-AV7.2-AJ24.2 might not belong to the semi-variant TCR of MAIT cells, but recognize antigens binding to *HLA-C*0701* molecules. However, this hypothesis needs more evidences in the future.

To identify the antigen coding plasmid from the five promising reconstructed plasmids (Table 3-14, # C-09 to # C-13), subpools of *E.coli* culture proceeded as describe in Figure 2-3. The results of reactivation assay from the first round of subpools of *E.coli* culture are presented in Figure 3-25. The reactivation assay was repeated with two independent experiments. Obviously, two green T cells ($sGFP^{+}$) were detected in some batches of plasmids, but stronger activated signals were only detected in one or two batches of plasmids with higher numbers of green T cells ($N \geq 3$). These promising batches for each reconstructed plasmids (Figure 3-25, marked with asterisks) were used for the second round of subpools of *E.coli* culture until the antigen coding plasmid is finally identified. However, the activation signals are never enhanced by the following subpools (Data not shown).

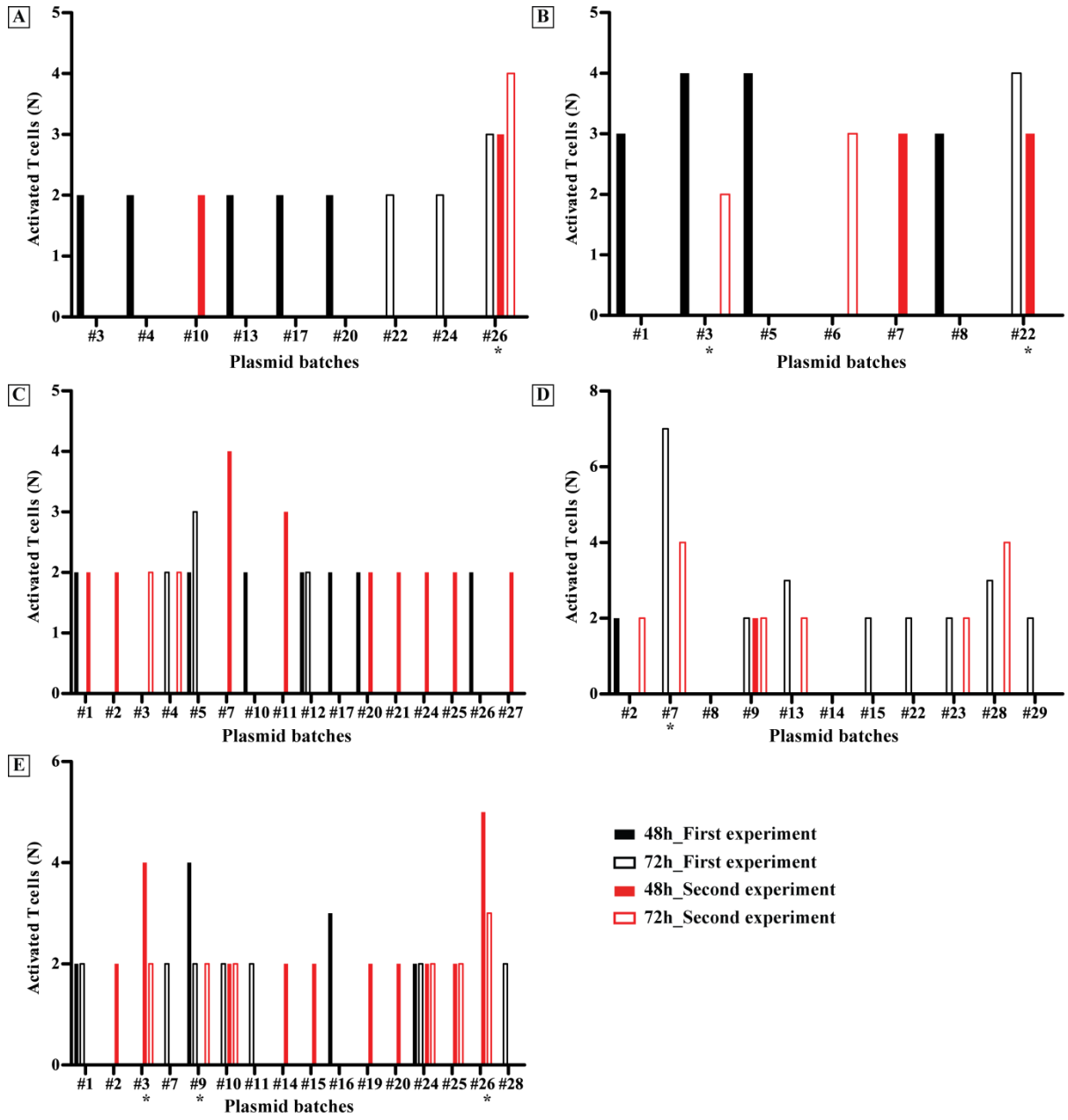

Figure 3-25: Reactivation of TCR BV1-BJ2.3-AV7.2-AJ24.2 in 30 probes of plasmids from 1st subpool

As mentioned in Table 3-14, five promising reconstructed plasmids from $C7^9$ Library continued the subpools of *E.coli* culture for enrichment of antigen coding plasmid. In 1st subpool, reactivation assay from 30 probes of plasmids was carried out and examined under fluorescence microscope after transfection for 48 and 72 hours, which were repeated with two independent experiments (black: first experiment; red: second experiment). Histogram shows the numbers of activated T cells ($sGFP^+$) in each probe of plasmids, which were recognized by the following reconstructed plasmids: Plasmid # C-09 **(A)**, Plasmid # C-10 **(B)**, Plasmid # C-11 **(C)** Plasmid # C-12 **(D)**, and Plasmid # C-13 **(E)**. In 30 probes of plasmids, only the probes that showed activated T cells are presented here, and the probes marked with asterisks will continue for the following subpools of *E.coli* culture.

Thus, during the antigen identification for TCR BV1-BJ2.3-AV7.2-AJ24.2, we detected higher numbers of activated T cells in the samples transfected with $C7^9$ library, and successfully isolated the positive APCs underneath. After plasmids recovery and reconstruction *in vitro*, the activated signals were re-detected in reactivation assay with five promising reconstructed plasmids. However, the positive signals were disappeared gradually in the subpools' experiments. Re-picking of positive APCs in the reactivation assay might help to achieve the activated signals again. In addition, distinguishing the activated signals from the spontaneous activated background is crucial for the recognition of the real antigen.

The positive APCs underneath are successfully isolated and used for plasmid recovery and reconstruction. The positive signals detected in reactivation assay indicate that the antigen coding plasmid might indeed be included in these reconstructed plasmids. However, the positive signals are lost in the subpools for enrichment of antigen coding plasmid. In the future, the method for enrichment of antigen coding plasmid should be optimized.

4 Discussion

4.1 Localization of Immune Cells in MS Brain

Brain-infiltrating $CD8^+$ T cells persist as expanded clones in the CSF and blood of MS patients (Skulina et al., 2004), but there might be other immune cells that infiltrate in brain lesions. In the previous study, αβ-TCRs of some $CD4^+$/$CD8^+$ T cells and MAIT cells were identified from MS brain lesions (Held et al., 2015; Junker et al., 2007; Kim et al., 2012; Seitz et al., 2006). Here, we located immune cells in histological sections of MS brain biopsy morphologically (Section 4.1.1). Particularly for activated $CD8^+$ T cells, many clusters were detected in some blocks of brain biopsies (Section 4.1.2). Lastly, we predict some possibilities for investigation of immune cells in future experiments (Section 4.1.3).

4.1.1 Immunofluorescence Staining of Immune Cells

Beside resident cells in the CNS, like neurons, glial cells, and neural stem cells some immune cells might migrate into the inflammatory lesions through BBB. Examples are T and B lymphocytes, dendritic cells, macrophages and NK cells. To verify this assumption, we identified these immune cells in histological sections of MS brain (Section 3.1). The chosen commercial antibodies needed to meet three conditions, which are (i) the antibodies apply to immunofluorescence staining, (ii) the antibodies should be suitable for frozen sections, and, (iii), they should not cross-react irrelevant brain-specific target cells. However, not all the commercial antibodies met these conditions. We initially tested them on frozen tonsil sections, and then the ones that had specifically detected the target cells were used for MS brain biopsy.

In MS, activated T cells entering the CNS could trigger an inflammatory cascade that facilitates the recruitment of other immune cells migrating to MS lesions (Krumbholz et al., 2005). T lymphocytes were specifically detected on tonsil and brain sections. However, of four antibodies against CD8 α-

and β-chains, one anti-CD8β antibody (clone F-5) did not specifically detect the $CD8^+$ T cells on brain sections (Figure 3-1). Therefore, it may not be applied on frozen tissues, especially for brain sections, which rather stained unspecific brain-specific target cells and not confined to the cell surfaces.

To figure out $CD8^+$ T cells in brain lesions activated or not, we examined eight commercial antibodies that target for three common activation markers (CD69, CD134, and CD137). After tested on tonsil sections, five of them specifically detected their targets with the appropriate working concentrations. However, only three of them could distinctively detect these targets (CD69, CD134, and CD137) on brain sections without any unspecific staining background (Figure 3-2). Brain contains a lot of fat, which may impede antibody binding to the target antigens on the surface of cells. In addition, most commercial antibodies are not tested against brain tissue, which might cross-react to brain-specific targets, such as neurons, microglia, Astrocytes, and oligodendrocytes.

Dendritic cells and macrophages served as cognate APCs might be recruited to present autoantigens to the autoreactive T cells in brain lesions of MS patients. In previous study, Melanie Greter et al. discovered that dendritic cells are vital for antigen recognition of autoreactive T cells further to mediate CNS inflammation and demyelination in an animal model of MS. (Greter et al., 2005). Deletion of macrophage and microglia functions is effective to reduce the inflammation and demyelination within the CNS (Benveniste, 1997). Moreover, a recent study demonstrated the NK cells play a critical role in controlling T-cell activity in the clinical progression of MS (Gross et al., 2016). Here in the thesis, dendritic cells and macrophages in brain tissue were detected by one anti-CD83 antibody (Clone HB15e) and two anti-CD68 antibodies (Clone EBM11 and Clone KP1), respectively (Figure 3-3). They were more often found in the perivascular space of brain.

Thus, we successfully located $CD8^+$ T cells, dendritic cells and macrophages in MS brain tissues morphologically. They might be related to the immunopathogenesis of MS. Some possible issues that might influence the staining results are summed up. (i) Not all commercial antibodies can work properly on brain biopsies. (ii) Brain biopsy contains much fat that might prevent antibody to bind to

specific antigen on the surface of target cells. (iii) Some antibodies might cross-react to irrelevant brain-specific targets. (iv) Non-specific binding of antibodies and the ionic and hydrophobic interaction may result in the non-specific background of the antibody.

4.1.2 Distribution of Clusters of Activated $CD8^+$ T-Cells

In MS brain biopsy investigated here, activated $CD8^+$ T cells were specifically detected by two anti-CD8α and anti-CD137 antibodies. Next, it was of interest to see how these activated $CD8^+$ T cells are distributing in different blocks (#2, #6, and #12) of MS brain biopsies. In line with the previous study by Anna G. Niedl, we discovered that block #12 has the highest number of $CD8^+$ T cells especially in the meninges, perivascular and parenchymal spaces (Figure 3-5). Most of them are activated ($CD137^+$). It indicates that actively demyelinating brain lesions infiltrated with large numbers of activated $CD8^+$ T cells might be located in this brain block. However, only a few single activated $CD8^+$ T cells but rare cluster were found in block #2 (Figure 3-4), where obviously no inflammation occurred. If single activated $CD8^+$ T cells from block #6 and #12 could be isolated and used for characterization of αβ-TCRs, it would be likely that these cells might be autoaggressive T cells involved in the immunopathogenesis of MS.

During the investigation of activated $CD8^+$ T cells in MS brain lesions, we noticed that many cells are not alone, but tightly contacting another cell that are unknown so far (Figure 3-6). In line with previous research on psoriasis vulgaris (PV) disease, different T cells with identical TCR molecules were detected in direct contact with other cells that exhibit the dendritic or epithelial morphology (Arakawa et al., 2015). In future research, it will be interesting to figure out the cell types of these contacting cells for activated $CD8^+$ T cells. It will bring new insight into the characterization of auto-antigens recognized by autoreactive $CD8^+$ T cells in MS.

4.1.3 Prospects for Investigation of Immune Cells in MS Brain

Inflammatory cells existing in CNS lesions may have effector functions in the immunopathogenesis of MS. These cells could be either the systemic immune cells translocated from the peripheral system through BBB or the CNS-resident cells that initiate, regulate and maintain an immune response (Becher et al., 2000). In the thesis, we only detected four systemic immune cells, i.e., T cells, $CD8^+$ T cells, dendritic cells and macrophages in the brain lesions of MS patients morphologically. However, the CNS-resident cells might also be the potential APCs presenting autoantigens to the encephalitic $CD4^+$/$CD8^+$ T subsets, leading to demyelination and axonal damage. Höftberger et al. reported that MHC class I molecules are highly expressed on astrocytes, axons, neurons and oligodendrocytes which may be potential targets for Class I MHC-restricted $CD8^+$ T-lymphocytes (Höftberger et al., 2004). Another research on Theiler's murine encephalomyelitis virus-induced demyelinating disease (TMEV-IDD) demonstrates that the resident microglia and the infiltrating macrophages are the mainly antigen-presenting phenotypes in the contribution of CNS demyelination (Mack et al., 2003). Therefore, in future experiments, it will be interesting to investigate other immune cells as well as the CNS-resident cells, and the relationships between them in brain lesions of MS patients.

4.2 Identification of the MS-Related TCR αβ-Chains

Two strategies have been established to identify the complete TCR αβ-heterodimers of the tissue-infiltrating T cells from frozen histological samples (Kim et al., 2012; Seitz et al., 2006). (i) Clonally expanded TCR β-chains in muscle sections were identified using CDR3 spectratyping. Then, those $Vβ^+$ T cells that were considered as myocytotoxic $CD8^+$ T cells morphologically were identified by immunohistochemistry, and then isolated by laser microdissection. Next, the paired TCR α- and β-chains were identified by a multiplex RT-PCR based clonally specific protocol, which can amplify both α- and β-chains from the single T cells. (ii) This approach was further developed, so that all α- and β-TCR chains may be detected, even without knowledge of the Vβ elements.

To identify paired αβ-TCRs from the single activated $CD8^+$ T cells with high efficiency in MS brain tissues, we optimized the protocol of rapid immunostaining to distinguish the activated $CD8^+$ T cells from irrelevant bystanders and maximally preserved RNA from histological sections (Section 4.2.1 and 4.2.2). Next, the multiplex RT-PCR-based approach was improved to yield higher number of TCR α- and β-chains (Section 4.2.3).

4.2.1 **Distinguishing of Activated $CD8^+$ T Cells from Irrelevant Bystanders**

Immunofluorescence staining was used to distinguish the cells of interest from irrelevant bystanders. However, the routine use of this approach in frozen or fixed tissue accelerates RNA degradation. The consequence is that no enough intact RNA is left for unbiased amplification of TCR α- and β-chains. Thus, a rapid immunostaining method was introduced here and developed not only for visualizing T cells of interest but also for preserving RNA quality (Section 3.3.1). CD137, as an activations marker, was chosen for staining with CD8α molecule to identify the activated $CD8^+$ T cells morphologically on brain sections of MS patients. In Section 3.1, it is shown that one anti-CD137 antibody (Clone BBK-2) specifically detected its target cells on brain sections by the conventional protocol of immunofluorescence staining. Along with the staining protocol that was adjusted to preserve more RNA in a slide, an acceptable staining was obtained on brain sections when a higher concentration of anti-CD137 antibody was used. Thus, by combining the anti-CD8α-Cy3 antibody (Clone LT8) with the anti-CD137 antibody, single activated $CD8^+$ T cells were clearly distinguished from irrelevant bystander T cells on brain sections, and then isolated by laser microdissection (Figure 3-8).

In summary, we adjusted the period for tissue fixing, blocking and incubation with antibodies during staining. The steps of fixation and blocking are necessary to reduce the unspecific staining background. Addition of RNase inhibitor is significant for RNA preservation during staining. In addition, rinse steps were deleted, which compromise the cellular adherence to slides and accelerate RNA degradation. The whole staining procedure performed at 4°C, from which we got the acceptable staining results. Low temperature may also be helpful to reduce RNA degradation (Figure 3-10).

4.2.2 **Minimization of RNA Degradation**

RNA quality is vital for the subsequent amplification of αβ-TCRs from single T cells on brain sections. However, four main technical obstacles might significantly influence the integrity of RNA. (i) Repeated unfreezing of brain biopsy leads to the loss of RNA (Section 4.2.2.1). (ii) Various thicknesses in brain tissue sections affect the cell shape and the RNA integrity in the cell (Section 4.2.2.2). (iii) Immunofluorescence staining of target cells on histological sections accelerates RNA degradation (Section 4.2.2.3). Addition of RNase inhibitor does matter for RNA preservation. (iv) Image quality and correct operation during laser microdissection also matter to the isolation of single T cells (Section 4.2.2.4).

4.2.2.1 Storage of MS brain biopsy

The initial RNA quality in tissue biopsy is crucial for RNA preservation. The brain biopsy of MS patient FE was surgically removed in 1996, as he was initially diagnosed with a malignant glioma in the brain area. Considering of the rarely available human brain autopsies, we seized the occasion to investigate the immunopathogenesis of MS with the rare brain biopsy. It was divided into several blocks and frozen at -80°C. Hereafter, the brain blocks were transferred numerous times from -80°C to -20°C and backward for the preparation of tissue sections. These warming and cooling cycles during the last 20 years severely influence the RNA integrity nowadays.

4.2.2.2 Cell-positions in tissue sections

During the preparation of tissue sections by freezing microtome, the T cells of interest might be broken, and RNA might be lost. After immunofluorescence staining, the single T cells appeared as dots under the fluorescence microscope, which were marked and isolated by laser microdissection. The isolated single T cells might not be the amount of cell included in the tissue section, which are decided by the thickness of tissue section.

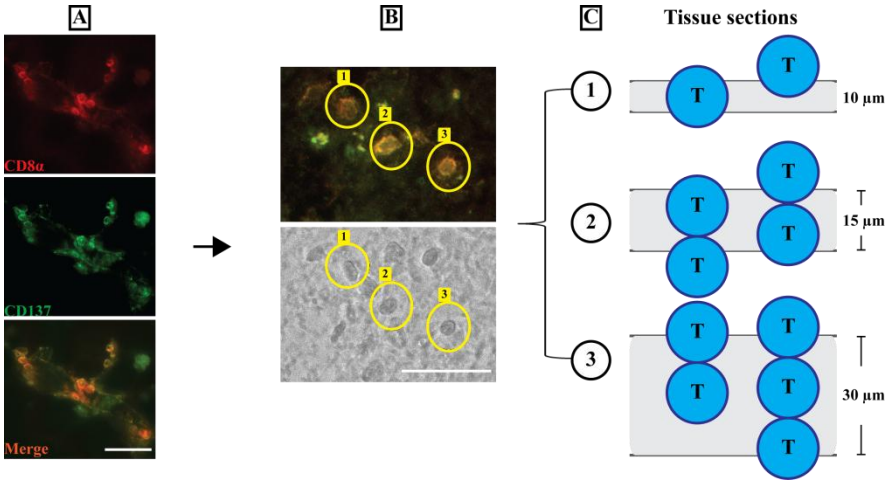

Figure 4-1: Vary thickness of tissue sections influences the subsequent single cell TCR analyses

(A) Improved rapid immunostaining approach was used to stain the activated $CD8^+$ T cells (CD8α and CD137 double positive) on frozen brain sections. **(B)** Single $CD8\alpha^+CD137^+$ T cells were isolated by laser microdissection. **(C)** T cells (~15 µm) are distributed in three different thicknesses of tissue sections. ① In the tissue sections with a thickness of 10 µm, the T cells are cut in different layers, which contain either most of the cell nuclei or small piece of cytoplasm. ②-③ In the tissue sections with a thickness of 15 µm or greater, the opportunity of cutting entire T cells is higher, but the overlapped T cells (more than two cells located in the same position) might appear as one T cell on microscopy. Scale bars=25 µm.

The approximate diameter of T cells is up to 15 µm. If tissue sections are cut with a thickness <15 µm (Figure 4-1, ①), the T cells might be damaged by cutting and their RNAs may diffuse off the slice. Moreover, the cell nucleus may not be included in the slice either. If cut with a thickness of 15 µm or greater (Figure 4-1, ②-③), two T cells in one position may probably be isolated and used to amplify the αβ-TCRs. In this case, it is hard to tell the TCR α- and β-chains coming from one T cell or another. To avoid this problem, in the thesis, we prepared the tissue sections with a diameter of 10 µm for all the experiments. Hence, approximately 50% of isolated single T cells had enough RNA for amplification of αβ-TCRs.

4.2.2.3 RNA retaining during staining

The incubation and washing steps during staining severely influence RNA quality of tissue sections. In Section 3.3.2, different ways were tested to minimize RNA degradation during staining. Compared to the RNA quality after staining without any treatment, the employment of RNase/DNase-free BSA solution as a blocking reagent additionally with the dehydration steps effectively minimized RNA

degradation (Figure 3-10). Thus, RNase inhibitor is necessary for maintaining RNA quality during staining. Dehydration could take residual water out of tissue sections after staining, thus further blocking RNases. After these effective treatments, the preserved RNA might be enough for subsequent TCR amplification (Figure 3-11).

4.2.2.4 Image quality and operation of laser microdissection

To obtain high resolution of fluorescence images with high contrast, we usually covered the tissue sections with fluorescence mounting medium and a glass cover slip, which allow the light to pass through straightly. However, because single cells of interest shall be catapulted into a reaction tube by a laser ray, the tissue section must not be covered with a glass cover slip. Instead, we cover the tissue sections with isopropanol solution that may impede the detection of strong auto-fluorescence from the stained cells, and seclude contact with water for RNA preservation. However, isopropanol covered tissue may refract the light rays in different directions, which reduces the apparent resolution of fluorescence images. In addition, because of the volatility of isopropanol, the amount of isopropanol covered on tissue sections should be increased again during the searching of appropriate T cells under the microscope.

4.2.3 **Molecular Analysis of Paired αβ-TCRs from Single T Cells in MS Patients**

For a higher yield of TCR α- and β-chains from single T cells, the multiplex RT-PCR based approach was optimized (Section 4.2.3.1). In the CSF specimens of MS patients, one Vβ and two different Vα-chain rearrangements (termed as dual TCRs) are detected (Section 4.2.3.2). However, there are still some technological obstacles in identifying the clonally expanded αβ-TCRs (Section 4.2.3.3).

4.2.3.1 Improvement of the technique for T cell repertoire studies

An unbiased RT-PCR based approach was established to amplify TCR α- and β-chains of single T cells without a prior knowledge of particular TRBV/TRAV usage (Kim et al., 2012). For a higher yield of paired αβ-TCRs from histological samples of MS brain biopsies, this method was optimized

during the thesis (Section 3.3.3). The unbiased approach is independent of applying monoclonal antibodies against TCR Vβ regions that are identified earlier by CDR3 spectratyping (Seitz et al., 2006). As long as the single T cells of interest are isolated from brain sections with sufficient RNA quality, in theory, the paired α/β chains should be amplified by the unbiased approach. In fact, however, the yield of αβ-receptors from MS brain biopsies was not as expected.

In the RT reaction, the concentration of two TRAC and TRBC primers (Cα-RT-imp and Cβ-RT-2) might be too high to influence PCR efficiency. Here the final concentration was reduced for better yield of PCR product. However, this yield was still low (Table 3-3), which indicates that the following multiplex PCRs should be optimized as well. A set of nine degenerated primers was designated by Song-Min Kim to cover all functional variable segments of TCR β-chains. Together with nested reverse primers annealing to the TRBC regions, the whole TCR β-chain rearrangements are possible to be reconstructed. In the pre-amplification of TCR α- and β-chains, one primer (Cβ-out) is not specifically annealing to the cDNA of TCR β-chains (Section 3.3.3.3). A new primer (Cβ-mid4) was designed to anneal to the inner site of TRBC region to avoid the unproductive TCR β-chains. Significant higher yields of TCR β-chains were obtained, which indicates that primer design is critical to the PCR efficiency. Except for the primers, the thermocycling conditions were also optimized. Obviously, two annealing temperatures (60°C and 53°C) are not sufficient to amplify all the TRAV and TRBV repertoire. In addition, if the annealing temperature is too low, the primers could not effectively anneal to the template, and the PCR efficiency might be reduced. Therefore, the touchdown PCR with three phases may satisfy the requirement of all primers involved in the PCR.

Before specific amplification of TCR β-chains, a set of anchor sequences was added to the 5’ end of V-regions of β-chains through a run-off reaction, which reacts to one direction (Kim et al., 2012). Because this reaction might bring unspecific PCR products and lead to the interaction of primers, a reverse primer was introduced into the reaction, which might help to improve the PCR efficiency. Moreover, the melting temperatures of primers are different, which may also influence the PCR

efficiency. Therefore, annealing temperature and amplification cycles were increased to gain more specific PCR products.

The even more variable α-chain repertoire makes the amplification even more challenging. Thus the number and the variability of Vα elements are more variable than that of β-chains, so that the number of primers was significantly increased (Seitz et al., 2006). With the pre-amplification product as a template, the corresponding α-chain was successfully amplified by nested PCR from freshly prepared, FACS-sorted single T cells. However, this approach might not be efficient when cryosections of human biopsies (not fresh cells) are used, because of RNA degradation during long-term storage. Here, we tried to optimize this protocol for higher yields of TCR α-chains; however, there was no significant difference before and after improvement. The unspecific interactions between these primers may also impede the amplification of α-chains.

4.2.3.2 Detection of dual TCRs

Due to the high sensitivity of this method, we could detect dual TCRs in single T cells. In CSF specimens of MS patients, we identified some T cells that express two different TCR α-chains associated with one identical β-chain (Table 3-9). It was found that 20% of influenza-primed $CD8^+$ T cells express functional dual TCRs (Dash et al., 2011; Padovan et al., 1993). There are two possibilities of dual TCRs involved in the immune response. (i) T cells express two functional αβ-TCRs which contain one identical β-chain but two different α-chains. These specific T cells can recognize the similar antigens presented by different APCs. (ii) During T-cell development, only one α-chain is chosen to form the functional pathogenic receptor expressed on the surface. In brain biopsies, because of RNA degradation, it was hard to identify the dual TCRs from single $CD8^+$ T cells. On the contrary, with the fresh CSF specimens, some T cells were detected to express dual TCRs. Because of the limited numbers of single T cells, we could not tell yet whether the dual TCRs mainly identified from a $CD4^+$ T-cell subset or a $CD8^+$ T-cell subset.

4.2.3.3 Technical challenges in characterization of clonally expanded αβ-TCRs

High yields of TCR α- and β-chains obtained from freshly isolated, single T cells demonstrate the successful application of this optimized method. However, the yield of paired αβ-TCR was restricted by some technical challenges, especially for frozen sections of biopsy samples.

The first challenge is generated due to the unstable RNA in a tissue section. During the fluorescence staining of target cells on frozen sections, RNA might be degraded by RNases. It is also explained by the high yields of TCR clones with better RNA quality from freshly isolated single T cells (Section 3.3.5). It is well-known that histological samples of human tissue biopsies provide evidence of autoreactive T cells involved in the immunopathogenesis of autoimmune disorders (Dornmair et al., 2003). By combining morphological identification with reconstruction *in vitro*, in theory, we could characterize any TCR molecular from any histological sample of human diseases. Therefore, RNA degradation has to be minimized to the utmost extent.

The second challenge is TCR repertoire analysis. With the single cell PCR, it is hard to identify clonal expansions, because very high number of single T cells would be analyzed. Therefore, flanking NGS experiments are usually required. In a recent study, the investigation of $CD161^{hi}TRAV1\text{-}2^{+}$ T cells by pyrosequencing and single cell analyses demonstrates that this cell subset does not exclusively contain semi-invariant MAIT cells, but also conventional MHC-restricted T-cell subpopulations with hypervariable TCR α- and β-chains (Held et al., 2015). Likewise, NGS results from a melanoma patient reveal that some clonally expanded T-cell subsets are detected in the CSF, but not in the melanoma (Gerdes et al., 2016). Therefore, combining NGS technology with single cell analysis will be the best choice to identify the clonally expanded receptors of autoreactive T cells on MS brain lesions.

A research group introduced one method that combines 5'RACE with multiplex PCR to amplify TCR α- and β-chains from single FACS-sorted $CD8^{+}$ T cells of human peripheral blood (Sun et al., 2012). There is still room to optimize the protocol to improve the yield of rearranged α-chains. Similar to

amplify TCR β-chains, we might modify the PCR with the ligation of an anchor to the entire possible variable segments of α-chains associated with a single primer targeting at the conserved constant regions (Gao and Wang, 2015).

4.3 Subcloning of 58-BV1-BJ2.3-AV7.2-AJ24.2 T hybridoma cells

Before searching antigens for TCR JM22 and BV1-BJ2.3-AV7.2-AJ24.2, it is necessary to validate expression of each transfected molecule in the transfected T hybridoma cells, including the recombinant αβ-TCR, CD8 co-receptor, and NFAT-sGFP upon TCR activation. No or low expression of any of these molecules mentioned above will abrogate subsequent antigen identification. In Section 3.4.1, we checked the expression of each molecule for these two transfected T hybridoma cell lines before antigen identification. Expression of CD8 β-chains on 58-BV1-BJ2.3-AV7.2-AJ24.2 T hybridoma cells was initially low as compared to that on 58-JM22 T hybridoma cells (Figure 3-15). The low expression might be caused by unstable transfection with plasmids. However, the actual reason is still unknown so far. Purification by MACS® technology might help to resolve this problem. After separation and subcloning, 100% T hybridoma cells were validated to express CD8 β-chain that was not lost in the following cultivation.

4.4 Investigation of HLA Restriction of the TCR BV1-BJ2.3-AV7.2-AJ24.2

The TCR BV1-BJ2.3-AV7.2-AJ24.2 identified from brain-infiltrating $CD8^+$ T cells of a MS patient was investigated to determine its HLA restriction. As described in Section 1.6.3, the α-chain contains the typical "V" element (Vα7.2) for MAIT cells, even though the CDR3 region is longer than that for conventional MAIT cells. Therefore, except for $CD8^+$ T cells, we examined whether this TCR recognize antigens presented by MR1 molecules or not. The tested HLA molecules are MS patient FE matched MHC Class I molecules (*HLA-A*0101, -B*0801,* and *-C*0701*) and MR1 molecule. We used COS-7 cells as APCs that were co-transfected with each MHC molecule mentioned above, as well as matched PECP library ($A1^{39}$, $B8^{359}$, $C7^{9}$, or N27). These cells were co-cultivated with the 58-BV1-

BJ2.3-AV7.2-AJ24.2 T hybridoma cells. The TCR activation was subsequently analyzed. However, the T cell activation was significantly different amongst different HLA molecules. The highest level of activation was observed in the *HLA-C*0701* restricted $C7^9$ library, and in the presence of the MR1 restricted N27 library, an intermediate level of activation was also detected (Figure 3-22). This suggests that the *HLA-C*0701* might be the correct HLA molecule to present auto-antigen to the MS-derived TCR BV1-BJ2.3-AV7.2-AJ24.2, which is responsible for restricting the antigen presentation to this particular MS-related TCR.

4.5 Technical Challenges of Antigen Identification

Several technical challenges influence the antigen identification for TCR JM22 and BV1-BJ2.3-AV7.2-AJ24.2. Avoiding the activation background in antigen search is crucial for distinguishing the "real" activated T-cell clusters from spontaneously activated T cells (Section 4.5.1). In addition, the biggest problem was how to apply the subpools of *E.coli* culture effectively to identify the antigenic plasmid (Section 4.5.2).

4.5.1.1 Activation Background of TCR BV1-BJ2.3-AV7.2-AJ24.2

During the experiments of antigen identification, activation background caused by the spontaneously activated T cells was detected for the TCR BV1-BJ2.3-AV7.2-AJ24.2. This activation background fluctuated in different experiments. Two reasons might cause this problem, which are (i) spontaneous calcium influx, and, (ii), TCR activation by an endogenous antigen. The spontaneous activation may be caused by Ca^{2+} influx involved in T cells (Kawakami, 2016) (Section 1.8). In a previous study, MAIT cells recognize an endogenous ligand binding to MR1 molecule that is expressed on hematopoietic cells in the thymus (Chua et al., 2011; Gold et al., 2015). However, if there is an endogenous antigen in the T hybridoma cells, much more cells should be green. This was obviously not the case here. T hybridoma cells were re-cloned to select the ones that have rare spontaneous activation without exogenous stimuli (Section 3.5.2).

4.5.2 Identification of the Antigenic Plasmid by *E.coli* Subpools

Even a positive APC that activates this particular MS-related TCR was successfully isolated; the antigenic plasmid should be identified from hundreds of irrelevant bystander plasmids. In section 3.5.5, subpools of *E.coli* culture were used to determine the antigenic plasmid. Unfortunately, the antigenic signal was lost after these *E.coli* subpools. Several rounds of *E.coli* culture and separation might lead to the loss of the antigenic plasmid. In the future experiments, we might increase the numbers of probes of plasmids in subpools to cover all the *E.coli* clones. Then with the help of the auto-scanning system, reactivation assay performs under the fluorescence microscope.

4.6 Outlook

$CD8^+$ T cells, a main component of the adaptive immune system, are predominate in the brain lesions and significantly related to the immunopathogenesis involved in multiple sclerosis (Hohlfeld et al., 2016). Strategies for identifying the clonally expanded TCR repertoire and investigating the specificities of their target antigens in patients with multiple sclerosis are important approaches for neuroimmunological research of autoimmune diseases.

A universal strategy for identification of paired αβ-TCRs from single T cells (Kim et al., 2012) was improved in the present work. It is developed from earlier work that identified the TCRs from those myocytotoxic $CD8^+$ T cells in frozen biopsies of myositis patients (Seitz et al., 2006). The optimized unbiased approach continued the previous work to the frozen brain biopsies and CSF specimens of MS patients. So far, several TCR β-chains of interest T cells (that usually belonged to an *in situ* activated population) were obtained from brain biopsies. Because of the hypervariability of α-chains and RNA degradation, amplification of corresponding α-chains has proved more difficult. Future research should be focused to large extents on optimizing the existing protocols. Without considering RNA degradation, prior knowledge of TCR repertoire from single $CD4^+$ and $CD8^+$ T cells persisting in the CSF of MS patients was required. However, by combining NGS technology and single cell analysis,

we may identify the paired αβ-TCRs that belong to the clonally expanded population. With the universal approach, any T cells of interest may be identified, such as (i) fresh T cell populations in blood and CSF, (ii) T cells that secrete cytotoxic factors or express an activation marker, and, (iii), T cells that contact their target cells.

Once the TCR of interest is identified and then revived in a hybridoma cell line, the searching of its target antigens *in vitro* is started. Anti-myelin recognition by a particular MHC class I-restricted TCR is successfully mimicked through the antigen searching system (Ruhl et al., 2016). However, Because of the spontaneous activation background and huge work of screening the plasmids subpools, in the thesis, identification of the potential mimotope for an MS-related TCR was failed. Further efforts should be undertaken to develop this antigen searching system for high efficiency. In the future research, we may simplify the procedure of screening antigenic plasmid from thousands of irrelevant plasmids subpools. In addition, antigen-processing machinery and affinity between the mimotope and TCR should be taken into consideration.

5 Appendix

5.1 Abbreviations

List of Abbreviations:

A	Adenosine
AA	Amino Acid
APC	Allophycocyanin (a fluorescent dye)
APCs	Antigen presenting cells
Amp	Ampicillin
BBB	Blood-brain barrier
bp	Base pairs
BSA	Bovine Serum Albumin
C	Constant region of TCR chains
C	Cytosine
CD	Cluster of differentation
cDNA	Complementary DNA
CDRs	Complementarity determining regions
cfu	Colony forming units
CIDP	Chronic inflammatory demyelinating polyneuropathy
CIS	Clinically isolated syndrome of multiple sclerosis
CNS	Central nervous system
CSC	China Scholarship Council
CTLs	Cytotoxic T cells
Cy3	Cytochrome 3 (a fluorescent dye)
D	Diversity region of TCR β-chain
DAPI	4',6-diamidino-2-phenylindole (fluorescent stain)
DCs	Cendritic cells
DEPC	Diethylpyrocarbonate
DMSO	Dimethylsulfoxid
DNA	Deoxyribonucleic acid
dNTP	Desoxy-nucleoside-triphosphate
EAE	Experimental Autoimmune Encephalomyelitis
EBV	Epstein-Barr virus
E.coli	*Escherichia coli*
EDTA	Ethylenediamine tetraacetic acid
ELISA	Enzyme linked immunosorbent assay
ER	Endoplasmic reticulum
FACS	Fluorescence-activated cell sorting
FBS	Fetal bovine serum
FCM	Flow cytometry
FDA	Food and Drug Administration
FITC	Fluoresceinisothiocyanate (a fluorescent dye)
FU	Fluorescence Unit
G	Guanine
G418	Geneticin
HLA	Human leukocyte antigen
hMR1	Human MHC Class I related protein
ID	Identification code
IL-2	Interleukin-2

IL-4	Interleukin-4
IMGT®	The international ImMunoGeneTics information system®
INF-γ	Interferon gamma
ITAMs	Immunoreceptor tyrosine-based activation motifs
J	Joining region of TCR chains
JM22	A T cell receptor that recognizes flu(58-66) peptide from influenza matrix protein
K	K-nucleotide, represents the random insertion of guanine or thymine nucleotides
kb	Kilo base pairs
LB	Luria-Bertani culture medium
LCM	Laser capture microdissection
mAb	Monoclonal Antibody
MAIT	Mucosal-associated invariant T cells
MACS	Magnetic Cell Separation
MBP	Myelin basic protein
MEM	Minimum essential medium
MHC	Major histocompatibility complex
MOG	Myelin oligodendrocyte protein
MP	Melanoma patient
MRI	Magnetic resonance imaging
MS	Multiple sclerosis
N	Non-germline
N	N- or non-templated nucleotide, represents the random insertion of any nucleotide
NFAT	Nuclear factor of activated T cells
NK cells	Natural killer cells
NGS	Next generation sequencing
OCB	Oligoclonal bands
OD	Optical density
ori	Origin of replication
P	Palindromic
PBS	Phosphate buffered saline
PBMC	Peripheral Blood Mononuclear Cell
PCR	Polymerase chain reaction
PE	Phycoerythrin (a fluorescent dye)
PECP	Plasmid-encoded combinatorial peptide libraries
PFA	Paraformaldehyde
pH	Potential of hydrogen
pMHC	Peptide-MHC complex
PPMS	Primary progressive MS
PRMS	Progressive relapsing MS
PS-SCL	Synthetic combinatorial peptide libraries in positional scanning format
RFLP	Restriction fragment length polymorphisms
RIN	RNA Integrity Number
RIS	Radiologically isolated syndrome of multiple sclerosis
RNA	Ribonucleic acid
RNase	Ribonuclease
rpm	Rounds per minute
RPMI	Roswell Park Memorial Institute medium
RRMS	Relapsing-remitting MS
rRNA	Ribosomal ribonucleic acid
RT	Room temperature
RT-PCR	Reverse Transcription polymerase chain reaction
sGFP	Superfolder green fluorescent protein
SH2	Src Homology 2
SLE	Systemic lupus erythematosus
SPMS	Secondary progressive MS
SV40	Simian vacuolating virus 40

T	Thymine
T_a	Annealing temperature
TAP	Transporter associated with antigen processing transporter
Taq	Polymerase of Thermophilus aquaticus
TBE	Tris/Borate/EDTA buffer
TCR	T-cell receptor
Th1	T helper 1
Th2	T helper 2
T_m	Melting Temperature
TMEV-IDD	Theiler's murine encephalomyelitis virus-induced demyelinating disease
TNF-α	Tumor necrosis factor alpha
Tris	Tris(hydroxymethyl)-aminomethane
U	Unit
U	Uracil
UV	Ultraviolet Light
V	Variable region of TCR chains
v/v	Volume per volume
w/v	Weight per volume

5.2 Indexes of Figures and Tables

Figure Index:

Figure 1-1: TCR gene recombination and the formation of TCR-pMHC I complex 4
Figure 1-2: Crystal structure of a TCR–pMHC complex 7
Figure 1-3: Overview of the progress and diagnosis of MS 11
Figure 1-4: Sequences of paired T-cell receptor (TCR) α- and β-chains derived from MS patient 13
Figure 1-5: Overview of an approach for antigen identification from putatively disease-related TCR molecules 17
Figure 2-1: PCR strategy for identifying the paired TCR α- and β-chains from single T cells 34
Figure 2-2: Workflow of TCR repertoire analysis from the blood and CSF samples from MS patients 49
Figure 2-3: Workflow for the enrichment of positive *E.coli* clones in subpools 55
Figure 2-4: Streets of 30 bacteria colonies were marked on LB^{amp} agar plate 56
Figure 3-1: Immunofluorescence staining of immune cells in tonsil and brain tissues. (Part 1) 59
Figure 3-2: Immunofluorescence staining of immune cells in tonsil and brain tissues. (Part 2) 61
Figure 3-3: Immunofluorescence staining of immune cells in tonsil and brain tissues. (Part 3) 63
Figure 3-4: Identification of activated $CD8^+$ T cells in different brain blocks of MS patient FE 65
Figure 3-5: Clusters of activated $CD8^+$ T cells infiltrated in the MS brain tissue 66
Figure 3-6: Detection of the activated $CD8^+$ T cells in directly contact with another cells in the MS brain tissue 67
Figure 3-7: Steps and examinations within the rapid immunostaining method 69
Figure 3-8: Pathogenic $CD8^+$ T cells located in the MS brain and isolated by laser microdissection 71

Figure 3-9: Comparison of RNA qualities in brain tissues before and after fluorescence staining.....72
Figure 3-10: Comparison of RNA qualities in tonsil tissues with different treatments.....74
Figure 3-11: Minimization of RNA degradation on brain biopsy with the improved rapid immunostaining.....75
Figure 3-12: Strategically steps and optimization to identify paired TCR α- and β-chains from dissected tissue-infiltrating T cells.....77
Figure 3-13: TCR α and β transcripts obtained from single CSF T cells of MS patients.....89
Figure 3-14: Distribution of TCR α and β transcripts obtained from single CSF T cells of MS patients.....90
Figure 3-15: Expression of recombinant TCRs and co-receptor CD8 molecules before subcloning....93
Figure 3-16: Expression of CD8β in 58-FE-BV1-BJ2.3-AV7.2-AJ24.2 T hybridoma cells before and after separation.....94
Figure 3-17: TCR activation *in vitro* by CD3 cross-linking.....95
Figure 3-18: Spontaneous activation of TCR BV1-BJ2.3-AV7.2-AJ24.2 reduced by cell re-cloning..98
Figure 3-19: Expression of HLA-A2 in the stably transfected COS-7-A2 cell line.....99
Figure 3-20: TCR JM22 activation by $A2^{269}$ library.....100
Figure 3-21: Micromanipulation of the COS-7 cell beneath the activated T hybridoma cells.....101
Figure 3-22: TCR BV1-BJ2.3-AV7.2-AJ24.2 activation by PECP libraries presented by different MHC molecules.....104
Figure 3-23: Detection of plasmid recovery PCR products by gel electrophoresis.....106
Figure 3-24: Reactivation of TCR JM22 by antigen pools isolated from single APCs.....107
Figure 3-25: Reactivation of TCR BV1-BJ2.3-AV7.2-AJ24.2 in 30 probes of plasmids from 1^{st} subpool.....110
Figure 4-1: Vary thickness of tissue sections influences the subsequent single cell TCR analyses....119
Figure 5-1: Isotype control of each antibody in tonsil and brain tissues (Part 1).....134
Figure 5-2: Isotype control of each antibody in tonsil and brain tissues (Part 2).....135
Figure 5-3: Isotype control of each antibody in tonsil and brain tissues (Part 3).....136

Table Index:

Table 2-1: List of devices.....19
Table 2-2: List of chemical kits and specific reagents.....20
Table 2-3: List of buffers, medium, and solutions.....21
Table 2-4: Primers used for reverse transcription (RT) reaction of single T cells.....22
Table 2-5: Primers used for specific amplification of TCR β-chain of single T cells.....23
Table 2-6: Primers used for pre-amplification of TCR α-chain of single T cells.....23
Table 2-7: Primers used for the specific amplification of TCR α-chain of single T cell.....24
Table 2-8: Primers used for recovery of antigen-coding plasmids.....25

Table 2-9: Plasmid constructions 25
Table 2-10: Antibodies employed for immunofluorescence staining 26
Table 2-11: Antibodies employed for flow cytometers 27
Table 2-12: List of eukaryotic cell lines and *E.coli* strains 27
Table 2-13: HLA typing results of MS patients FE and RF 29
Table 2-14: Diagnostic performance of HLA typing for MS patients. 29
Table 2-15: Antibiotic selection for stable transfection of eukaryotic cell lines 43
Table 3-1: Detection of different immune cells with the specific antibodies 57
Table 3-2: Summary of staining results obtained from different conditions 70
Table 3-3: TCR β-chains obtained from unbiased PCR protocol with various concentrations of RT primers 78
Table 3-4: TCR β-chains obtained from unbiased PCR protocol with various reverse Cβ primers 79
Table 3-5: TCR β-chains obtained from unbiased PCR protocol with different thermocycling conditions 81
Table 3-6: TCR β-chains obtained from unbiased PCR protocol with different PCR setups 82
Table 3-7: TCR α-chains obtained from the nested PCRs with different PCR setups 83
Table 3-8: TCR β-chains obtained from the single dissected T cells using the improved unbiased PCR approach 85
Table 3-9: TCR chains obtained from single T cells of the MS CSF specimens 86
Table 3-10: Identical TCR α- and β-chains obtained from single cell analysis and NGS 87
Table 3-11: Frequency of TCR α- and β-chains discovered from different MS patients 88
Table 3-12: PECP library employed for antigen search 97
Table 3-13: Summary of APCs isolation in different antigen libraries recognized by two transfected T hybridoma cell lines 102
Table 3-14: Reactivation of TCR BV1-BJ2.3-AV7.2-AJ24.2 by antigen pools isolated from single APCs 108

5.3 Control Staining with Isotype Antibody

In Section 3.1, the potential immune cells in the space of brain of MS patients were detected with the appropriate antibodies. Meanwhile, the control staining with isotype antibodies proceeded to measure the non-specific staining background signals caused by the interaction of immunoglobulin binding to Fc receptors on the cell surface. The isotype control has the same host species and isotype as the specific primary antibody. Additionally, we examined the specific antibodies and the isotype

antibodies on tonsil and brain sections with the same fluorescence staining protocol. The staining results for isotype control are presented in Table 5-1 to 5-3.

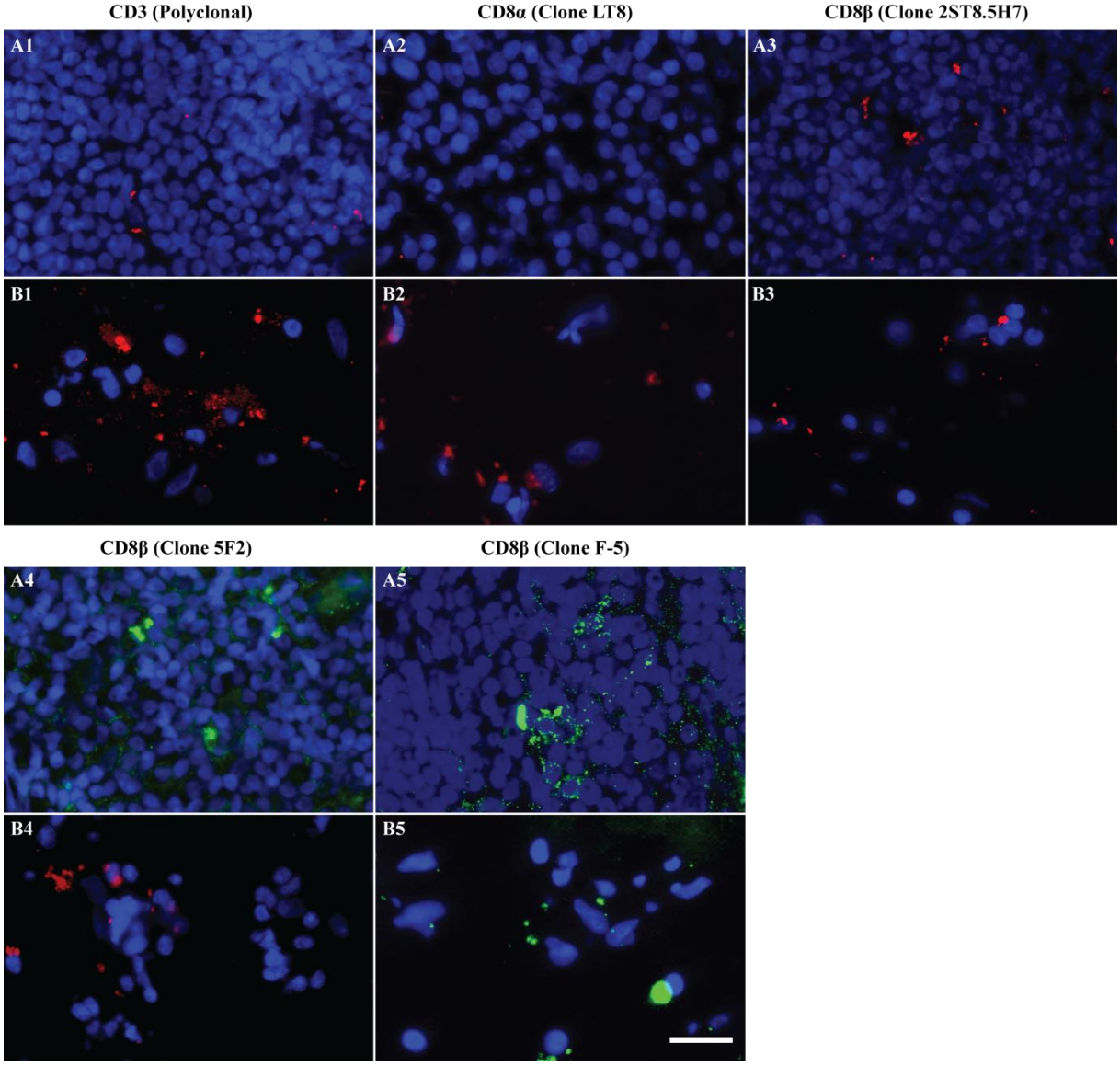

Figure 5-1: Isotype control of each antibody in tonsil and brain tissues (Part 1)

Isotype controls were given parallel with the staining of different antibodies both on frozen tonsil sections **(A)** and MS brain sections **(B)**. All nuclei were stained with DAPI (blue). The isotype control antibodies were labeled with same dyes (Red and green dyes) as the antibodies for $CD8^+$ T cells. The names of antibodies (Clone ID) are written on the top of each image. Scale bar=20 µm.

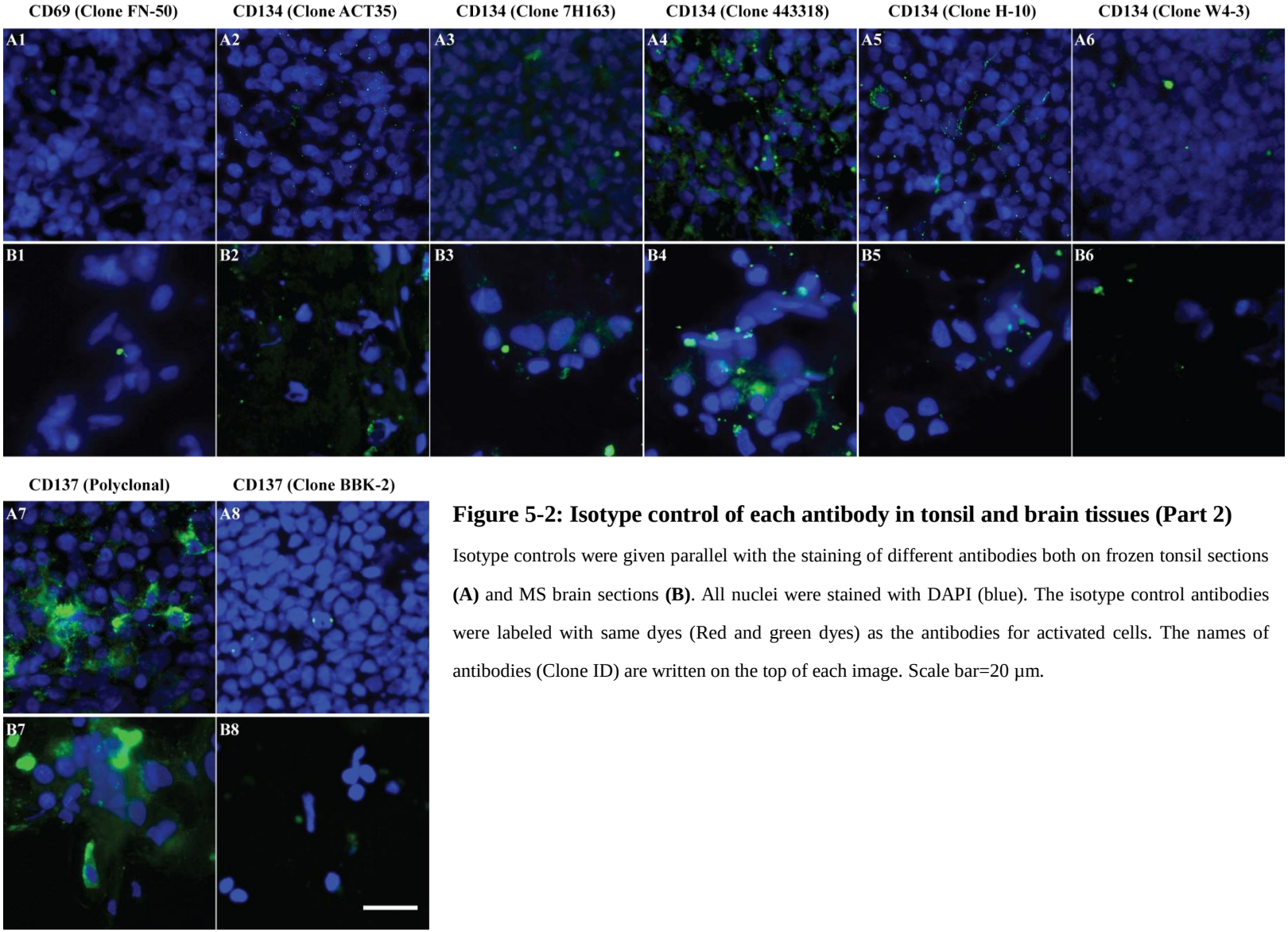

Figure 5-2: Isotype control of each antibody in tonsil and brain tissues (Part 2)

Isotype controls were given parallel with the staining of different antibodies both on frozen tonsil sections **(A)** and MS brain sections **(B)**. All nuclei were stained with DAPI (blue). The isotype control antibodies were labeled with same dyes (Red and green dyes) as the antibodies for activated cells. The names of antibodies (Clone ID) are written on the top of each image. Scale bar=20 µm.

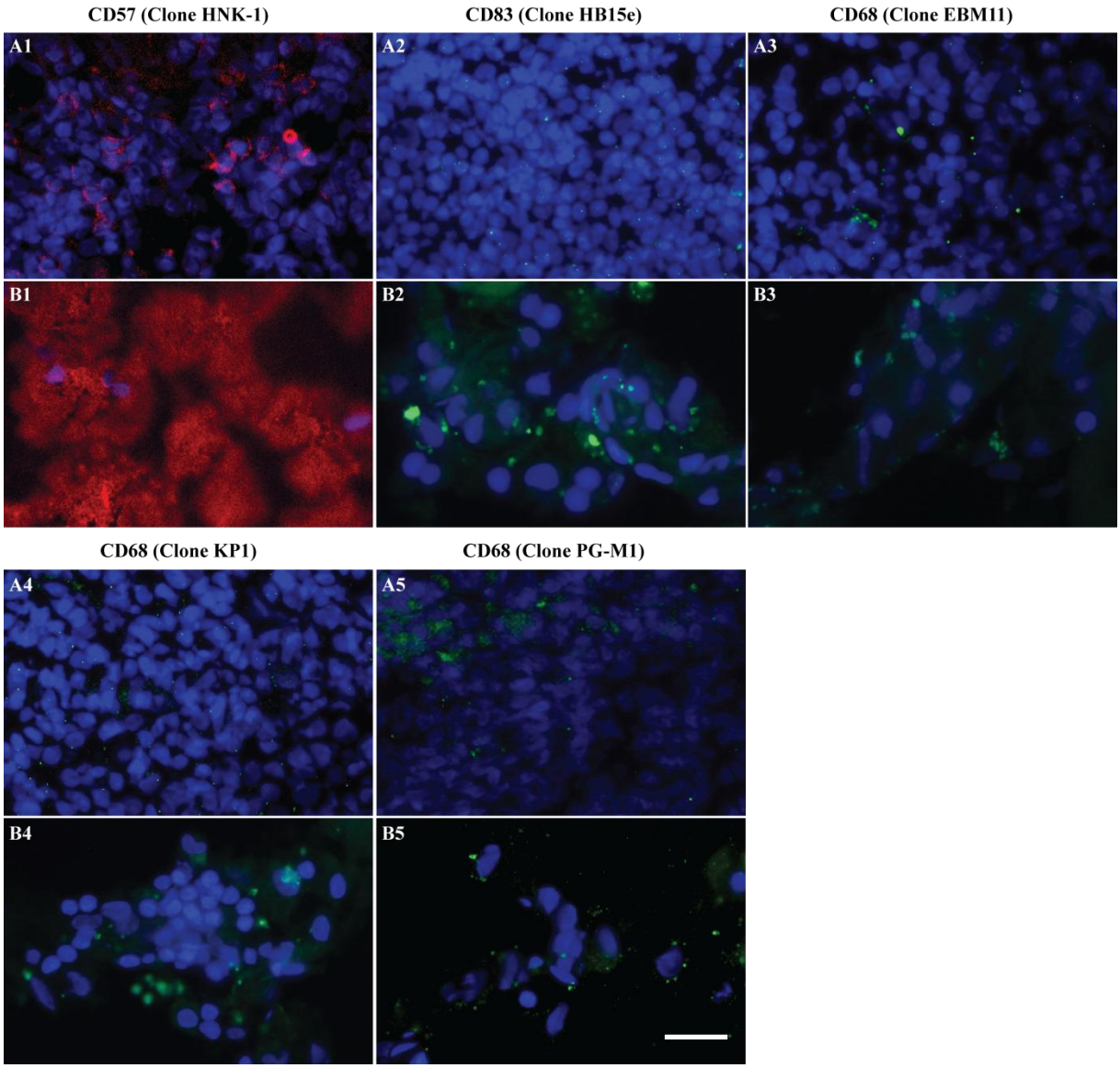

Figure 5-3: Isotype control of each antibody in tonsil and brain tissues (Part 3)

Isotype controls were given parallel with the staining of different antibodies both on frozen tonsil sections **(A)** and MS brain sections **(B)**. All nuclei were stained with DAPI (blue). The isotype control antibodies were labeled with same dyes (Red and green dyes) as the antibodies for NK cells, dendritic cells, and macrophages. The names of antibodies (Clone ID) are written on the top of each image. Scale bar=20 µm.

5.4 Vector Maps

5.4.1 Map of pcDNA™ 6/V5-His

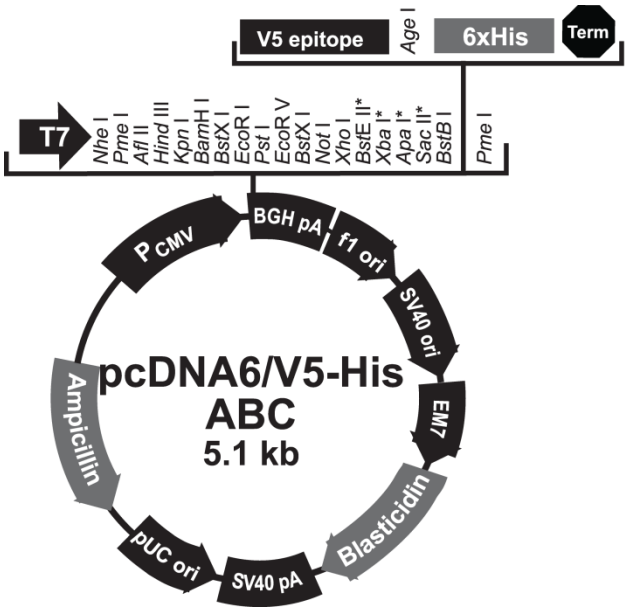

Comments for pcDNA6/V5-His A
5144 nucleotides

CMV promoter: bases 209-863
T7 promoter priming site: bases 863-882
Multiple cloning site: bases 895-1008
V5 epitope: bases 1009-1050
Polyhistidine tag: bases 1060-1077
BGH reverse priming site: bases 1100-1117
BGH polyadenylation sequence: bases 1103-1330
f1 origin: bases 1376-1804
SV40 promoter and origin: bases 1832-2139
EM7 promoter: bases 2187-2242
Blasticidin resistance gene (ORF): bases 2261-2659
SV40 early polyadenylation sequence: bases 2817-2947
pUC origin: bases 3330-4003
Ampicillin resistance gene (ORF): bases 4148-5008

invitrogen™

5.4.2 Map of pcDNA™ 3.1D/V5-His-TOPO®

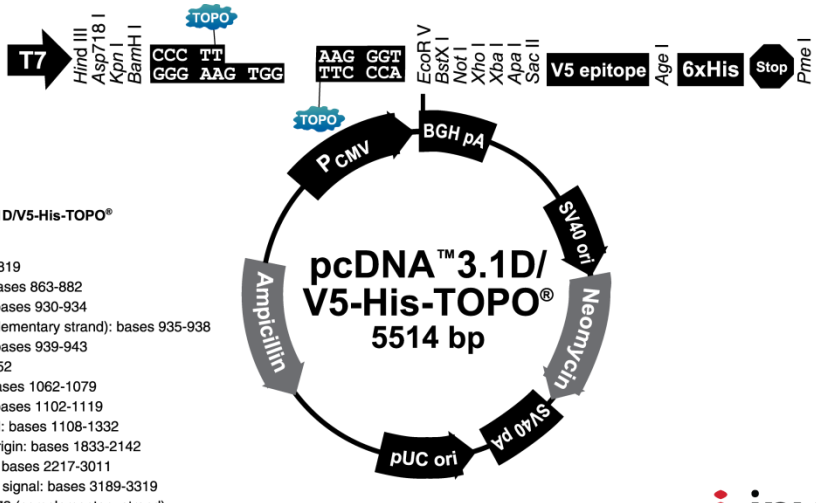

Comments for pcDNA™3.1D/V5-His-TOPO®
5514 nucleotides

CMV promoter: bases 232-819
T7 promoter/priming site: bases 863-882
TOPO® recognition site 1: bases 930-934
Overhang sequence (complementary strand): bases 935-938
TOPO® recognition site 2: bases 939-943
V5 epitope: bases 1011-1052
Polyhistidine (6xHis) tag: bases 1062-1079
BGH reverse priming site: bases 1102-1119
BGH polyadenylation signal: bases 1108-1332
SV40 early promoter and origin: bases 1833-2142
Neomycin resistance gene: bases 2217-3011
SV40 early polyadenylation signal: bases 3189-3319
pUC origin: bases 3700-4373 (complementary strand)
Ampicillin (*bla*) resistance gene: bases 4518-5378 (complementary strand)
bla promoter: bases 5379-5477 (complementary strand)

invitrogen™

5.4.3 Map of pCR™ 2.1-TOPO®

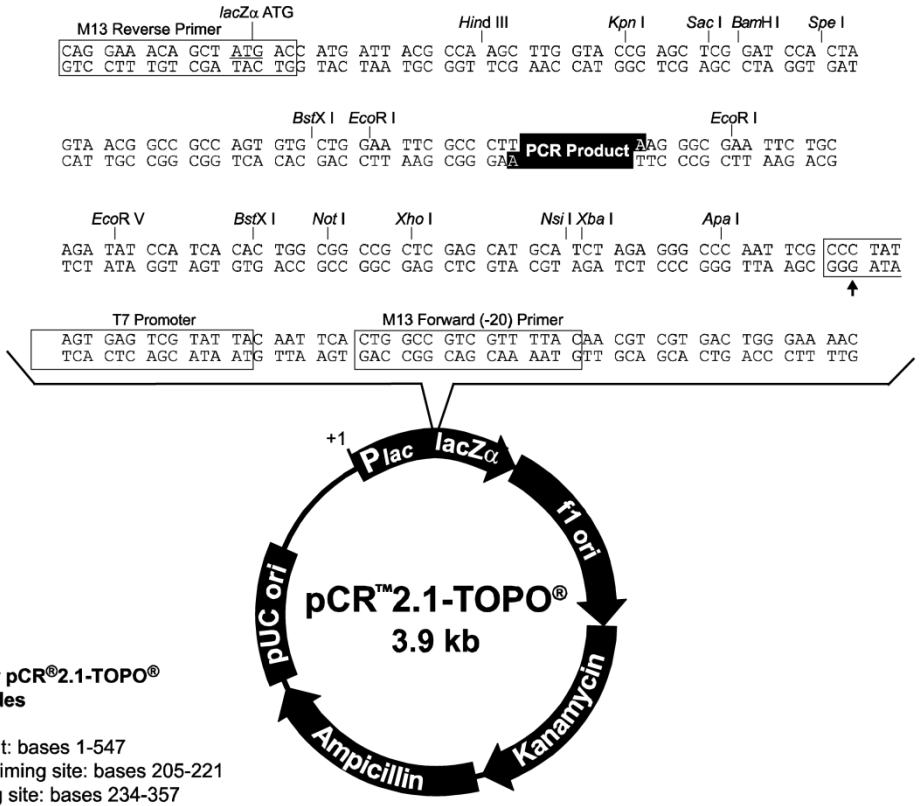

Comments for pCR®2.1-TOPO®
3931 nucleotides

*Lac*Zα fragment: bases 1-547
M13 reverse priming site: bases 205-221
Multiple cloning site: bases 234-357
T7 promoter/priming site: bases 364-383
M13 Forward (-20) priming site: bases 391-406
f1 origin: bases 548-985
Kanamycin resistance ORF: bases 1319-2113
Ampicillin resistance ORF: bases 2131-2991
pUC origin: bases 3136-3809

life technologies™

5.5 Curriculum Vitae

Personal Data

Name	Qingqing Zhou
Birthday	18th October 1986
Place of Birth	Xinyang, Henan, China
Nationality	Chinese

Educational experience

Since Oct. 2012	PhD student in the Institute of Clinical Neuroimmunology of Ludwig Maximilians University, Munich, Germany Supervisor: Dr. Klaus Dornmair Major: Medicine Doctoral thesis: Detection of autoreactive $CD8^+$ T cells *in situ* and investigation of their antigen-specificities
Sep. 2009 - Jun. 2012	Master student in the School of life science, Zhengzhou University, Zhengzhou, China Supervisor: Prof. Qiaozhen Kang Major: Biochemistry & Molecular Biology Diploma Thesis: Effects of the Deficiency of Protein 4.1R on the Changes of $CD4^+$ T cells through developing EAE model
Aug. 2005 - Jun. 2009	Bachelor student in the College of Life Science, Xinyang Normal University, Xinyang, China Major: Bioscience

Honors and Awards

2012 - 2016	National Research Scholarship for Graduate Students from China Scholarship Council-Ludwig Maximilian University Munich, Germany Joint Program
2009 - 2010	Scholarship from Postgraduate's Academic Forum of Zhengzhou University
2008 - 2009	National Encouragement Scholarship for Excellent Studies in Bioscience
2007 - 2008	National Encouragement Scholarship for Excellent Studies in Biotechnology

Publications and Patents

1. Liu, X., **Zhou, Q**., Ji, Z., Fu, G., Li, Y., Zhang, X., Shi, X., Wang, T., and Kang, Q. (2014). Protein 4.1R attenuates autoreactivity in experimental autoimmune encephalomyelitis by suppressing CD4+ T cell activation. Cellular Immunology *292*, 19-24.
2. **Zhou, Q**., Yan, H., Sun, L., JI, Z., Dong, Q., Guo, H., Shi, Y., Gao, Y., Qi, Y., and Kang, Q. (2011). Introducing and Breeding of 4.1R Gene Knockout Mice. Journal of Zhengzhou University *46*, 179-182.
3. Li, L., **Zhou, Q**., Wang, Y., Yan, H., Shi, Y., Liu, X., and Kang, Q. (2011) Validate the antigenicity of MOG through establishing an EAE model in C57BL/6 mice. Shandong Medical Journal *51*, 29-30.
4. Detection of autoreactive $CD8^+$ T cells *in situ* and investigation of their antigen-specificities in Multiple Sclerosis. (in preparation)
5. Application Nr. CN 201010119587
   Zhou, Q., An, X., Kang, Q., Ji, Z., Wang, T., Yan, H., and Chen, l. (2010). Preparation method of antitumor drug screening model with 4.1R and CD29 as target spots and application thereof. Zhengzhou University.
6. Application Nr. CN 201010177875
   Liu, W., **Zhou, Q**., Kang, Q., Duan, G., ji, Z., Qi, Y., and Gao, Y. (2011). Fusion protein MBP-NAP and preparation method and application thereof. Zhengzhou University.

Scientific Research Project

2012-2016 (CSC-LMU Joint Program)	Targets of adaptive immune responses in patients with multiple sclerosis: characterization of the antigens of $CD8^+$ T cells
2010-2012 NFSC (National Natural Science Fund of China)	1. Molecular mechanism of the mast cell degranulation regulated by protein 4.1 R 2. Protein 4.1 R regulating $CD4^+$ T cell-dependent immune response 3. Regulatory mechanism of protein 4.1 R for $CD4^+$ T cell activation and TCR/CD3-mediated signal transduction

5.6 References

Anderson, M.W., Zhao, S., Freud, A.G., Czerwinski, D.K., Kohrt, H., Alizadeh, A.A., Houot, R., Azambuja, D., Biasoli, I., Morais, J.C., et al. (2012). CD137 is expressed in follicular dendritic cell tumors and in classical hodgkin and T-cell lymphomas. The American journal of pathology *181*, 795-803.

Arakawa, A., Siewert, K., Stöhr, J., Besgen, P., Kim, S.-M., Rühl, G., Nickel, J., Vollmer, S., Thomas, P., and Krebs, S. (2015). Melanocyte antigen triggers autoimmunity in human psoriasis. The journal of experimental medicine *212*, 2203-2212.

Arden, B., Clark, S.P., Kabelitz, D., and Mak, T.W. (1995). Human T-cell receptor variable gene segment families. Immunogenetics *42*, 455-500.

Ascherio, A., Munger, K.L., White, R., and et al. (2014). Vitamin d as an early predictor of multiple sclerosis activity and progression. JAMA neurology *71*, 306-314.

Awad, A., Hemmer, B., Hartung, H.P., Kieseier, B., Bennett, J.L., and Stuve, O. (2010). Analyses of cerebrospinal fluid in the diagnosis and monitoring of multiple sclerosis. J Neuroimmunol *219*, 1-7.

Babbe, H., Roers, A., Waisman, A., Lassmann, H., Goebels, N., Hohlfeld, R., Friese, M., Schröder, R., Deckert, M., and Schmidt, S. (2000). Clonal expansions of $CD8^+$ T cells dominate the T cell infiltrate in active multiple sclerosis lesions as shown by micromanipulation and single cell polymerase chain reaction. The journal of experimental medicine *192*, 393-404.

Babij, R., and Perumal, J.S. (2015). Comparative efficacy of alemtuzumab and established treatment in the management of multiple sclerosis. Neuropsychiatric disease and treatment *11*, 1221-1229.

Bar-Or, A. (2016). Multiple sclerosis and related disorders: evolving pathophysiologic insights. The lancet neurology *15*, 9-11.

Beall, S.S., Concannon, P., Charmley, P., McFarland, H.F., Gatti, R.A., Hood, L.E., McFarlin, D.E., and Biddison, W.E. (1989). The germline repertoire of T cell receptor beta-chain genes in patients with chronic progressive multiple sclerosis. J Neuroimmunol *21*, 59-66.

Becher, B., Prat, A., and Antel, J.P. (2000). Brain-immune connection: Immuno-regulatory properties of CNS-resident cells. Glia *29*, 293-304.

Beltrán, E., Obermeier, B., Moser, M., Coret, F., Simó-Castelló, M., Boscá, I., Pérez-Miralles, F., Villar, L.M., Senel, M., and Tumani, H. (2014). Intrathecal somatic hypermutation of IgM in multiple sclerosis and neuroinflammation. Brain *137*, 2703-14.

Benveniste, E.N. (1997). Role of macrophages/microglia in multiple sclerosis and experimental allergic encephalomyelitis. Journal of molecular medicine *75*, 165-173.

Beringer, D.X., Kleijwegt, F.S., Wiede, F., van der Slik, A.R., Loh, K.L., Petersen, J., Dudek, N.L., Duinkerken, G., Laban, S., Joosten, A., et al. (2015). T cell receptor reversed polarity recognition of a self-antigen major histocompatibility complex. Nat Immunol *16*, 1153-1161.

Berthelot, L., Laplaud, D.A., Pettre, S., Ballet, C., Michel, L., Hillion, S., Braudeau, C., Connan, F., Lefrere, F., Wiertlewski, S., et al. (2008). Blood $CD8^+$ T cell responses against myelin determinants in multiple sclerosis and healthy individuals. Eur J Immunol *38*, 1889-1899.

Biddison, W.E., Beall, S.S., Concannon, P., Charmley, P., Gatti, R.A., Hood, L.E., McFarland, H.F., and McFarlin, D.E. (1989). The germline repertoire of T-cell receptor beta-chain genes in patients with multiple sclerosis. Research in immunology *140*, 212-215.

Bielekova, B., Sung, M.-H., Kadom, N., Simon, R., McFarland, H., and Martin, R. (2004). Expansion and functional relevance of high-avidity myelin-specific $CD4^+$ T cells in multiple sclerosis. The journal of immunology *172*, 3893-3904.

Blank, U., Boitel, B., Mege, D., Ermonval, M., and Acuto, O. (1993). Analysis of tetanus toxin peptide/DR recognition by human T cell receptors reconstituted into a murine T cell hybridoma. Eur J Immunol *23*, 3057-3065.

Boon, T., Coulie, P.G., Van den Eynde, B.J., and van der Bruggen, P. (2006). Human T cell responses against melanoma. Annu Rev Immunol *24*, 175-208.

Brändle, S.M., Obermeier, B., Senel, M., Bruder, J., Mentele, R., Khademi, M., Olsson, T., Tumani, H., Kristoferitsch, W., and Lottspeich, F. (2016). Distinct oligoclonal band antibodies in multiple sclerosis recognize ubiquitous self-proteins. Proceedings of the national academy of sciences *113*, 7864-7869.

Brownlee, W.J., Hardy, T.A., Fazekas, F., and Miller, D.H. (2017). Diagnosis of multiple sclerosis: progress and challenges. Lancet *389*, 1336-1346.

Callan, M.F.C., Fazou, C., Yang, H., Rostron, T., Poon, K., Hatton, C., and McMichael, A.J. (2000). $CD8^+$ T-cell selection, function, and death in the primary immune response in vivo. The journal of clinical investigation *106*, 1251-1261.

Carboni, S., Aboul-Enein, F., Waltzinger, C., Killeen, N., Lassmann, H., and Peña-Rossi, C. (2003). CD134 plays a crucial role in the pathogenesis of EAE and is upregulated in the CNS of patients with multiple sclerosis. Journal of neuroimmunology *145*, 1-11.

Chua, W.-J., Kim, S., Myers, N., Huang, S., Yu, L., Fremont, D.H., Diamond, M.S., and Hansen, T.H. (2011). Endogenous MHC-related protein 1 is transiently expressed on the plasma membrane in a conformation that activates mucosal-associated invariant T cells. The journal of immunology *186*, 4744.

Comi, G., Radaelli, M., and Soelberg Sorensen, P. (2017). Evolving concepts in the treatment of relapsing multiple sclerosis. Lancet *389*, 1347-1356.

Compston, A. (1988). The 150th anniversary of the first depiction of the lesions of multiple sclerosis. Journal of neurology, neurosurgery, and psychiatry *51*, 1249-1252.

Compston, A., and Coles, A. (2008). Multiple sclerosis. Lancet *372*, 1502-1517.

Crawford, F., Jordan, K.R., Stadinski, B., Wang, Y., Huseby, E., Marrack, P., Slansky, J.E., and Kappler, J.W. (2006). Use of baculovirus MHC/peptide display libraries to characterize T-cell receptor ligands. Immunological reviews *210*, 156-170.

Dash, P., McClaren, J.L., Oguin, T.H., 3rd, Rothwell, W., Todd, B., Morris, M.Y., Becksfort, J., Reynolds, C., Brown, S.A., Doherty, P.C., et al. (2011). Paired analysis of TCR-alpha and TCR-beta chains at the single-cell level in mice. J Clin Invest *121*, 288-295.

Davis, M.M., and Bjorkman, P.J. (1988). T-cell antigen receptor genes and T-cell recognition. Nature *334*, 395-402.

Deckx, N., Lee, W.-P., Berneman, Z.N., and Cools, N. (2013). Neuroendocrine immunoregulation in multiple sclerosis. Clinical and developmental immunology *2013*, 705232.

Diamond, B., Katz, J.B., Paul, E., Aranow, C., Lustgarten, D., and Scharff, M.D. (1992). The role of somatic mutation in the pathogenic anti-DNA response. Annu Rev Immunol *10*, 731-757.

Dooms, H., and Abbas, A.K. (2002). Life and death in effector T cells. Nat Immunol *3*, 797-798.

Dornmair, K., Goebels, N., Weltzien, H.-U., Wekerle, H., and Hohlfeld, R. (2003). T-cell-mediated autoimmunity: novel techniques to characterize autoreactive T-cell receptors. The American journal of pathology *163*, 1215-1226.

Dornmair, K., Meinl, E., and Hohlfeld, R. (2009). Novel approaches for identifying target antigens of autoreactive human B and T cells. Seminars in immunopathology *31*, 467-477.

Filippi, M., Rocca, M.A., Ciccarelli, O., De Stefano, N., Evangelou, N., Kappos, L., Rovira, A., Sastre-Garriga, J., Tintore, M., Frederiksen, J.L., et al. (2016). MRI criteria for the diagnosis of multiple sclerosis: MAGNIMS consensus guidelines. The lancet neurology *15*, 292-303.

Friese, M.A., and Fugger, L. (2009). Pathogenic $CD8^+$ T cells in multiple sclerosis. Annals of neurology *66*, 132-141.

Gao, F., and Wang, K. (2015). Ligation-anchored PCR unveils immune repertoire of TCR-beta from whole blood. BMC biotechnology *15*, 39.

Gass, A., Rocca, M.A., Agosta, F., Ciccarelli, O., Chard, D., Valsasina, P., Brooks, J.C., Bischof, A., Eisele, P., Kappos, L., et al. (2015). MRI monitoring of pathological changes in the spinal cord in patients with multiple sclerosis. The lancet neurology *14*, 443-454.

Gerdes, L.A., Held, K., Beltrán, E., Berking, C., Prinz, J.C., Junker, A., Tietze, J.K., Ertl-Wagner, B., Straube, A., and Kümpfel, T. (2016). CTLA4 as immunological checkpoint in the development of multiple sclerosis. Annals of neurology *80*, 294-300.

Global Burden of Disease Study, C. (2015). Global, regional, and national incidence, prevalence, and years lived with disability for 301 acute and chronic diseases and injuries in 188 countries, 1990-2013: a systematic analysis for the Global Burden of Disease Study 2013. Lancet *386*, 743-800.

Gold, M.C., Napier, R.J., and Lewinsohn, D.M. (2015). MR1-restricted mucosal associated invariant T (MAIT) cells in the immune response to Mycobacterium tuberculosis. Immunological reviews *264*, 154-166.

Gotch, F., Rothbard, J., Howland, K., Townsend, A., and McMichael, A. (1987). Cytotoxic T lymphocytes recognize a fragment of influenza virus matrix protein in association with HLA-A2. Nature *326*, 881-882.

Greter, M., Heppner, F.L., Lemos, M.P., Odermatt, B.M., Goebels, N., Laufer, T., Noelle, R.J., and Becher, B. (2005). Dendritic cells permit immune invasion of the CNS in an animal model of multiple sclerosis. Nat Med *11*, 328-334.

Griesemer, A.D., Sorenson, E.C., and Hardy, M.A. (2010). The role of the thymus in tolerance. Transplantation *90*, 465-474.

Gross, C.C., Schulte-Mecklenbeck, A., Rünzi, A., Kuhlmann, T., Posevitz-Fejfár, A., Schwab, N., Schneider-Hohendorf, T., Herich, S., Held, K., Konjević, M., et al. (2016). Impaired NK-mediated regulation of T-cell activity in multiple sclerosis is reconstituted by IL-2 receptor modulation. Proceedings of the national academy of sciences *113*, E2973-E2982.

Held, K., Beltrán, E., Moser, M., Hohlfeld, R., and Dornmair, K. (2015). T-cell receptor repertoire of human peripheral CD161 hi TRAV1-2^{+} MAIT cells revealed by next generation sequencing and single cell analysis. Human immunology *76*, 607-614.

Held, K., Bhonsle-Deeng, L., Siewert, K., Sato, W., Beltrán, E., Schmidt, S., Rühl, G., Ng, J.K., Engerer, P., and Moser, M. (2015). αβ T-cell receptors from multiple sclerosis brain lesions show MAIT cell-related features. Neurology-neuroimmunology neuroinflammation *2*, e107.

Hellebrand, E., Mautner, J., Reisbach, G., Nimmerjahn, F., Hallek, M., Mocikat, R., and Hammerschmidt, W. (2006). Epstein-Barr virus vector-mediated gene transfer into human B cells: potential for antitumor vaccination. Gene therapy *13*, 150-162.

Hemmer, B., Gran, B., Zhao, Y., Marques, A., Pascal, J., Tzou, A., Kondo, T., Cortese, I., Bielekova, B., Straus, S.E., et al. (1999). Identification of candidate T-cell epitopes and molecular mimics in chronic Lyme disease. Nat Med *5*, 1375-1382.

Hemmer, B., Kerschensteiner, M., and Korn, T. (2015). Role of the innate and adaptive immune responses in the course of multiple sclerosis. The lancet neurology *14*, 406-419.

Hinterberger, M., Aichinger, M., da Costa, O.P., Voehringer, D., Hoffmann, R., and Klein, L. (2010). Autonomous role of medullary thymic epithelial cells in central $CD4^+$ T cell tolerance. Nat Immunol *11*, 512-519.

Hofbauer, M., Wiesener, S., Babbe, H., Roers, A., Wekerle, H., Dornmair, K., Hohlfeld, R., and Goebels, N. (2003). Clonal tracking of autoaggressive T cells in polymyositis by combining laser microdissection, single-cell PCR, and CDR3-spectratype analysis. Proc Natl Acad Sci U S A *100*, 4090-4095.

Höftberger, R., Aboul-Enein, F., Brueck, W., Lucchinetti, C., Rodriguez, M., Schmidbauer, M., Jellinger, K., and Lassmann, H. (2004). Expression of major histocompatibility complex class l molecules on the different Cell types in multiple sclerosis lesions. Brain pathology *14*, 43-50.

Hohlfeld, R., and Dornmair, K. (2007). Revisiting the immunopathogenesis of the inflammatory myopathies. Neurology *69*, 1966-1967.

Hohlfeld, R., Dornmair, K., Meinl, E., and Wekerle, H. (2015). The search for the target antigens of multiple sclerosis, part 1: autoreactive $CD4^+$ T lymphocytes as pathogenic effectors and therapeutic targets. The lancet neurology *15*, 198-209.

Hohlfeld, R., Dornmair, K., Meinl, E., and Wekerle, H. (2016). The search for the target antigens of multiple sclerosis, part 2: $CD8^+$ T cells, B cells, and antibodies in the focus of reverse-translational research. The lancet neurology *15*, 317-331.

Hohlfeld, R., Meinl, E., and Dornmair, K. (2008). B- and T-cell responses in multiple sclerosis: novel approaches offer new insights. Journal of the neurological sciences *274*, 5-8.

Hohlfeld, R., and Wekerle, H. (2001). Immunological update on multiple sclerosis. Current opinion in neurology *14*, 299-304.

Hu, W., and Lucchinetti, C.F. (2009). The pathological spectrum of CNS inflammatory demyelinating diseases. Seminars in immunopathology *31*, 439-453.

Huang, S., Gilfillan, S., Cella, M., Miley, M.J., Lantz, O., Lybarger, L., Fremont, D.H., and Hansen, T.H. (2005). Evidence for MR1 antigen presentation to mucosal-associated invariant T cells. The Journal of biological chemistry *280*, 21183-21193.

Illes, Z., Shimamura, M., Newcombe, J., Oka, N., and Yamamura, T. (2004). Accumulation of Valpha7.2-Jalpha33 invariant T cells in human autoimmune inflammatory lesions in the nervous system. International immunology *16*, 223-230.

Junker, A., Ivanidze, J., Malotka, J., Eiglmeier, I., Lassmann, H., Wekerle, H., Meinl, E., Hohlfeld, R., and Dornmair, K. (2007). Multiple sclerosis: T-cell receptor expression in distinct brain regions. Brain *130*, 2789-2799.

Kass, I., Buckle, A.M., and Borg, N.A. (2014). Understanding the structural dynamics of TCR-pMHC complex interactions. Trends Immunol *35*, 604-612.

Kawakami, N. (2016). In vivo imaging in autoimmune diseases in the central nervous system. Allergology international : official journal of the Japanese society of allergology *65*, 235-242.

Kim, S.-M., Bhonsle, L., Besgen, P., Nickel, J., Backes, A., Held, K., Vollmer, S., Dornmair, K., and Prinz, J.C. (2012). Analysis of the paired TCR α-and β-chains of single human T cells. PloS one *7*, e37338.

Kjer-Nielsen, L., Patel, O., Corbett, A.J., Le Nours, J., Meehan, B., Liu, L., Bhati, M., Chen, Z., Kostenko, L., Reantragoon, R., et al. (2012). MR1 presents microbial vitamin B metabolites to MAIT cells. Nature *491*, 717-723.

Krishnamoorthy, G., Saxena, A., Mars, L.T., Domingues, H.S., Mentele, R., Ben-Nun, A., Lassmann, H., Dornmair, K., Kurschus, F.C., Liblau, R.S., et al. (2009). Myelin-specific T cells also recognize neuronal autoantigen in a transgenic mouse model of multiple sclerosis. Nat Med *15*, 626-632.

Krumbholz, M., Theil, D., Cepok, S., Hemmer, B., Kivisäkk, P., Ransohoff, R.M., Hofbauer, M., Farina, C., Derfuss, T., Hartle, C., et al. (2005). Chemokines in multiple sclerosis: CXCL12 and CXCL13 up-regulation is differentially linked to CNS immune cell recruitment. Brain *129*, 200.

Lassmann, H., Brück, W., and Lucchinetti, C. (2001). Heterogeneity of multiple sclerosis pathogenesis: implications for diagnosis and therapy. Trends in molecular medicine *7*, 115-121.

Le Bourhis, L., Guerri, L., Dusseaux, M., Martin, E., Soudais, C., and Lantz, O. (2011). Mucosal-associated invariant T cells: unconventional development and function. Trends Immunol *32*, 212-218.

Lefranc, M.-P., Giudicelli, V., Ginestoux, C., Jabado-Michaloud, J., Folch, G., Bellahcene, F., Wu, Y., Gemrot, E., Brochet, X., Lane, J., et al. (2009). IMGT®, the international ImMunoGeneTics information system®. Nucleic acids research *37*, D1006-D1012.

Lefranc, M.P., and Lefranc, G. (2001). The T Cell Receptor FactsBook (London, UK: Academic Press).

Letourneur, F., and Malissen, B. (1989). Derivation of a T cell hybridoma variant deprived of functional T cell receptor alpha and beta chain transcripts reveals a nonfunctional alpha-mRNA of BW5147 origin. Eur J Immunol *19*, 2269-2274.

Lublin, F.D. (2014). New multiple sclerosis phenotypic classification. European neurology *72*, 1-5.

Mack, C.L., Vanderlugt-Castaneda, C.L., Neville, K.L., and Miller, S.D. (2003). Microglia are activated to become competent antigen presenting and effector cells in the inflammatory environment of the Theiler's virus model of multiple sclerosis. Journal of neuroimmunology *144*, 68-79.

Mahad, D.H., Trapp, B.D., and Lassmann, H. (2015). Pathological mechanisms in progressive multiple sclerosis. The lancet neurology *14*, 183-193.

Mantegazza, R., Andreetta, F., Bernasconi, P., Baggi, F., Oksenberg, J.R., Simoncini, O., Mora, M., Cornelio, F., and Steinman, L. (1993). Analysis of T cell receptor repertoire of muscle-infiltrating T lymphocytes in polymyositis. Restricted V alpha/beta rearrangements may indicate antigen-driven selection. Journal of clinical investigation *91*, 2880-2886.

Marcus, J.F., and Waubant, E.L. (2013). Updates on clinically isolated syndrome and diagnostic criteria for multiple sclerosis. The neurohospitalist *3*, 65-80.

Matsumoto, Y., Yoon, W.K., Jee, Y., Fujihara, K., Misu, T., Sato, S., Nakashima, I., and Itoyama, Y. (2003). Complementarity-determining region 3 spectratyping analysis of the TCR repertoire in multiple sclerosis. Journal of immunology *170*, 4846-4853.

Milo, R., and Kahana, E. (2010). Multiple sclerosis: Geoepidemiology, genetics and the environment. Autoimmunity reviews *9*, A387-A394.

Miyazaki, Y., Miyake, S., Chiba, A., Lantz, O., and Yamamura, T. (2011). Mucosal-associated invariant T cells regulate Th1 response in multiple sclerosis. International immunology *23*, 529-535.

Munger, K.L., Zhang, S.M., O'Reilly, E., Hernán, M.A., Olek, M.J., Willett, W.C., and Ascherio, A. (2004). Vitamin D intake and incidence of multiple sclerosis. Neurology *62*, 60-65.

Nikolic-Zugic, J., and Bevan, M.J. (1990). Role of self-peptides in positively selecting the T-cell repertoire. Nature *344*, 65-67.

Obermeier, B., Lovato, L., Mentele, R., Brück, W., Forne, I., Imhof, A., Lottspeich, F., Turk, K.W., Willis, S.N., and Wekerle, H. (2011). Related B cell clones that populate the CSF and CNS of patients with multiple sclerosis produce CSF immunoglobulin. Journal of neuroimmunology *233*, 245-248.

Obermeier, B., Mentele, R., Malotka, J., Kellermann, J., Kumpfel, T., Wekerle, H., Lottspeich, F., Hohlfeld, R., and Dornmair, K. (2008). Matching of oligoclonal immunoglobulin transcriptomes and proteomes of cerebrospinal fluid in multiple sclerosis. Nat Med *14*, 688-693.

Oksenberg, J.R., Baranzini, S.E., Barcellos, L.F., and Hauser, S.L. (2001). Multiple sclerosis: Genomic rewards. Journal of neuroimmunology *113*, 171-184.

Ontaneda, D., Thompson, A.J., Fox, R.J., and Cohen, J.A. (2017). Progressive multiple sclerosis: prospects for disease therapy, repair, and restoration of function. Lancet *389*, 1357-1366.

Padovan, E., Casorati, G., Dellabona, P., Meyer, S., Brockhaus, M., and Lanzavecchia, A. (1993). Expression of two T cell receptor alpha chains: dual receptor T cells. Science *262*, 422-424.

Pannetier, C., Even, J., and Kourilsky, P. (1995). T-cell repertoire diversity and clonal expansions in normal and clinical samples. Immunology today *16*, 176-181.

Pellkofer, H.L., Voltz, R., Goebels, N., Hohlfeld, R., and Dornmair, K. (2009). Cross-reactive T-cell receptors in tumor and paraneoplastic target tissue. Archives of neurology *66*, 655-658.

Porcelli, S., Yockey, C.E., Brenner, M.B., and Balk, S.P. (1993). Analysis of T cell antigen receptor (TCR) expression by human peripheral blood $CD4^-8^-$ alpha/beta T cells demonstrates preferential use of several V beta genes and an invariant TCR alpha chain. J Exp Med *178*, 1-16.

Ruhl, G., Niedl, A.G., Patronov, A., Siewert, K., Pinkert, S., Kalemanov, M., Friese, M.A., Attfield, K.E., Antes, I., Hohlfeld, R., et al. (2016). Multiple sclerosis: Molecular mimicry of an antimyelin HLA class I restricted T-cell receptor. Neurology-neuroimmunology neuroinflammation *3*, e241.

Salem, A.A., Douglas-Jones, A.G., Sweetland, H.M., and Mansel, R.E. (2003). Intraoperative evaluation of axillary sentinel lymph nodes using touch imprint cytology and immunohistochemistry: I. Protocol of rapid immunostaining of touch imprints. European journal of surgical oncology *29*, 25-28.

Sawcer, S., Franklin, R.J., and Ban, M. (2014). Multiple sclerosis genetics. The lancet neurology *13*, 700-709.

Seitz, S., Schneider, C.K., Malotka, J., Nong, X., Engel, A.G., Wekerle, H., Hohlfeld, R., and Dornmair, K. (2006). Reconstitution of paired T cell receptor α-and β-chains from microdissected single cells of human inflammatory tissues. Proceedings of the national academy of sciences *103*, 12057-12062.

Serriari, N.E., Eoche, M., Lamotte, L., Lion, J., Fumery, M., Marcelo, P., Chatelain, D., Barre, A., Nguyen‐Khac, E., and Lantz, O. (2014). Innate mucosal-associated invariant T (MAIT) cells are activated in inflammatory bowel diseases. Clinical & experimental immunology *176*, 266-274.

Siewert, K., Malotka, J., Kawakami, N., Wekerle, H., Hohlfeld, R., and Dornmair, K. (2012). Unbiased identification of target antigens of $CD8^+$ T cells with combinatorial libraries coding for short peptides. Nature medicine *18*, 824-828.

Skulina, C., Schmidt, S., Dornmair, K., Babbe, H., Roers, A., Rajewsky, K., Wekerle, H., Hohlfeld, R., and Goebels, N. (2004). Multiple sclerosis: brain-infiltrating $CD8^+$ T cells persist as clonal expansions in the cerebrospinal fluid and blood. Proceedings of the national academy of sciences of the United States of America *101*, 2428-2433.

Sprent, J., Lo, D., Gao, E.-K., and Ron, Y. (1988). T cell selection in the thymus. Immunological reviews *101*, 173-190.

Stangel, M., Fredrikson, S., Meinl, E., Petzold, A., Stuve, O., and Tumani, H. (2013). The utility of cerebrospinal fluid analysis in patients with multiple sclerosis. Nature reviews neurology *9*, 267-276.

Starr, T.K., Jameson, S.C., and Hogquist, K.A. (2003). Positive and negative selection of T cells. Annu Rev Immunol *21*, 139-176.

Stewart-Jones, G.B.E., McMichael, A.J., Bell, J.I., Stuart, D.I., and Jones, E.Y. (2003). A structural basis for immunodominant human T cell receptor recognition. Nat Immunol *4*, 657-663.

Sun, X., Saito, M., Sato, Y., Chikata, T., Naruto, T., Ozawa, T., Kobayashi, E., Kishi, H., Muraguchi, A., and Takiguchi, M. (2012). Unbiased analysis of TCRα/β chains at the single-cell level in human $CD8^+$ T-cell subsets. PloS one *7*, e40386.

Tilloy, F., Treiner, E., Park, S.H., Garcia, C., Lemonnier, F., de la Salle, H., Bendelac, A., Bonneville, M., and Lantz, O. (1999). An invariant T cell receptor alpha chain defines a novel TAP-independent major histocompatibility complex class Ib-restricted alpha/beta T cell subpopulation in mammals. J Exp Med *189*, 1907-1921.

Uccelli, A., and Mancardi, G. (2010). Stem cell transplantation in multiple sclerosis. Current opinion in neurology *23*, 218-225.

Van Der Bruggen, P., Zhang, Y., Chaux, P., Stroobant, V., Panichelli, C., Schultz, E.S., Chapiro, J., Van Den Eynde, B.J., Brasseur, F., and Boon, T. (2002). Tumor-specific shared antigenic peptides recognized by human T cells. Immunological reviews *188*, 51-64.

Vyas, J.M., Van der Veen, A.G., and Ploegh, H.L. (2008). The known unknowns of antigen processing and presentation. Nat Rev Immunol *8*, 607-618.

Wong, F.S., Karttunen, J., Dumont, C., Wen, L., Visintin, I., Pilip, I.M., Shastri, N., Pamer, E.G., and Janeway, C.A., Jr. (1999). Identification of an MHC class I-restricted autoantigen in type 1 diabetes by screening an organ-specific cDNA library. Nat Med *5*, 1026-1031.

Wucherpfennig, K.W., Newcombe, J., Li, H., Keddy, C., Cuzner, M.L., and Hafler, D.A. (1992). T cell receptor V alpha-V beta repertoire and cytokine gene expression in active multiple sclerosis lesions. J Exp Med *175*, 993-1002.

Zerrahn, J., Held, W., and Raulet, D.H. (1997). The MHC reactivity of the T cell repertoire prior to positive and negative selection. Cell *88*, 627-636.

Zhao, Y., Gran, B., Pinilla, C., Markovic-Plese, S., Hemmer, B., Tzou, A., Whitney, L.W., Biddison, W.E., Martin, R., and Simon, R. (2001). Combinatorial peptide libraries and biometric score matrices permit the quantitative analysis of specific and degenerate interactions between clonotypic TCR and MHC peptide ligands. The journal of immunology *167*, 2130-2141.

Ziegler, S.F., Ramsdell, F., and Alderson, M.R. (1994). The activation antigen CD69. Stem cells *12*, 456-465.